Fisheries New Zealand
Tini a Tangaroa

Local-scale spatial risk assessment of inshore commercial fisheries on Hector's dolphins

New Zealand Aquatic Environment and Biodiversity Report No. 308

J.O. Roberts,
D.N. Webber

ISSN 1179-6480 (online)
ISBN 978-1-991080-37-0 (online)

April 2023

Te Kāwanatanga o Aotearoa
New Zealand Government

Disclaimer

Requests for further copies should be directed to:

Fisheries Science Editor
Fisheries New Zealand
Ministry for Primary Industries
PO Box 2526
Wellington 6140
NEW ZEALAND

Email: Fisheries-Science.Editor@mpi.govt.nz
Telephone: 0800 00 83 33

This publication is also available on the Ministry for Primary Industries websites at:
http://www.mpi.govt.nz/news-and-resources/publications
http://fs.fish.govt.nz go to Document library/Research reports

Please cite this report as:

Roberts, J.O.; Webber, D.N. (2023). Local-scale spatial risk assessment of inshore commercial fisheries on Hector’s dolphins. *New Zealand Aquatic Environment and Biodiversity Report No. 308.* 99 p.

TABLE OF CONTENTS

EXECUTIVE SUMMARY

Roberts, J.O.[1]; Webber, D.N.[2] (2023). Local-scale spatial risk assessment of inshore commercial fisheries on Hector's dolphins.

***New Zealand Aquatic Environment and Biodiversity Report No. 308*. 99 p.**

The spatially explicit fisheries risk assessment (SEFRA) of Hector's dolphins (*Cephalorhynchus hectori hectori*) and Māui dolphins (*Cephalorhynchus hectori maui*) was updated and outputs were reported for Hector's dolphins in three local-scale areas: the north coast of the South Island (NCSI), the Kaikōura coast (KAIK), and the south coast of the South Island (SCSI). Inputs that were updated included the summer/winter spatial distribution layers for South Island Hector's dolphins and the commercial fishing effort data (observed and unobserved) to include the fishing years 2017–18 to 2019–20.

Spatial distribution models were fitted to all available sightings-based spatial data for Hector's dolphins around the South Island of New Zealand (including from aerial surveys, boat-based mark-recapture surveys, fishery observer data, and public sightings) and included environmental covariates. Model selection was done using a novel model cross-validation procedure, which resulted in the selection of a model including sea surface turbidity, the percentage of mud in benthic sediments, and a seasonal spatial smoother. This model and two sensitivity model runs predicted a more heterogenous spatial distribution in each area than was previously assumed, with regions of elevated density within Golden Bay, off the coast to the north of Kaikōura, and in Te Waewae Bay.

Using the revised Hector's dolphin spatial distribution layers in the SEFRA model resulted in: a decrease in estimated annual risk associated with commercial set nets within SCSI across the 2014–15 to 2016–17 fishing seasons, increased risk within NCSI, and around the same level of risk within KAIK, in comparison with the model using the previous Hector's dolphin spatial distribution layers. Risk associated with inshore trawls remained about the same in all three areas. Shifting the period for calculating risk to 2017–18 to 2019–20 resulted in commercial set net risk being about the same in SCSI and this reduced the estimated risk in both NCSI and KAIK. For inshore trawl, the risk was slightly lower in the more recent period in both SCSI and NCSI, and slightly higher in KAIK.

Alternative SEFRA model runs indicated that the approach was reasonably insensitive to the spatial distribution model used. It was concluded that the degree of cryptic mortality and the level of observer coverage are likely to be the greatest sources of residual uncertainty with respect to the estimation of commercial fisheries risk in these areas and could be prioritised by future research.

---

[1] Anemone, New Zealand.
[2] Quantifish Ltd., New Zealand.

1. INTRODUCTION

1.1 Background

Hector's dolphins (*Cephalorhynchus hectori hectori*) and the closely related subspecies Māui dolphin (*Cephalorhynchus hectori maui*), are endemic to the coastal waters of the New Zealand mainland. Hector's dolphins are widespread around the South Island, whereas Māui dolphin are only found off the west coast of the North Island. Historically, inshore commercial fisheries, especially set nets (gill nets), are considered to have impacted on the population status of both subspecies, particularly Māui dolphin and Hector's dolphins off the east coast of the South Island (ECSI) (e.g., Slooten & Dawson 2010, MacKenzie 2022). It is likely that mortalities increased substantially after the mid-1970s following the development and widespread use of polymer gill nets, and that mortality rates have since declined with the sequential implementation of new fishing area restrictions in locations of high abundance (Roberts et al. 2019a).

The design of the most recent fishing area restrictions was informed by a spatial risk assessment model that was developed to inform the 2020 Hector's and Māui dolphin Threat Management Plan (TMP) (Roberts et al. 2019a, Department of Conservation & Fisheries New Zealand 2021). The new restrictions were implemented 1 October 2020 and included increased protection in Golden Bay / Tasman Bay, around Kaikōura Canyon, and off Te Waewae Bay, in addition to other areas (Department of Conservation & Fisheries New Zealand 2021). The assessment by Roberts et al. (2019a) used the spatially explicit fisheries risk assessment (SEFRA) approach (See chapter 3 of Fisheries New Zealand 2022), which uses spatial layers of species density and relates this to spatial fishery effort in order to derive fishery overlap, and ultimately to estimate annual deaths and population risk (detailed in Section 2.4). One of the principal advantages of this approach, which can be considered as a spatial (and typically Bayesian) extension of the Potential Biological Removal (PBR) approach (Wade 1998), is that it can produce spatially disaggregated outputs that can be used for spatial planning.

The spatial distribution layers used by the Roberts et al. (2019a) SEFRA model were produced by a spatial distribution model fitted to sighting-based count data from aerial surveys off the South Island of New Zealand (MacKenzie & Clement 2014, 2016, 2018). The final model included two spatial habitat covariates: surface turbidity, derived from satellite-based ocean colour data (Pinkerton et al. 2018); and the probability of presence of key Hector's and Māui dolphin prey species, derived from research trawl survey catch and effort data (see appendix 5 of Roberts et al. 2019a). From this spatial model, separate 'summer' (1 November to 30 April) and 'winter' (1 May to 31 October) spatial density layers were produced, which were then rescaled using population rescaling strata to account for regional variation in abundance from aerial surveys and other sources that were not explained by the habitat model. The rescaled summer/winter spatial layers were then used by the SEFRA model to derive overlap and estimate annual captures, deaths, and risk.

Roberts et al. (2019a) identified some locations of elevated risk from commercial fisheries (e.g., off the coasts of Kaikōura and Timaru). However, the lack of prey species information at some locations (e.g., off the south coast of the South Island, and regions of the north coast of the South Island) may have impaired the quality of predictions at these locations. Furthermore, three additional years of fishery data were available that could be used to update the SEFRA model.

1.2 Research objectives

This project (Fisheries New Zealand project PMM2020-09) produced updated SEFRA model estimates of deaths and risk of Hector's dolphins at selected local-scale areas around the South Island of New Zealand. SEFRA model inputs that were updated included:

- the summer/winter South Island Hector's dolphin density layers (see Appendix A for plots of the previous layers used for each local-scale area);

- commercial fishery observer-reported catch and effort data; and
- commercial fishery effort data (including observed and unobserved fishing effort).

The overall objective of PMM2020-09 was to:

> *Estimate the spatial density of Hector's dolphins, including seasonal variability, for local populations of particular interest for fisheries management, and evaluate the consequences for estimation of fisheries risk.*

The specific objectives of this project were:

1. *Identify and compile data potentially indicative of Hector's dolphin spatial distributions in up to three local populations or local habitats of particular interest.*
2. *Applying an appropriate spatial modelling statistical method, estimate the spatial density of Hector's dolphins in the local area(s) of interest, including seasonal variation.*
3. *Intersect predicted spatial densities under Objective 2 with fishing effort data to estimate spatial overlap and fisheries risk, including changes over time, in the local population(s) of interest. In consultation with Fisheries New Zealand working groups, test alternate structural assumptions potentially affecting estimation of fisheries risk.*
4. *Using model sensitivities, test the extent to which the spatial distribution(s) from Objective 2 and the estimates of overlap/ risk from Objective 3 are sensitive to alternate plausible model parameterisations.*

This document summarises research under all of these objectives. Note that this document does not report estimates of Hector's dolphin spatial distribution, commercial fishery deaths, or risk outside the three local-scale areas. Also, this assessment did not update the non-fishery inputs used by Roberts et al. (2019a), or report estimates of overlap, deaths, or risk for non-commercial fishery threats.

1.3 Selection of local-scale areas

In consultation with Fisheries New Zealand, the following areas were selected for the local-scale analysis of spatial distribution and commercial fishery risk assessment:

- The **north coast of the South Island** (NCSI), including the Golden Bay / Tasman Bay regions as well as the Marlborough Sounds;
- The **Kaikōura coast** (KAIK), including the region between Cape Campbell in the north and Motunau in the south; and
- The **south coast of the South Island** (SCSI), including the region between Nugget Point in the east to Fiordland in the west.

The NCSI and SCSI areas align with South Island population rescaling strata used by Roberts et al. (2019a), which were used to rescale spatial distribution model predictions for the latest mean estimates of population size in each area (Table 1 and Figure 1a). The KAIK area sits within a larger population rescaling stratum.

Specific place names referenced by this document are located in Figure 1b.

Table 1: Population rescaling strata used to define the local-scale areas of this study and to rescale spatial distribution model predictions for population size in each area. See Roberts et al. (2019a) for the rationale for each population size value. Also, the local-scale areas that were the focus of this study.

Rescaling stratum (label)	Population size (scaling factor)	Local-scale area (label)
West coast North Island (WCNI)	65	–
Taranaki to Kapiti (TAKA)	15 Summer 17 Winter	–
North Island Other (NI)	10	–
East coast South Island (ECSI)	9728	Northern and southern along-shore boundaries of ‘Clarence’ and ‘Kaikōura’ aerial survey strata defined by MacKenzie & Clement (2014) (KAIK).
North coast South Island (NCSI)	214	Entire area (NCSI)
West coast South Island (WCSI)	5482	–
South coast South Island (SCSI)	332	Entire area (SCSI)

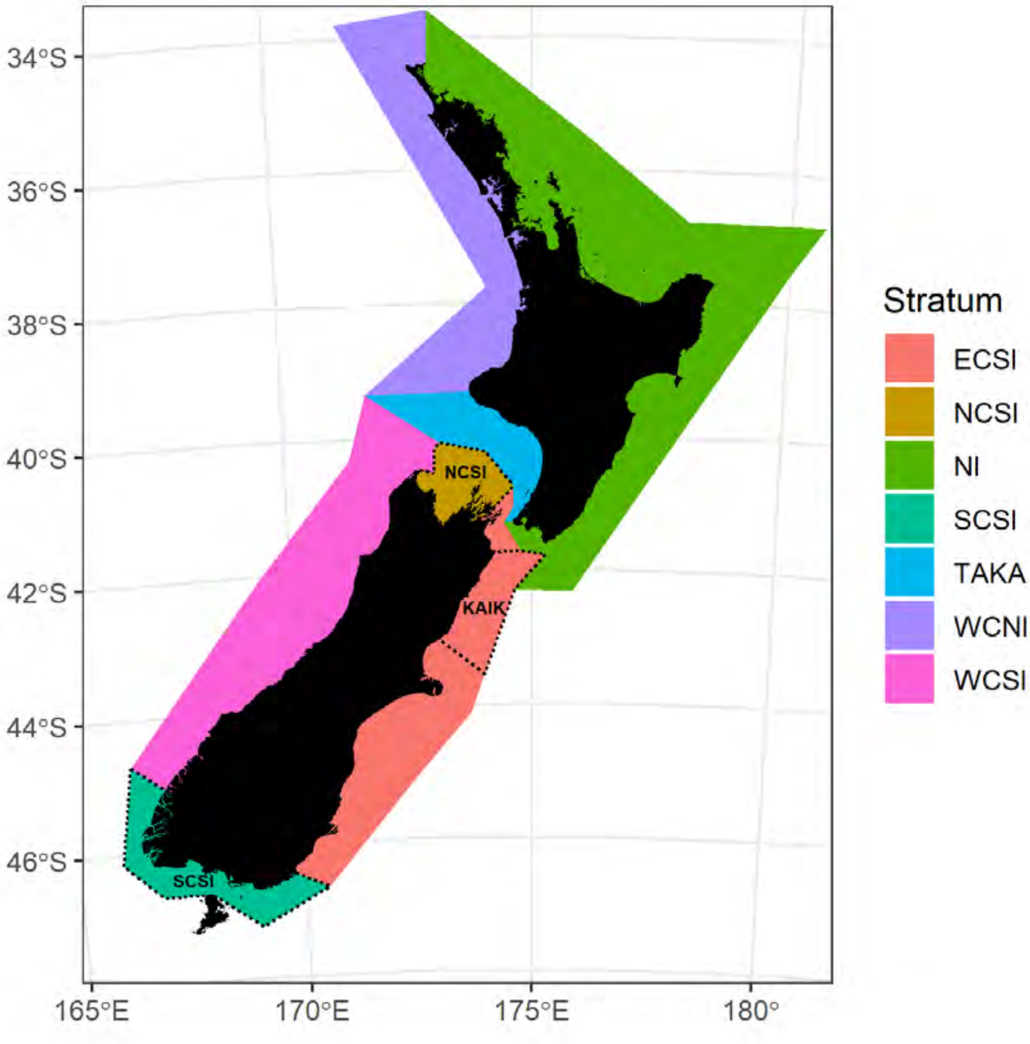

Figure 1a: Population rescaling strata (coloured polygons) and the local-scale areas for which this assessment updated the spatial distribution of Hector’s dolphins and the estimation of fisheries risk (polygons with local area labels and dashed outlines) (see Table 1).

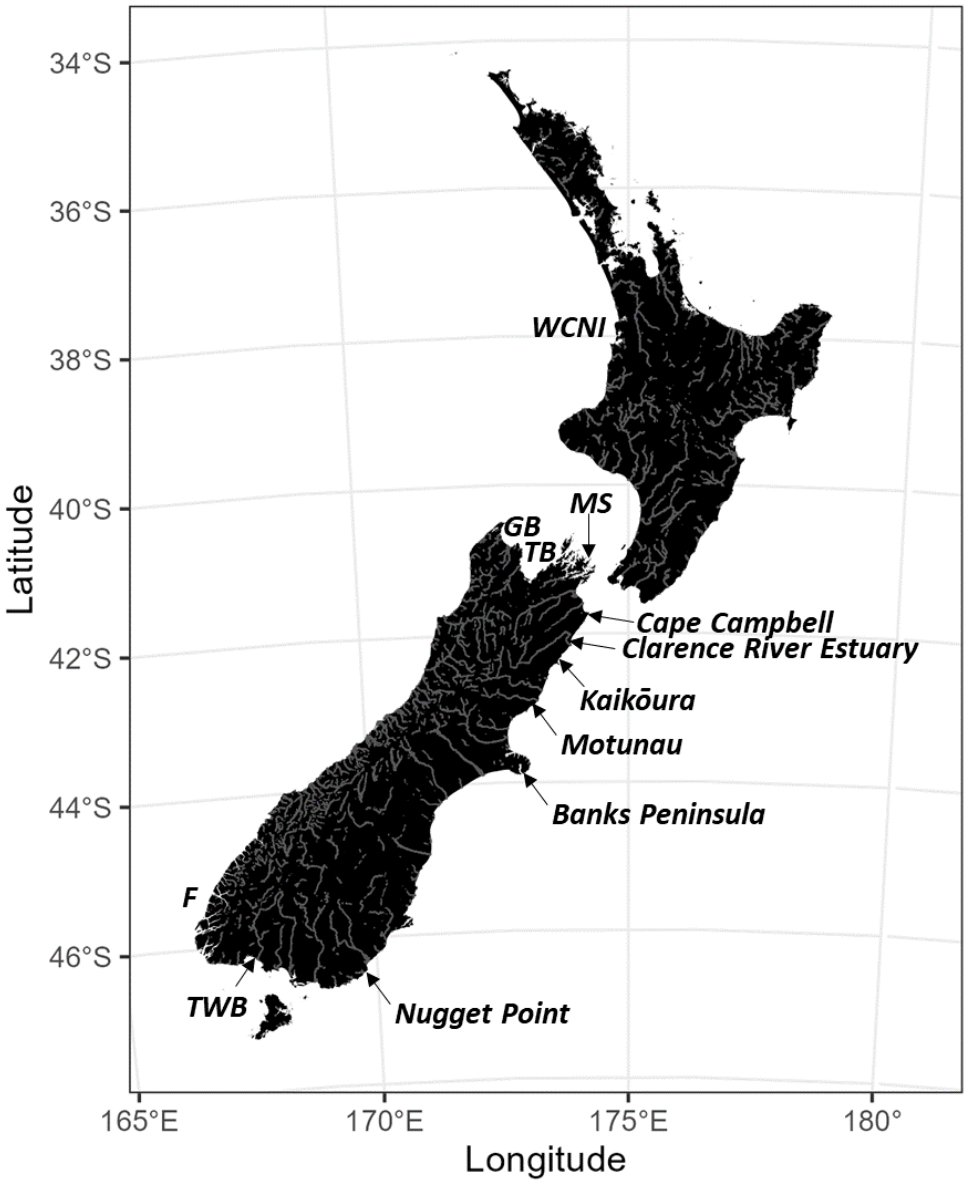

Figure 1b: The locations of place names mentioned in this document. Abbreviated place names include: Fiordland ('F'), Golden Bay ('GB'), Milford Sound ('MS'), Tasman Bay ('TB'), and Te Waewae Bay ('TWB'),

2 METHODS

2.1 Sources of spatial distribution information

Nearly all the spatial information for Hector's dolphins comes from sightings data. Other sources of spatial information include extremely limited tracking data studies from the Banks Peninsula region (Department of Conservation 2005), and acoustic detection data (Banks Peninsula and west coast of the North Island) (e.g., Rayment et al. 2009), i.e., not within the study areas of this project. The available sightings-based data include observations made by formal aerial surveys of distribution and abundance, by fisheries observers on inshore fishing vessels, by boat-based mark-recapture studies, and sightings reported by the public on an *ad hoc* basis.

2.1.1 Aerial survey sightings

Formal government-funded aerial surveys of Hector's dolphin abundance and distribution were completed around the South Island of New Zealand, in summer and winter, from 2010 to 2018 (not inclusive) (e.g., MacKenzie & Clement 2014, 2018). These surveys provide a good along-shore/offshore spatial coverage of sighting effort during the time periods of each respective survey. Unlike the mark-recapture and public sightings data, data on the spatial distribution of sighting effort (i.e., including locations without positive sightings) are readily available for the aerial surveys.

2.1.2 Fisheries observer sightings

Since 2009, government fisheries observers placed on inshore commercial fishing vessels have made marine mammal observation counts during deck-based observation periods, recorded on 'nomad' GPS devices (see Richard et al. 2020). The nomad effort and sightings data were linked and provided by the Department of Conservation (DOC) for the spatial risk assessment of threats the Hector's and Māui dolphins (see Roberts et al. 2019a). These data, which include zero counts, provide Hector's dolphin spatial information in areas overlapping with commercial fishing.

2.1.3 Mark-recapture sightings

Academic researchers have collected and analysed geolocated Hector's dolphin counts done during boat-based mark-recapture (MR) studies (e.g., Bräger 1998, Weir & Sagnol 2015). These studies were not specifically designed for estimating the spatial distribution of Hector's dolphins. One of the primary issues with using these data for spatial distribution modelling is that they often lack robust methods for recording observations at locations where dolphins were not seen (true of Kaikōura coast studies, but not at Te Waewae Bay, SCSI) (Weir & Sagnol 2015, Rodda 2016). Behavioural interactions with the dolphins can also be problematic for spatial distribution modelling using boat-based observations. However, they do provide intensive sampling at certain locations of interest for the purposes of spatial risk modelling.

2.1.4 Public sightings

Public sightings data provide informal spatial information of Hector's dolphin presence around New Zealand. Records of this species are routinely checked for validity off the west coast of the North Island, where Māui dolphin occur, but are not normally vetted around the South Island. They also lack any direct information of spatial sighting effort (zero counts) to accompany the sightings (positive counts). As such these data are the lowest quality of the various sources of spatial data. However, there are good numbers of public sightings in certain low-density regions, where formal surveys rarely encounter dolphins (e.g., the NCSI). Also, indirect approaches for producing relevant spatial sighting effort layers can be explored (see below).

2.2 Processing spatial information

For all data sources, counts were aggregated (where necessary) across age stages, to give a total count of all Hector's dolphins for each sighting event.

2.2.1 Aerial survey

Aerial survey sightings data from government surveys of the ECSI ('aerial_ecsi') and WCSI ('aerial_wcsi') were obtained. For these surveys, the data were converted into summed counts of Hector's dolphins (calves and non-calves) recorded along 1-km survey line segments.

Aerial survey sighting data for the SCSI surveys in 2010 and 2018 were provided by D. MacKenzie on 9 Aug 2021. The methods used by these surveys were described by Clement et al. (2011) and MacKenzie & Clement (2014, 2018). In 2010, two different survey approaches were used:

- a line transect survey, characterised by an onshore-offshore path in regions of high and low density, with two observers on each side of the plane; and
- an effective strip width (ESW) survey, characterised by an along-shore path in regions of high Hector's dolphin density, with observers placed on one side of the plane only.

These data were also converted into summed counts along 1-km line segments. The ESW and line surveys were treated as separate data sources for the purposes of spatial modelling ('aerial_scsi_2010_esw' and 'aerial_scsi_2010_line', respectively), given the differences in survey approach that would be likely to affect relative sighting rate. These were also kept separate from the 2018 survey data ('aerial_scsi_2018').

2.2.2 Fisheries observer sightings and effort

Since 2009, New Zealand government fisheries observers have recorded sightings of marine mammals, made using nomad GPS devices during deck-based observation periods ('nomad'). These sightings data were linked to associated effort data by DOC (up to partway through 2017), and the linked data were provided to the research team undertaking the 2019 TMP risk assessment (these data are mapped in Roberts et al. 2019a).

These data were subsetted to keep only total counts of Hector's dolphins per on-effort sighting event. Typically, observers completed sighting events approximately every 20 minutes. A previous analysis (focussing on seabirds) aggregated these data across longer time periods, partly to reduce the incidence of double counting of the same individuals/groups (Richard et al. 2020). This was not done here, since we deemed that this would be less likely to occur when observing marine mammals.

2.2.3 Boat-based survey sightings

Hector's dolphin sightings data were obtained from boat-based mark-recapture surveys of:

- different regions of the South Island in 1993–1997 (Bräger 1998);
- Te Waewae Bay in 2004–2006 (Rodda 2016); and
- the Kaikōura coast in 2013–2020 (e.g., see Weir & Sagnol 2015).

The 1990s data ('brager') were extracted, with permission, from an appendix in Bräger (1998). Although this survey did not routinely undertake and record negative sighting events, some zeros were recorded where environmental measurements were taken but dolphins were not seen.

The Te Waewae data ('rodda') were provided by J. Rodda on 20 August 2021. These data consisted of on-effort sightings made by monthly surveys in 2004–2006 (including start and end times for each group), and on-effort track locations at 10–30 second intervals along track lines. The positive sightings were linked to the effort data by closest time and date. The linked effort data were then aggregated into 10-minute blocks, summing the total number of dolphins seen across each block. This final step was done to minimise double-counting of the same dolphins while maximising the precision of the effort locations (10-minute blocks were determined to optimise this trade-off).

The Kaikōura coast data were provided by Jody Weir on 8 and 10 September 2021. There was no consistent recording of effort locations by this survey. However, waypoints (with zero Hector's dolphin counts attributed) were more regularly recorded on each trip from 22 December 2014 to 4 April 2015, and from 11 October 2015 to 30 March 2018. Also, sightings of other marine mammal species (with zero Hector's dolphin counts attributed) were regularly recorded on each trip from 13 November 2018 to 7 November 2020. These negative sightings events were combined with the positive events for these respective time periods. Given the differences in the 'effort' data used in the two time periods, these were kept separate (up to 30 March 2018 = 'weir1', and since 13 November 2018 = 'weir2') for the purposes of spatial distribution modelling to allow for the estimation of differential sighting rate given the same underlying density of dolphins.

A boat-based survey of Golden Bay, within the north coast South Island area, has been undertaken by DOC intermittently since 2014. Of the 'non-targeted' survey days (i.e., not responding to a report of a Hector's dolphin sighting by a member of the public) there was just one sighting event, of a pair of Hector's dolphins (Figure C.6). Given the lack of spatial information from this source, these data were not used for the spatial distribution modelling.

2.2.4 Boat-based public sightings and effort

For the north coast of the South Island only, this analysis used boat-based public sightings data of Hector's dolphins ('public'), which was combined with recreational fishing boat locations obtained from aerial surveys of these in 2005 and 2006 (SEC2007-01) (e.g., Hartill et al. 2011).

All public sightings of Hector's dolphin were extracted from the DOC sightings database. The first extract of this database was obtained on 5 April 2021 (Department of Conservation 2021), which was used for model optimisation and prediction. A second extract was obtained 1 May 2022 (Department of Conservation 2022a), which included a large number of sightings along the NCSI and which was used for a model sensitivity run (see later). Sightings of Hector's dolphins are not typically subjected to species-level validation around the South Island, as they are off the North Island. Hence, these data were not filtered by validation status. Public boat-based sightings were defined as those with 'Platform' = 'Charter vessel' or 'Private vessel'.

Recreational fishing boat locations were recycled from those provided to the TMP risk assessment (Roberts et al. 2019a). A subset of boat locations around the north coast of the South Island was then made, and public boats were defined as those with 'type' = 'Charter', 'Launch', 'Trailer', or 'Yacht'.

All boat locations were assigned a zero for the total number of Hector's dolphins seen and were then combined with the positive boat-based sighting counts from public sighting data.

Two alternative public sightings datasets were fitted to: public sightings data up until the end of 2020 (used for model optimisation and some model predictions) and a data extract up until 2022 (used for sensitivity model run predictions). Note that the second dataset also included a larger number of positive sightings in years up until 2020, which were excluded from the first dataset because the full set environmental covariates of spatial distribution were not available for these data. These were included for the second dataset, so long as there were corresponding environmental data for covariates that were in the final model (sea surface turbidity and percentage mud in benthic sediments).

2.2.5 Other public sightings

All other public sightings of Hector's dolphin were extracted from the DOC sightings database, obtained on 5 April 2021 Department of Conservation 2021). However, these were not used for model fitting since no reliable corresponding source of spatial effort data could be identified.

2.3 Spatial models of Hector's dolphin distribution

Predictive models of Hector's dolphin spatial distribution were developed by fitting to the sightings-based spatial data from around the South Island of New Zealand. The optimal model and sensitivity runs were then used to make seasonal (meaning summer and winter) predictions of spatial density within the three local-scale areas specified by Fisheries New Zealand. Models were fitted to observations of dolphin counts per event. Spatial covariates were included in models to help predict dolphin counts in areas with little or no data, and their inclusion was determined by a model optimisation process. For all model fits, a variant of generalised additive models (GAMs) for large datasets (called BAMs) was implemented, using the *R* package *mgcv* (Wood 2017).

2.3.1 Candidate covariates

Several candidate environmental covariates were offered to the spatial models including temporally static variables, temporally dynamic variables (a separate value for each month and year), and quarterly climatologies. These covariates included:

- Bathymetric depth and slope
- Sea surface temperature (SST) and SST gradient
- Sea surface wind speed
- Sea level anomaly
- Sea surface turbidity (two different ocean-colour based proxies)
- Sea surface chlorophyll-a concentration
- Distance to shore
- Composition of benthic sediment type
- Presence of key prey species

All candidate covariates are summarised in Table B.1 and plotted spatially in Figure B.1 to Figure B.10. The respective covariate value was extracted for each covariate at the location and time (year, month, and/or day) of each sighting event.

Data source was included as a non-spatial fixed effect. Year and month of observation were also offered but were generally not found to be influential given the model structures used or were confounded with the data source effect. At least some of the raw data used in each of the study areas (e.g., aerial survey observations) lacked time stamps, precluding the use (across the full dataset) of time-specific variables that could also affect sighting rate, such as time of day and sun altitude.

2.3.2 Model development

Throughout this document, we represent a Gaussian process (GP) spatial smoother as $GP(k)$ or $GP(k|t)$ where k represents the dimension of the basis used to represent the smooth term and t represents a season. A one-dimensional smoother of variable x is represented as $s(x, k)$ and a fixed-effect as x. For example, a model structure may have the form

$$\mu = GP(k = 50) + s(\log(\text{chla}), k = 3) + \text{source}$$

which specifies a model that includes: a GP spatial smoother with an initial basis dimension of 50; a spline of chlorophyll-a in log-space with an initial basis dimension of 3; and data source as a fixed effect. The coordinate reference system (CRS) used for model inputs and outputs was "+proj=aea +lat_0=-40 +lon_0=175 +lat_1=-30 +lat_2=-50 +x_0=0 +y_0=0 +datum=WGS84 +units=m +no_defs" or European Petroleum Survey Group (EPSG) 9191 (Mormede et al. 2022).

Habitat terms were added as univariate splines. The dimension of the basis used to represent univariate smooth terms for each explanatory variable using a starting value ($k = 3$) that would allow non-linear shapes while avoiding overly wiggly relationships.

For all model runs, the negative binomial distribution was assumed, parameterised in terms of its mean μ and variance σ^2

$$p = \frac{\sigma^2 - \mu}{\sigma^2},$$

and

$$r = \frac{\mu^2}{\sigma^2 - \mu},$$

where

$$\Pr(X=k)=\binom{k+\frac{\mu^2}{\sigma^2-\mu}-1}{k}\left(\frac{\sigma^2-\mu}{\sigma^2}\right)^k\left(\frac{\mu}{\sigma^2}\right)^{\mu^2/(\sigma^2-\mu)}.$$

Estimated parameters included the coefficients for each explanatory variable and the variance.

Initially, separate models were fitted to the sightings for each of the three local areas. Two types of modelling approach were trialled:

1. Smooth models, for which 2-dimensional spatial smooths (of easting and northing) were the only spatial model predictors.
2. Habitat models, for which spline smooths of environmental covariates were the only spatial model predictors.

However, this approach resulted in models that produced highly unrealistic predictions, which was attributed to there being insufficient spatial information within each local-scale area (i.e., typically only one or two locations of high density) to produce habitat models with good predictive power. Tellingly, the models for each area contained different combinations of environmental covariates, which was deemed by the researchers to be improbable for the same species.

This finding prompted a revision of the approach for spatial distribution modelling, whereby models were simultaneously fitted to sightings-based observations from off the South Island, and the same optimal models were then used to make predictions across each of the three local-scale areas.

The final model development process was as follows:

1. Data source was treated as a fixed effect and forced as the first model term.

2. Environmental covariates were treated as splines and iteratively added based on the percentage of model deviance explained, stopping when less than 0.2% additional deviance was explained with the addition of any of the remaining candidate environmental covariates (following a modification of the standard approach used in fishery catch-per-unit-effort analyses for Fisheries New Zealand).
3. Model cross-validation procedures were then used to evaluate the relative predictive power of the final and intermediate models developed under step 2 (see below).
4. A 2-dimensional GP spatial smooth (to account for spatial correlation between adjacent observations) was then added if this explained an additional 0.2% of model deviance. This was then allowed to be seasonal (i.e., a separate smooth for summer and winter), if this explained an additional 0.2% of model deviance above the non-seasonal smooth model.
5. Any non-significant environmental covariates were then removed from the model to arrive at the final model structure.

Two alterative model cross-validation procedures were trialled for assessing the predictive power of alterative habitat model formulations. The first was a standard *k*-fold random cross-validation procedure, where the data were divided at random into 10 subsets (i.e., folds), which were iteratively held back from model fitting using the remaining ‘training’ dataset, before validating the model on the remaining ‘test’ data. The second approach was similar to the *k*-fold procedure, except that data source was used as the folds, so that, e.g., in one iteration the model was fitted to all data except public sightings data, then tested using these data only, then in the next iteration another data source was held back and used as the test dataset, etc. For both approaches, the root-mean-square-error (RMSE) of the predicted values versus observed values was used to assess model predictive power.

2.3.3 Model prediction

Summer and winter spatial distributions were generated by predicting the expected count at a 250-m resolution using the optimal fitted model for each species. During the model fitting step, the closest covariate possible was used (e.g., sea surface temperature during the month/year of the observation). However, during the model prediction step, the seasonal average value of each covariate was used (see Appendix B).

The coordinate reference system (CRS) for this raster was "+proj=aea +lat_0=-40 +lon_0=175 +lat_1=-30 +lat_2=-50 +x_0=0 +y_0=0 +datum=WGS84 +units=m +no_defs" or European Petroleum Survey Group (EPSG) 9191 (Mormede et al. 2022) (the standardised grid for New Zealand marine science outputs), i.e., the same as was used for model fitting. Note that spatial predictions did not always fill the entire extent of the predicted raster, because some of the environmental covariate layers do not cover the entire raster extent (e.g., in some of the smaller/narrower harbours).

2.3.4 Rescaling for regional population size

The model predictions were then rescaled using the South Island population rescaling strata, following the approach of Roberts et al. (2019a) (Table 1 and Figure 1a). The purpose of this step was to rescale the spatial model predictions, so that the estimated density of the raster cells in each rescaling stratum summed to the latest mean estimate of the total number of Hector's dolphin in each stratum.

2.4 Spatial risk assessment

2.4.1 Spatial risk model to assess commercial fishery-related deaths

The SEFRA method was used to estimate commercial fishery-related deaths for Hector's/Māui dolphins, which were reported for Hector's dolphins in the three local-scale areas (Figure 1a). The conceptual and mathematical basis of the SEFRA method, including the data inputs and underlying structural assumptions, are described by Sharp (2018) and the latest application of SEFRA to Hector's/Māui dolphins is described by Roberts et al. (2019a).

An extract of the Protected Species Captures (PSC) database was provided by Fisheries New Zealand, on the 31 of January 2022, including:

1. commercial fishing effort data, per fishing event;
2. observed commercial fishing effort data, per fishing event; and
3. fisheries observer-recorded protected species captures, per capture event.

These data, along with seasonal species distribution maps and priors for all model parameters, inform the SEFRA model. All variables used to describe the model can be found in Table 2. Fishing events were either observed (i.e., an observer is on-board the fishing vessel during a fishing event) or unobserved. Hector's dolphin captures recorded by fisheries observers on the observed portion of the fishing effort were used to estimate model parameters by fitting a relationship between observed fishing effort and observed dolphin captures. Observed dolphin captures were recorded as being alive or dead and this is also reflected in the model and subsequently used to estimate the number of deaths, assuming not all animals captured alive and released will die. The combination of observed and unobserved effort, along with the estimated parameters, was used to estimate the total number of commercial fishery related captures, deaths, and risk.

This implementation of the SEFRA method included two commercial fishing methods known to pose a risk to Hector's/Māui dolphins: set netting and inshore trawling. Six different model runs were presented including five new model runs (summarised in Table 3), consisting of a model run using the previous Hector's dolphin spatial distribution layers of Roberts et al. (2019a) **(previous)**, a model run using the spatial distributions predicted by the *hab2_s50_season* model from this assessment (**update**), another that was the same as the **update** model run, except that it specified separate vulnerabilities for fishing events targeting cartilaginous fish (see Table 4) versus non-cartilaginous fish (**vuln**), and two runs that were the same as the **update** model run, except that they used Hector's dolphin spatial distributions predicted using *hab2_s50* (**alt_dist1**) or *hab2_s50_season_ncsi* (**alt_dist2**).

Table 2: Variable symbols, support, and descriptions. Estimated parameters are estimated within the model while random variables are simulated from a prior outside the model (i.e., within the generated quantities block of the *Stan* code).

Symbol	Support	Description
Indices		
i	$i = \{1,2,\dots\}$	A fishing event (e.g., a net is set or a trawl tow begins) that occurs at a time and location
s	$s = \{1,2\}$	Population – Hector's dolphin or Māui dolphin
r	$r = \{1,2,3\}$	Region – Kaikoura (KAIK), north coast of the South Island (NCSI), or south coast of the South Island (SCSI)
g	$g = \{1,2\}$	Commercial fishery group – set net or inshore trawl
c	$c = \{1,2,\dots\}$	A cell in a map
Data		
$\left(C_{sg}^{\text{live}}\right)'$	≥ 0	Number of observed live captures
$\left(C_{sg}^{\text{dead}}\right)'$	≥ 0	Number of observed dead captures
Covariates		
a_{gi}', a_{gi}	≥ 0	Observed fishing intensity and fishing intensity (km of net for set net and number of tows for inshore trawl)
$p_{si}^{\text{S}}, p_{si}^{\text{W}}$	$\in [0,1)$	Relative density during summer and winter
O_{sg}', O_{sg}	≥ 0	Observed overlap and overlap
Estimated parameters		
v_g	≥ 0	Vulnerability
p_g^{obs}	$\in (0,1)$	Probability that an event is observable
ψ_g	$\in (0,1)$	Probability of an individual being alive given that it is caught
N_s	> 0	Population size for each sub-species
Random variables		
$r_s^{\max}$	> 0	Intrinsic population growth rate for each sub-species
ω_g	$\in (0,1)$	Live release survival rate
S_s^{1+}	$\in (0,1)$	Non-calf annual survival rate
Fixed parameters		
ϕ	$\in (0,1)$	Calibration coefficient
Derived quantities		
$C_{sg}^{\text{live}}, C_{sg}^{\text{dead}}$	≥ 0	Live and dead captures
D_{sg}	≥ 0	Deaths
PST_s	≥ 0	Population sustainability threshold
R_{pg}	≥ 0	Risk ratio
k_g	≥ 0	Cryptic mortality rate (the inverse of the probability that a capture event was observable)

Table 3: SEFRA model runs compared by this assessment.

SEFRA model name	Fishing years used to summarise risk	Spatial distribution model label	Posterior distribution
previous	2014–15 to 2016–17	From Roberts et al. (2019a)	From Roberts et al. (2019a)
update	2014–15 to 2016–17	*hab2_s50_season*	New
update	2017–18 to 2019–20	*hab2_s50_season*	New
vuln	2017–18 to 2019–20	*hab2_s50_season*	New
alt_dist1	2017–18 to 2019–20	*hab2_s50*	New
alt_dist2	2017–18 to 2019–20	*hab2_s50_season_ncsi*	New

Table 4: Cartilaginous species.

Target species code	Common name	Scientific name
BSH	Seal shark	*Dalatias licha*
BWH	Bronze whaler shark	*Carcharhinus brachyurus*
EGR	Eagle ray	*Myliobatis tenuicaudatus*
ELE	Elephantfish	*Callorhinchus milii*
GSH	Ghost shark	*Hydrolagus novaezealandiae*
OSD	Sharks & dogfish not otherwise specified in Sch3, Part2 Reporting Regs 2001	Selachii (order)
SCH	School shark	*Galeorhinus galeus*
SHA	Shark (Unspecified)	–
SKA	Skates	Rajidae (family)
SPD	Spiny dogfish	*Squalus acanthias*
SPO	Rig	*Mustelus lenticulatus*
SSK	Smooth skate	*Dipturus innominatus*
STR	Stingray (Unspecified)	–

2.4.2 Estimating model parameters

Spatial distribution layers are a key input for SEFRA models, which may vary throughout the year, reflecting changes in at-sea foraging patterns during the breeding cycle (Fisheries New Zealand 2022). These spatial layers are used to calculate commercial fishery overlap, which is used twice during SEFRA modelling:

1. observed overlap is used during model fitting; and
2. total overlap is used to make inference about seabird/marine mammal captures for all fishing effort.

Observed and total overlap are both functions of fishing effort by different fishing groups (g). A fishing group is a subjective group of similar fishing types (e.g., snapper (*Chrysophrys auratus*) bottom longline fleet, butterfish (*Odax pullus*) set net fleet). Fishing effort for each fishing group during each fishing event (i) is represented as a a_{gi} and takes the units of each fishing group (i.e., kilometre of net for set nets and number of tows for trawl). Some fishing events are observed and represented using the prime symbol (′), thus observed effort is a a'_{gi}. Observed effort can be thought of as a subset of the total effort[3]

$$a'_{gi} \subset a_{gi},$$

which means that a_{gi} contains the observed fishing events a'_{gi} and the unobserved fishing events. For display purposes, fishing effort can be aggregated within raster cells (c)

$$a_{gc} = \sum_{i \in c} a_{gi} \quad \text{and} \quad a'_{gi} = \sum_{i \in c} a'_{gi},$$

where $i \in c$ denotes that fishing event i occurred in cell c.

Species distribution layers (rasters) are represented as p_{sc} for each species (s) and cell (c). Each species distribution is rescaled to have the property

$$\sum_{c} p_{sc} x_{sc} = 1 \quad \forall s,$$

where x_{sc} is the area in square kilometres of each cell (note that the area of each cell is not necessarily the same and may depend on the type of spatial projection being used). If N_s is the total population size for species s, then the abundance in each cell is defined as

$$y_{sc} = p_{sc} x_{sc} N_s \quad \text{where} \quad \sum_{c} y_{sc} = N_s,$$

and the density (mean number of individuals per square kilometre) in each cell is

$$z_{sc} = \frac{p_{sc} x_{sc} N_s}{x_{sc}} = p_{sc} N_s.$$

Using species distribution layers, the species distribution for each species (s) at the location of each fishing event (i), where fishing event i occurs in cell c (i.e., $i \in c$), is extracted and denoted p_{si} (i.e., p_{si} is derived from p_{sc}).

Two commercial fishery groups (g) were included in this model: set net and inshore trawl. Fishing effort is summarised per fishing event (i.e., not aggregated within cells); every fishing event (i) has an associated fishing intensity (a_{gi}) measured in kilometres of net length for set net and number of trawl tows for inshore trawl.

Māui dolphin are a closely related sub-species of Hector's dolphin (Pichler 2001). As such, several key model parameters are assumed to be the same and were estimated across the whole species. Parameters estimated (at the species level) in this way include vulnerability (i.e., probability of capture or death) in each commercial fisheries group (v_g), the probability that an event is observable (given that an observer is on watch) for each fisheries group (p_g^{obs}), the probability of an individual being alive (given that it is captured) for each fisheries group (ψ_g), and the live-release survival rate for each fisheries group (ω_g). Population size estimates (N_s) for each sub-species (s) were specified as priors in the model.

[3] Note that for a small number of 1-km grid cells, the aggregated fishing intensity for observed fishing events exceeded that of the total (observed and unobserved) fishing intensity. The reasons for this discrepancy in the input data were not identified or accounted for by this assessment

Vulnerability, the probability that an event is observable, the probability of an individual being alive given that it is captured, and the live release survival rate are all parameters that need to be estimated.

Fisheries observer data (protected species captures on observed fishing events) are used to estimate model parameters. Observed overlap is calculated for each sub-species (s) and commercial fisheries group (g) using data from 1995–96 to 2019–20

$$O'_{sg} = \begin{cases} \sum_i a'_{gi} p^{\text{S}}_{si} & i \in \text{summer} \\ \sum_i a'_{gi} p^{\text{W}}_{si} & i \in \text{winter} \end{cases}.$$

The probability of an individual being alive given that it is captured (ψ_g) is then used to calculate the expected number of observed alive ($\lambda^{\text{live}}_{sg}$) and dead ($\lambda^{\text{dead}}_{sg}$) captures

$$\lambda^{\text{live}}_{sg} = O'_{sg} N_s v_g p^{\text{obs}}_g \psi_g$$
$$\lambda^{\text{dead}}_{sg} = O'_{sg} N_s v_g p^{\text{obs}}_g (1 - \psi_g).$$

Using the posterior distribution for the model parameters $N_s v_g p^{\text{obs}}_g$, maps are generated to display the number of predicted observed captures (alive and dead)

$$C'_{sgc} = \sum_{i \in c} O'_{sgi} \times \mathbb{E}(N_s v_g p^{\text{obs}}_g),$$

where $i \in c$ means that fishing event i is in cell c and $\mathbb{E}(\cdot)$ is the expected value (or mean) of the product of the posterior samples. Note however that because fishing effort and fisheries observer data are utilised at the level of individual fishing events, cell size has no effect on model outcomes; and maps of captures and risk can be re-generated at any user-defined cell size.

Throughout this document reference is made to cryptic mortality rate which is defined as

$$k_g = \frac{1}{p^{\text{obs}}_g}.$$

All variables used throughout this report are provided in Table 2.

2.4.3 Bayesian inference

Priors relate to estimated model parameters. Random variables are simulated (in the generated quantities block in the *Stan* code) and are therefore not updated by data. The prior for the Hector's dolphin population size ($N_{s=\text{HDO}}$) is derived from Mackenzie & Clement (2016) who estimated a mean of 14 849 individuals by averaging the summer and winter abundance estimates for each of the ECSI, SCSI, and WCSI then summing these to get the total abundance estimate for the South Island. They provided a CV of 11% which was translated into a standard deviation for a lognormal distribution using

$$\sigma = \sqrt{\log(CV^2 + 1)} = 0.110.$$

Thus, the prior used was

$$N_{s=\text{HDO}} \sim \text{lognormal}(\log(14849), 0.110^2).$$

The prior for Māui dolphin population size ($N_{s=\text{HDM}}$) is derived from Baker et al. (2016) who estimated a mean of 63 and a CV of 11% also. Thus, the prior used was

$$N_{s=\text{HDM}} \sim \text{lognormal}(\log(63), 0.110^2).$$

Uninformative but non-uniform vulnerability priors were specified in log-space to help with Markov chain Monte Carlo (MCMC) mixing

$$\log(v_g) \sim \text{normal}(0, 10^2).$$

The prior for the probability that an event was observable was obtained from a review of the information relating to dolphin and porpoise species interactions with fishing gear (see Appendix 10 of Roberts et al. 2019a). Informed priors were assumed for set net captures

$$p^{\text{obs}}_{g=Set\ net} \sim \text{beta}(6.916, 6.916),$$

consistent with a 95% credible interval (CI) of 0.25 and 0.75; and for inshore trawl captures

$$p^{\text{obs}}_{g=Trawl} \sim \text{uniform}(0.5, 1.0).$$

A vaguely informative prior is used for the probability of an individual being alive given that it is caught in commercial fishery group (g)

$$\psi_g \sim \text{beta}(1, 3).$$

The live-release survival rate random variable was also obtained from a review of information across dolphin and porpoise species by Roberts et al. (2019a) and was simulated from

$$\omega_g \sim \text{uniform}(0.5, 0.9).$$

Beta priors were derived for adult survival (survival of individuals equal to or greater than one year old represented by 1+). For Hector's dolphin, a beta prior was specified (Roberts et al. 2019a)

$$S^{1+}_{s=\text{HDO}} \sim \text{beta}(164.0, 14.3).$$

For Māui dolphin, a beta distribution was fitted to the posterior samples based on demographic assessment fitted to genetic mark-recapture observations (Roberts et al. 2019b)

$$S^{1+}_{s=\text{HDM}} \sim \text{beta}(720.2, 86.4).$$

Priors for the intrinsic population growth rate (r^{max}_s) random variable were developed by fitting normal distributions to posterior samples produced by the analysis of Edwards et al. (2018), updated by Roberts et al. (2019a). The prior for Hector's dolphin is simulated from

$$r^{\text{max}}_{s=\text{HDO}} \sim \text{normal}(0.050, 0.011^2).$$

A summary of all priors and random variables is provided in Table 5.

A Poisson distribution was assumed for the observable alive and dead captures

$$\left(C^{\text{live}}_{sg}\right)' \sim \text{Poisson}\left(\lambda^{\text{live}}_{sg}\right)$$
$$\left(C^{\text{dead}}_{sg}\right)' \sim \text{Poisson}\left(\lambda^{\text{dead}}_{sg}\right),$$

noting that the Poisson distribution assumes the same mean and variance. Bayesian inference was done using *Stan* making use of its Hamiltonian Monte Carlo (HMC) algorithm (Stan Development Team 2016).

Table 5: Table of priors for each of the model parameters and simulated random variables.

Parameter	Symbol	Subscript	Prior type	Prior parameters	
Vulnerability	$\log(v_g)$	$\forall g$	normal	$\mu = 0$	$\sigma = 100$
Probability capture event is observable	p_g^{obs}	$g =$ Set net	beta	$\alpha = 6.916$	$\beta = 6.916$
		$g =$ Trawl	uniform	$a = 0.5$	$b = 1$
Probability an individual is alive when captured	ψ_g	$\forall g$	beta	$\alpha = 1$	$\beta = 3$
Total population size	N_s	$s =$ HDO	lognormal	$\mu = 8968$	$\sigma = 0.149$
		$s =$ HDM	lognormal	$\mu = 63$	$\sigma = 0.110$
Live-release survival probability	ω_g	$\forall g$	uniform	$a = 0.5$	$b = 0.9$
Non-calf annual survival	S_s^{1+}	$s =$ HDO	beta	$\alpha = 164.0$	$\beta = 14.3$
		$s =$ HDM	beta	$\alpha = 720.2$	$\beta = 86.4$
Intrinsic population growth rate	$r_s^{\max}$	$s =$ HDO	lognormal	$\mu = 0.050$	$\sigma = 0.011$

2.4.4 Model predictions

Model predictions were done using both observed and unobserved fishing events (a_{gi}). Mean annual overlap (observed and unobserved fishing events) is calculated by commercial fishery group (g) for both sub-species (s). To approximate 'current' patterns and intensity of fishing effort, the most recent three years of data were used (2017–18 to 2019–20), and the average annual overlap across these three years was estimated using

$$O_{sg} = \begin{cases} \frac{1}{n}\sum_i a_{gi} p_{si}^{S} & i \in \text{summer} \\ \frac{1}{n}\sum_i a_{gi} p_{si}^{W} & i \in \text{winter} \end{cases},$$

where n is the number of years that we are averaging across ($n = 3$).

A live-release survival rate parameter (ω_g) was used to calculate the number of deaths

$$D_{sg} = O_{sg} N_s v_g \left(1 - \psi_g \omega_g\right).$$

A mortality constraint (whereby total deaths are not allowed to exceed one minus the annual non-calf survival rate), as described by Sharp (2018) was not required because the number of deaths never approached $(1 - S_s^{1+})N_s$. However, this constraint was monitored to ensure it was not breached during any of the MCMC iterations.

The population sustainability threshold (PST) was calculated for each sub-species and region as

$$PST_{sr} = \frac{1}{2}\phi r_s^{\max} N_{sr},$$

where ϕ is a calibration coefficient set to the value of $\phi = 0.2$ specified by Fisheries New Zealand. This value of ϕ is consistent with population recovery to at least 90% of carrying capacity when assuming logistic population growth (Darryl Mackenzie unpublished data). The regional population size for each species (N_{sr}) is derived by summing the seasonal species distribution layer within each region and applying this fraction to the total population size (N_s).

The risk ratio for each species, fishing group, and region (R_{sgr}) was calculated as

$$R_{sgr} = \frac{D_{sgr}}{PST_{sr}},$$

where a risk ratio > 1 is consistent with annual deaths exceeding the PST for the population within each respective local-scale area.

3 RESULTS

3.1 Spatial distribution modelling

3.1.1 Summary of spatial information

The final data sources used for spatial modelling included:

- summer/winter aerial surveys of the ECSI in 2013 (‘aerial_ecsi’), the WCSI in 2015 (‘aerial_wcsi’), and the SCSI in 2010 (‘aerial_scsi_2010_line’ and ‘aerial_scsi_2010_esw’) and 2018 (‘aerial_scsi_2018’);
- Boat-based mark-recapture studies along the Kaikōura coast (‘weir1’ and ‘weir2’), at Te Waewae Bay on the SCSI (‘rodda’), and at multiple sites around New Zealand (‘brager’);
- Fisheries observer sightings data (‘nomad’); and
- Boat-based public sightings data (‘public’).

The temporal distribution of sighting events is summarised by data source in Table C.1 of Appendix C, and plotted spatially in Figure C.1 to Figure C.11 of Appendix C, including:

- presence/absence plots of all data from around the South Island (Figure C.1 and Figure C.2);
- presence/absence plots of data within local-scale areas (Figure C.3, Figure C.7, Figure C.9, and Figure C.10); and
- plots of mean count by 10 km grid cell within local-scale areas (Figure C.4, Figure C.5, Figure C.8, and Figure C.11).

In addition, the data from a boat-based survey of Golden Bay by DOC are shown in Figure C.6, although these data were not used in spatial modelling due to the sparsity of positive sighting events (a solitary on-effort sighting of a pair of Hector’s dolphins) (M. Ogle, unpublished data).

While all data sources were used for model fitting, the primary sources of spatial information varied by local-scale area:

- For the north coast of the South Island, boat-based public sightings data and the 2013 aerial survey of the east coast South Island were most informative (Figure C.3);
- For the Kaikōura coast, a number of sources were informative including multiple boat-based mark recapture studies (from 1993 to 2020), as well as the government aerial survey of the east coast South Island in 2013, and fisheries observer sightings data (Figure C.7);
- For the south coast of the South Island, the primary sources of spatial information were summer/winter government aerial surveys in 2010 and the summer of 2018, fisheries observer sightings data, and boat-based mark-recapture studies (Figure C.9 and Figure C.10).

The gridded mean count plots give an indication of locations of high and low sighting rate density, including the Golden Bay region of the NCSI (Figure C.4 and Figure C.5), the coastline to the north of Kaikōura (Figure C.8), and Te Waewae Bay (Figure C.11).

3.1.2 Model development

In the first stage of model development, splined environmental terms were iteratively added to the initial model (including only data source; lacking a spatial smooth) until the addition of any remaining term explained less than an additional 0.2% model deviance. Table 6 gives a comparison of the initial and terminal habitat models that resulted from this process. The terminal model (*hab10*) had ten environmental terms and was also the best model in terms of AIC (Akaike 1974). The model term plots for *hab10* are shown in Figure D.1. Based on this plot, this model is consistent with greater Hector's dolphin sighting rates in locations of relatively high sea surface turbidity and temperature, high prey species density, muddy and sandy benthic sediments, low SST gradient, over shallow seafloor, and regions of intermediate sea level anomaly.

However, *hab10* was identified as the poorest performing model by both model cross-validation variants, indicating that it had the worst predictive power of any of the model structures (see the two right-hand columns of Table 6). The models with lowest RMSE (best predictive power) varied by model cross-validation procedure. The *k*-fold method indicated that models with 1–9 environmental terms were approximately equally good, whereas models with only 1–3 model terms were optimal when data source was used to identify test and training datasets.

When RMSE was disaggregated by data source, this revealed that the optimal model was different based on the spatial information from each data source (Figure 2 and Figure 3). The trends in RMSE with increasing model structure complexity (i.e., from *hab0* to *hab10*, inclusive) (see Table 6 and the top left-hand plots of Figure 2 and Figure 3) differ from those for individual data sources (all other plots of Figure 2 and Figure 3).

It was clear that the best models, in terms of percentage deviance explained and model AIC, were the worst performing in terms of predictive power. With respect to model cross-validation approach, the data source method was deemed preferrable to the *k*-fold approach. In addition to testing models against data obtained from different source (i.e., different methods with different sighting rates and potential biases), because different data types were collected from different regions, using data source to identify test and training data sets will also have tested the power of the different models to predict in new spatial domains not used for model fitting. This was deemed a more stringent test of predictive power than the *k*-fold method, which will not naturally test models in new spatial domains. Therefore, data source-based model cross validation was used to inform final model selection.

The *hab3* was selected as the final habitat model structure, based on a trade-off between model predictive power using the data source method of model cross validation and the percentage of model deviance explained (Table 6). This model included data source as well as splined sea surface turbidity, presence of *Peltorhamphus* spp. flatfish, and percentage mud in benthic sediments.

Table 6: Comparison of different habitat model structures. Smoothed environmental terms are shown in the order in which they were selected; ‘turbidity1’ = summer/winter sea surface turbidity, ‘pelt’ = presence of *Peltorhamphus* spp. (flounder sp.), ‘mud’ = percentage of mud in benthic sediments, ‘rcod’ = presence of red cod (*Pseudophycis bachus*), ‘sst’ = mean sea surface temperature, ‘sand’ = percentage of sand in benthic sediments, ‘sprat’ =percentage of *Sprattus* spp. (sprat sp.), ‘sst_grad’ = mean sea surface temperature gradient, ‘depth’ = bathymetric depth, ‘wind’ = mean wind speed. Colours indicate the optimal model structure based on different means of comparison (blue = best model, red = worst model). The final habitat model structure carried forward for subsequent model development is in bold. ‘*N*’ = the number of dolphins observed.

				Model cross validation (RMSE)	
Model label	Model structure	% deviance explained	AIC	*k*-fold	By data source
hab0	*N* ~ *source*	34.5	51 487	2.34	2.39
hab1	*N* ~ *source* + s(sqrt(*turbidity1*))	48.1	48 830	2.27	2.29
hab2	*N* ~ *source* + s(sqrt(*turbidity1*)) + s(*pelt*)	50.9	48 187	2.24	2.32
hab3	***N* ~ *source* + s(sqrt(*turbidity1*)) + s(*pelt*) + s(*mud*)**	**51.9**	**47 955**	**2.24**	**2.33**
hab4	*N* ~ *source* + s(sqrt(*turbidity1*)) + s(*pelt*) + s(*mud*) + s(*rcod*)	52.7	47 760	2.30	2.62
hab5	*N* ~ *source* + s(sqrt(*turbidity1*)) + s(*pelt*) + s(*mud*) + s(*rcod*) + s(*sst*)	53.6	47 548	2.24	2.46
hab6	*N* ~ *source* + s(sqrt(*turbidity1*)) + s(*pelt*) + s(*mud*) + s(*rcod*) + s(*sst*) + s(*sand*)	54.2	47 391	2.25	2.59
hab7	*N* ~ *source* + s(sqrt(*turbidity1*)) + s(*pelt*) + s(*mud*) + s(*rcod*) + s(*sst*) + s(*sand*) + s(*sprat*)	54.6	47 302	2.24	2.73
hab8	*N* ~ *source* + s(sqrt(*turbidity1*)) + s(*pelt*) + s(*mud*) + s(*rcod*) + s(*sst*) + s(*sand*) + s(*sprat*) + s(*sst_grad*)	54.9	47 230	2.25	2.53
hab9	*N* ~ *source* + s(sqrt(*turbidity1*)) + s(*pelt*) + s(*mud*) + s(*rcod*) + s(*sst*) + s(*sand*) + s(*sprat*) + s(*sst_grad*) + s(sqrt(*depth*))	55.2	47 164	2.27	2.54
hab10	*N* ~ *source* + s(sqrt(*turbidity1*)) + s(*pelt*) + s(*mud*) + s(*rcod*) + s(*sst*) + s(*sand*) + s(*sprat*) + s(*sst_grad*) + s(sqrt(*depth*)) + s(*wind*)	55.4	47 108	2.53	2.73

Non-seasonal (temporally static) spatial smooths (of northing and easting) were added to model *hab3*, trialling alternative levels of spatial complexity, from the least complex (basis dimension value $k = 20$) to the most complex ($k = 60$) (see Table 7). The same 0.2% threshold value of percentage deviance explained was used to identify the optimal k-value, which was determined to be $k = 50$. So, model *hab3_s50* was carried forward to the next stage of model development.

Specifying a seasonal smooth ($k = 50$ for both the summer and winter periods) also resulted in a greater than 0.2% improvement in deviance explained (Table 7) and, so, model *hab3_s50_season* was carried forward to the next stage of model development.

On closer examination of *hab3_s50_season,* the splined term for the probability of presence of *Peltorhamphus* spp. flatfish (‘s(*pelt*)’) was found to offer no improvement in terms of % deviance explained (Table 7). This will have been a consequence of the introduction of the complex seasonal spatial smooth, which appears to have been sufficient to explain the spatial variability in sighting rate that the prey species term explained in model *hab3*. Hence the prey term was removed from the final model, resulting in *hab2_s50_season*, which comprised a seasonal spatial smooth, as well as splined sea surface turbidity and percentage mud in the benthic sediments. This model was used as the base case model for making predictions of the spatial distribution of Hector’s dolphins.

Table 7: Comparison of different spatial smooth configurations used in spatial distribution models. The final model structure carried forward to the next model development step is bolded. ‘*N*’ = the number of dolphins observed.

Model label	Model structure	% deviance explained	AIC
hab3	***N* ~ *source* + s(sqrt(*turbidity1*)) + s(*pelt*) + s(*mud*)**	**51.9**	**47 955**
hab3_s20	*N* ~ *source* + s(sqrt(*turbidity1*)) + s(*pelt*) + s(*mud*) + s(easting, northing, *k* = 20)	56.0	46 938
hab3_s30	*N* ~ *source* + s(sqrt(*turbidity1*)) + s(*pelt*) + s(*mud*) + s(easting, northing, *k* = 30)	57.8	46 490
hab3_s40	*N* ~ *source* + s(sqrt(*turbidity1*)) + s(*pelt*) + s(*mud*) + s(easting, northing, *k* = 40)	58.2	46 382
hab3_s50	***N* ~ *source* + s(sqrt(*turbidity1*)) + s(*pelt*) + s(*mud*) + s(easting, northing, *k* = 50)**	**58.8**	**46 238**
hab3_s60	*N* ~ *source* + s(sqrt(*turbidity1*)) + s(*pelt*) + s(*mud*) + s(easting, northing, *k* = 60)	58.9	46 208
hab3_s50_season	***N* ~ *source* + s(sqrt(*turbidity1*)) + s(*pelt*) + s(*mud*) + s(easting, northing, *k* = 50, by = season)**	**60.1**	**45 919**
hab2_s50_season	***N* ~ *source* + s(sqrt(*turbidity1*)) + s(*mud*) + s(easting, northing, *k* = 50, by = season)**	**60.1**	**45 919**

Model diagnostic plots are shown for model *hab2_s50_season* in Appendix D. The quantile-quantile plot for this model was not ideal (Figure D.2). However, there were no obvious spatial patterns in the residuals when viewed across the South Island area of model fitting (Figure D.3), or when viewed for each of the three local-scale areas (Figure D.4, Figure D.5 and Figure D.6).

Term plots for model *hab2_s50_season* are shown in Figure D.7. Based on this model, the sighting rate of Hector’s dolphins was estimated to be greatest in regions of elevated sea surface turbidity and at low to intermediate levels of mud in benthic sediments (peaking at around 40% mud). The aerial surveys were estimated to have lower sighting rate than the other sources of spatial information, noting that the effort layers were obtained by indirect means for many of the non-aerial survey data sources.

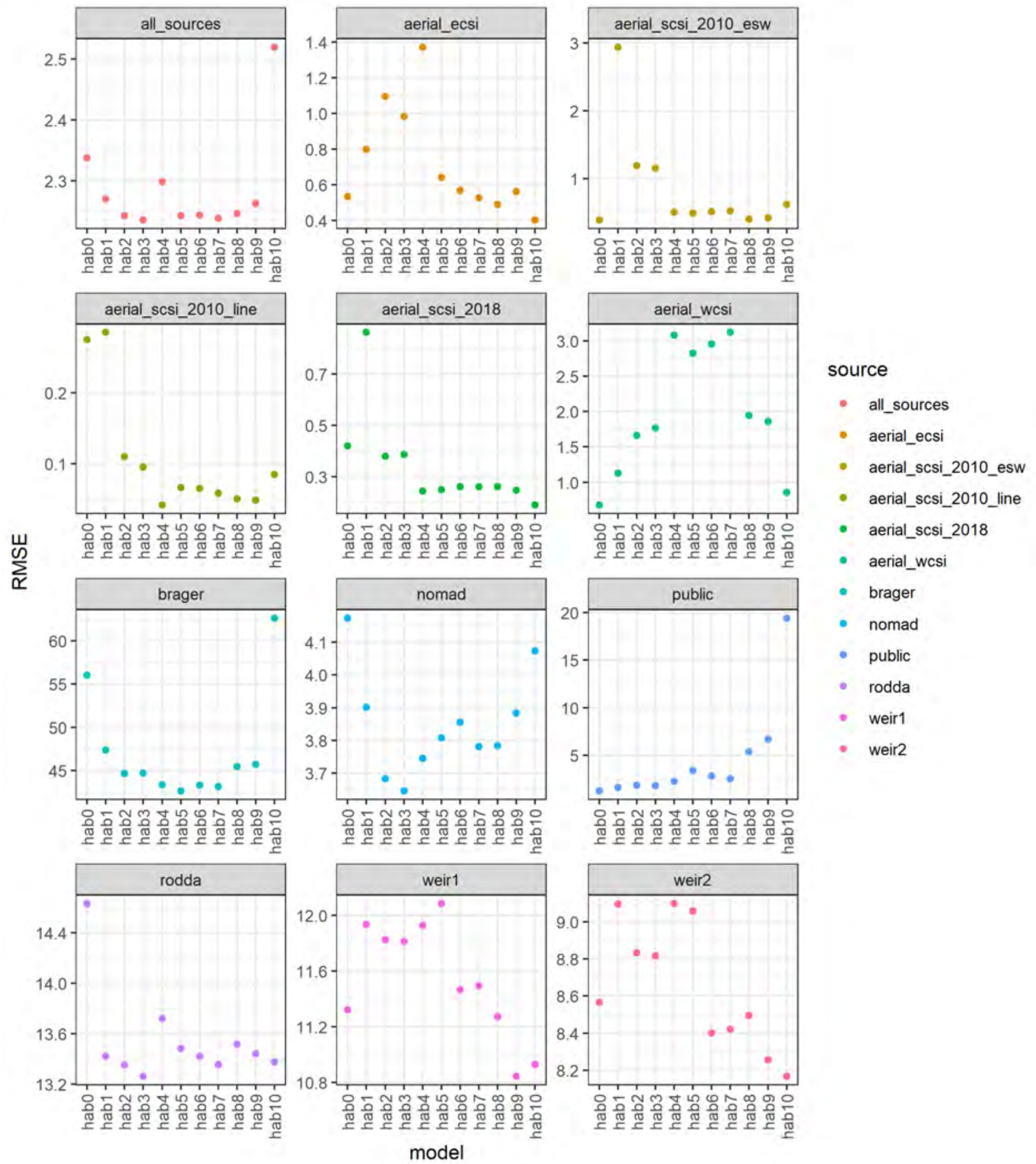

Figure 2: Comparison of habitat model structures by model cross validation using a random *k*-fold approach to define training and test datasets. The number in the model label denotes the number of environmental terms in each model. 'RMSE' = root-mean-square-error, here disaggregated by data source, where higher values indicate that a model has worse predictive power of the training dataset.

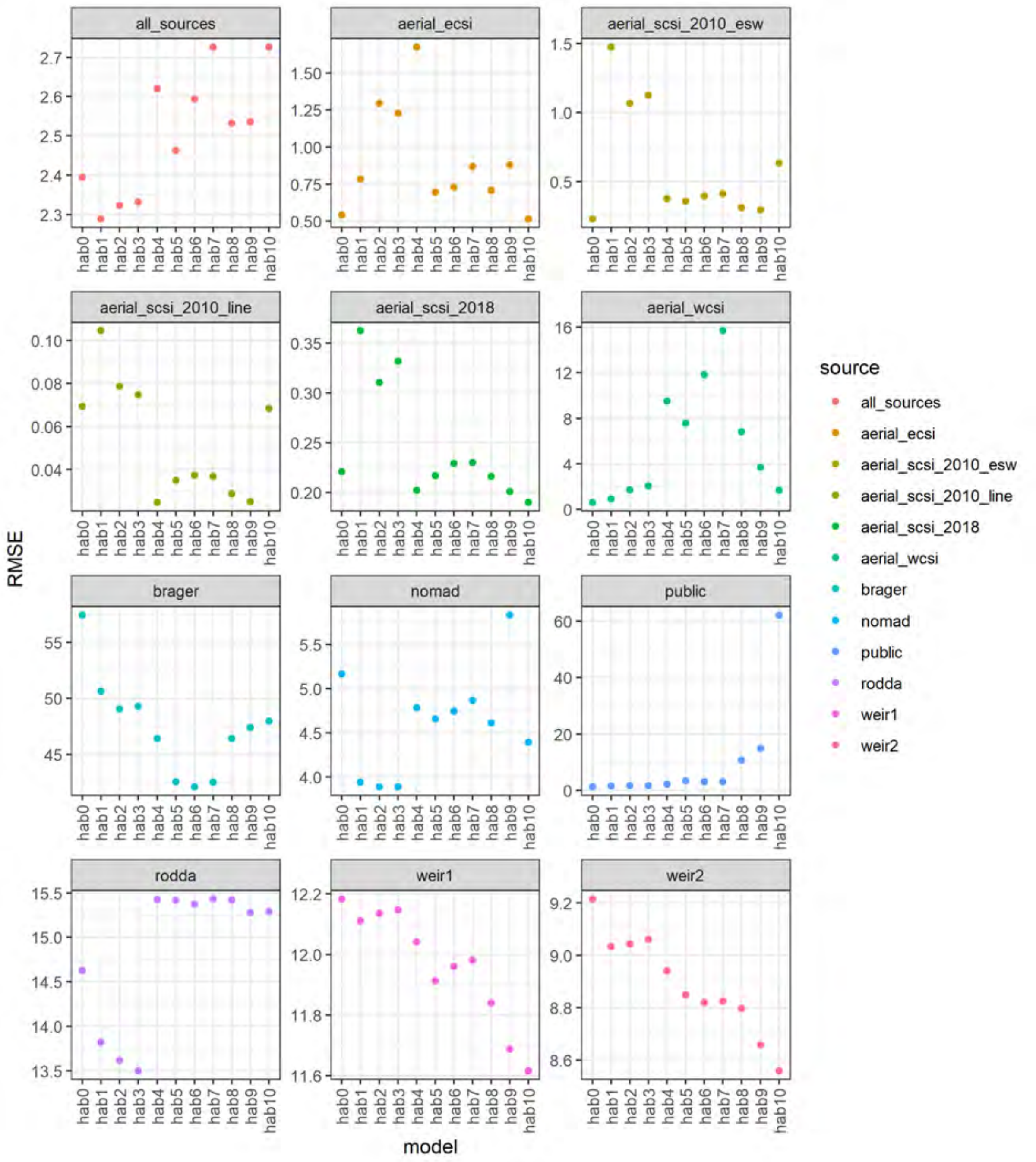

Figure 3: Comparison of habitat model structures by model cross validation <u>using data source</u> to define training and test datasets. The number in the model label denotes the number of environmental terms in each model. 'RMSE' = root-mean-square-error, here disaggregated by data source, where higher values indicate that a model has worse predictive power of the training dataset.

In addition to the base model (*hab2_s50_season*), spatial predictions were made using two sensitivity model runs:

- A version of *hab2_s50_season* with a non-seasonal surface smooth (*hab2_s50*).
- A rerun of *hab2_s50_season* fitted to the same data plus additional public sightings data when using the 2022 extract of the DOC public sightings database (*hab2_s50_season_ncsi*).

The spatial predictions of summer and winter Hector's dolphin distribution for each model are shown in Appendix E and can be compared with the predictions used by Roberts et al. (2019a) in Appendix A.

With respect to the NCSI, all models predicted greatest sighting density in western part of Golden Bay (e.g., Figure E.1 and Figure E.2). For the base model run (*hab2_s50_season*), dolphins were predicted to occur in the southern part of Tasman Bay in the winter period only, located near to the shore (Figure E.2). The spatial predictions from model *hab2_s50_season_ncsi* were similar to those of the base model run (e.g., compare Figure E.1 and Figure E.13).

Along the Kaikōura coast region, the greatest predicted sighting density was in the coastal region around and to the north of the Clarence River estuary, to the north of Kaikōura (Figure E.3 and Figure E.4). By comparison, the predicted density around Kaikōura itself was moderate, despite the very large number of sightings there (Figure C.7). This is because the relative sighting effort here was also very high (Figure C.7). This spatial pattern is consistent with sighting rates from the raw data (Figure C.8). There was minimal evidence for much seasonal variation in distribution within this stretch of coast (compare Figure E.3 and Figure E.4).

The predicted spatial distribution of sighting rate was more seasonal along the SCSI (compare Figure E.5 and Figure E.6). The greatest predicted density was in Te Waewae Bay in both seasons. However, this was less so in the winter period, with moderate density also predicted in other bays along the SCSI (Figure E.6).

The 2022 update to the public sightings data had only a minimal effect on the predicted sighting density of Hector's dolphins along the north coast of the South Island (e.g., compare Figure E.1 and Figure E.13).

3.2 Spatial risk assessment

3.2.1 Model inputs

The proportion of Hector's dolphin estimated to be within each local-scale area was derived from the spatial distribution layers (Table 8). These proportions were used to calculate the population size within each local-scale area, which was then used to derive the PST within each local-scale area for each of the different spatial distribution layers tested. Note that the proportions within the Kaikōura coast (KAIK) local-scale area can vary by season, particularly when predicting from spatial distribution models using a seasonal smooth (*hab2_s50_season* and *hab2_s50_season_ncsi*) (Table 8). This is because the KAIK area only comprises part of the ECSI population rescaling stratum (Figure 1a) and, therefore, the proportion of the assumed ECSI population of Hector's dolphins (Table 1) that is within the KAIK local-scale area can vary, depending on which spatial distribution model was used. For all other local-scale areas, the population size is constant across all runs, because they exactly correspond with population rescaling strata (Figure 1a). The SEFRA model posteriors of population size within each local-scale area are shown in Figure G.1 for each season.

Note that since the relative population of Hector's dolphins within KAIK can vary by model run and season, this can affect the estimated number of commercial fishery deaths within this area (since this will affect the degree of overlap). However, this will have a lesser effect on risk since the respective PST will also vary with population size.

All Hector's dolphin captures recorded by fisheries observers and fitted to by the SEFRA model are summarised in Table 9 and Table 10 and plotted spatially in Figure 4. Of these, a total of 16 Hector's dolphin captures were recorded during commercial set net operations, and 1 was captured by the inshore trawl fishery. All except one of the observed captures were in the summer period (1 October to 31 April), and all except for one of the set net captures were captured by fishing events recorded as targeting cartilaginous species. Four of the observed captures were within the KAIK local-scale area (Table 9) and were located to the south of Kaikōura town (Figure 1b and Figure 4).

Table 8: Proportion of Hector's dolphins estimated to be within each region, by season.

Distribution model	Local-scale area	Proportion of total Hector's dolphin density	
		Summer	Winter
Previous (Roberts et al. 2019a)	KAIK	0.0511	0.0525
	NCSI	0.0136	0.0136
	SCSI	0.0210	0.0210
hab2_s50_season	KAIK	0.0716	0.0458
	NCSI	0.0136	0.0136
	SCSI	0.0210	0.0210
hab2_s50	KAIK	0.0534	0.0565
	NCSI	0.0136	0.0136
	SCSI	0.0210	0.0210
hab2_s50_season_ncsi	KAIK	0.0872	0.0487
	NCSI	0.0136	0.0136
	SCSI	0.0210	0.0210

Table 9: Fisheries observer data fitted to by risk models by fishing method and target species group, summarising: the total observed effort (set net length in kilometres and number of tows for trawl), spatial overlap with Hector's dolphins (for model *update*), and the number of observed captures by state. 'SN' = set net; 'HDO' = Hector's dolphin; 'HDM' = Māui dolphin.

Method	Target	Species	Effort	Overlap	Observed captures	
					Alive	Dead
SN	Cartilaginous	HDO	5 027	0.0378	3	12
SN	Non-cartilaginous	HDO	2 377	0.0044	0	1
Trawl	–	HDO	19 618	0.1050	0	1
SN	Cartilaginous	HDM	5 027	0.0071	0	0
SN	Non-cartilaginous	HDM	2 377	0.0473	0	0
Trawl	–	HDM	19 618	0.5320	0	0

Table 10: All Hector's dolphin captures reported by government fisheries observers up until the 2019–20 fishing year, with summary information for each capture event. Note that no Māui dolphin captures were reported. Summer months are shaded yellow and winter months are blue, Kaikōura captures are shaded red, cartilaginous target species are shaded light purple. Target species are: 'SCH' = school shark (*Galeorhinus galeus*); 'RCO' = red cod (*Pseudophychis bachus*), 'SPO' = rig (*Mustelus lenticulatus*), 'TAR' = tarakihi (*Nemadactylus macropterus*), 'ELE' = elephantfish (*Callorhinchus milii*), 'SHA' = shark species.

Fishing year	Month	Region	Method	Target species	Hector's dolphins captured
1997–98	1	Timaru	Set net	SCH	2
1997–98	1	Banks Peninsula	Set net	SHA	2
1997–98	2	Timaru	Trawl	RCO	1
1997–98	3	Kaikōura	Set net	SHA	1
1997–98	3	Timaru	Set net	SHA	2
1997–98	11	Banks Peninsula	Set net	SHA	1
2006–07	11	Kaikōura	Set net	SPO	1
2007–08	2	Timaru	Set net	SPO	1
2008–09	5	Kaikōura	Set net	TAR	1
2009–10	1	Timaru	Set net	SPO	1
2009–10	11	Kaikōura	Set net	SCH	1
2012–13	10	Timaru	Set net	SPO	1
2013–14	11	Timaru	Set net	ELE	1
2016–17	2	Timaru	Set net	SPO	1

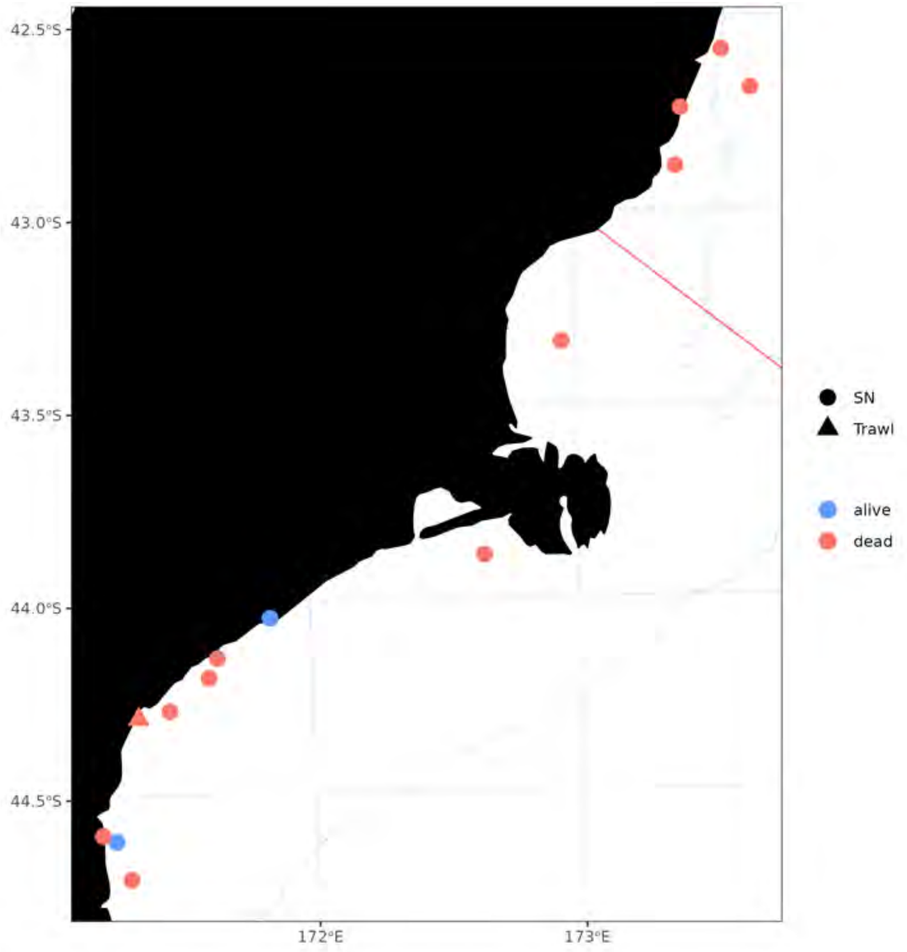

Figure 4: All Hector's dolphin capture locations reported by government fisheries observers by fishing method (SN = set net, Trawl = inshore trawl) from 1992–93 to 2019–20.

3.2.2 Model diagnostics

Diagnostic plots for the SEFRA model run **update** (using the *hab2_s50_season* spatial distribution model and assuming a single vulnerability parameter across all commercial set net events) can be found in Appendix F. MCMC mixing for all model parameters was acceptable across all four MCMC chains (Figure F.1). The prior and the posterior distributions were equivalent for the population size (N_s) and probability observable parameters (p_g^{obs}) (Figure F.2). The posterior updated the prior for the vulnerability parameters (v_g) and probability of live capture parameters (ψ_g) (Figure F.2). The model fit was excellent with respect to the observed and predicted number of captures (Figure F.3).

There were possibly too few observed captures within the KAIK local-scale area to evaluate the spatial correspondence with model-estimated observed captures. However, the location of these (all to the south of Kaikōura town) (Figure 4) had reasonably good agreement with the prediction of the **update** model, which estimated the greatest density of observed captures immediately to the south of Kaikōura (Figure H.3). There was excellent agreement between the location of observed Hector's dolphin captures and observed set net fishing effort (Figure F.4), observed overlap (Figure F.5), and the predicted number of observed captures (Figure H.3).

Model diagnostic plots were not provided for the other model runs but were all equally as good as the **update** model run.

3.2.3 Model outputs

The parameter estimates of the **update** model are summarised in Table 11 and are also summarised for all model runs in Table 12, showing only the mean values of each parameter.

Stepwise changes were made to the **previous** model (i.e., from Roberts et al. 2019a), so that it was possible to assess the effects of each change.

Firstly, the model runs **previous** (using the old spatial distribution model developed by Roberts et al. 2019a) and **update** (using the *hab2_s50_season* spatial distribution model) were used to predict average annual deaths and risk ratio across the same three fishing years (2014–15 to 2016–17), so that these could be compared directly. The **update** model had a relatively minor effect on estimated deaths within each area and had almost no effect on estimated deaths or risk for the inshore trawl fishery, or for commercial set net risk ratio within the KAIK area (Figure G.2). However, this change had a substantial increase in estimated risk ratio within the NCSI area (increasing the median risk ratio value to be above 1) and a decrease within the SCSI area (Figure 5).

The posteriors of annual deaths and risk ratio as estimated by the **update** model are summarised in (Table 13). The mean annual risk ratio for this period was estimated to be above a value of 1 in both the KAIK and NCSI local-scale areas. Given the value of ϕ (0.2) used to calculate the respective PSTs for each area, this would be consistent with the fishery overlap in this period being sufficient to drive or maintain the Hector's dolphin populations in KAIK and NCSI to below 90% of carrying capacity, when assuming logistic population growth and ignoring other potential anthropogenic sources of mortality (Darryl Mackenzie unpublished data).

Then, the **update** model was used to predict annual deaths and risk ratio comparing the set of fishing years used in the last comparison (2014–15 to 2016–17) with the latest three fishing years in the PSC database (2017–18 to 2019–20). Updating the fishing years increased the estimated risk ratio for the commercial set net fishery in NCSI and resulted in an even bigger decrease within KAIK. There was almost no effect on estimated risk for the inshore trawl fishery (Figure 6; also see Figure G.3).

None of the other model runs had much effect on the model posteriors of annual deaths and risk, when comparing across the same set of fishing years (i.e., 2017–18 to 2019–20) (Figure 7 and Figure G.4). This included: model **vuln**, which estimated separate vulnerabilities for set net events targeting cartilaginous versus non-cartilaginous fish species; and two models trialling alternative Hector's dolphin spatial distributions (**alt_dist1** and **alt_dist2**). Based on model **vuln**, the vulnerability of Hector's dolphins to capture was estimated to be greater in set nets targeting cartilaginous fish than those targeting non-cartilaginous fish (mean v_g = 0.059 and 0.034, respectively) (see Table 12 for all parameter values). Estimating separate vulnerability parameters for these fishery groups has the greatest effect on risk for the KAIK area, where the estimated annual risk ratio for commercial set nets from 2017–18 to 2019–20 was reduced from R = 1.941 (90% CI = 0.830–3.807) based on model **update** down to R = 1.619 (90% CI = 0.605–3.421) from model **vuln** (also see Table 13).

Table 11: Parameter summary for model *update*. For each parameter the following are shown: the mean, standard deviation (SD) of the mean, median (50%), 95% credible interval (2.5% and 97.5%), effective sample size (Effective N), and the potential scale reduction factor on split chains (Rhat; at convergence, Rhat = 1).

Output	Method	Species	Mean	SD	2.5%	50%	97.5%	Effective N	Rhat
v_g	SN		0.055	0.024	0.025	0.051	0.116	3 781	0.999
v_g	Trawl		0.002	0.001	0.000	0.001	0.005	3 783	1.000
ψ_g	SN		0.201	0.086	0.062	0.191	0.388	3 754	1.000
ψ_g	Trawl		0.170	0.140	0.006	0.135	0.517	4 008	1.000
ω_g	SN		0.699	0.114	0.512	0.695	0.889	3 999	1.000
ω_g	Trawl		0.699	0.114	0.510	0.699	0.889	3 862	0.999
p_g^{obs}	SN		0.498	0.129	0.251	0.498	0.749	4 096	1.000
p_g^{obs}	Trawl		0.748	0.143	0.513	0.749	0.985	3 573	1.000
N_s		HDO	14932	1646	11985	14828	18359	3 980	1.000
N_s		HDM	63.364	6.977	50.830	63.019	78.122	4 189	1.000
r_s^{max}		HDO	0.050	0.011	0.028	0.050	0.071	3 936	1.000
r_s^{max}		HDM	0.045	0.011	0.023	0.045	0.066	3 660	1.001
S_s^{1+}		HDO	0.920	0.028	0.858	0.923	0.965	3 703	1.002
S_s^{1+}		HDM	0.893	0.011	0.871	0.893	0.913	3 780	1.000
$\left(C_{sg}^{\mathrm{live}}\right)'$	SN	HDO	3.201	2.339	0.000	3.000	9.000	3 584	1.002
$\left(C_{sg}^{\mathrm{live}}\right)'$	Trawl	HDO	0.354	0.723	0.000	0.000	2.000	3 762	1.000
$\left(C_{sg}^{\mathrm{live}}\right)'$	SN	HDM	0.015	0.122	0.000	0.000	0.000	4 130	1.000
$\left(C_{sg}^{\mathrm{live}}\right)'$	Trawl	HDM	0.004	0.059	0.000	0.000	0.000	4 032	1.000
$\left(C_{sg}^{\mathrm{dead}}\right)'$	SN	HDO	12.785	5.017	4.000	12.000	24.000	3 958	1.000
$\left(C_{sg}^{\mathrm{dead}}\right)'$	Trawl	HDO	1.689	1.779	0.000	1.000	6.000	3 772	1.000
$\left(C_{sg}^{\mathrm{dead}}\right)'$	SN	HDM	0.071	0.271	0.000	0.000	1.000	4 066	0.999
$\left(C_{sg}^{\mathrm{dead}}\right)'$	Trawl	HDM	0.037	0.193	0.000	0.000	1.000	3 914	1.000
D_{sg}		HDO	39.580	14.538	18.849	37.150	74.301	3 864	0.999
D_{sg}		HDM	0.123	0.093	0.000	0.100	0.350	4 041	0.999
PST_s		HDO	74.595	18.872	40.184	74.091	113.546	4 035	1.000
PST_s		HDM	0.285	0.077	0.143	0.283	0.445	3 793	1.001

Table 12: Parameter summary for each model run showing the mean.

							Model
Output	Method	Species	previous	update	vuln	alt_dist1	alt_dist2
v_g	SN	–	0.039	0.055	0.059	0.047	0.056
v_g	SN – non- cartilaginous	–	–	–	0.034	–	–
v_g	Trawl	–	0.002	0.002	0.002	0.002	0.002
ψ_g	SN	–	0.199	0.201	0.197	0.201	0.198
ψ_g	Trawl	–	0.167	0.170	0.170	0.169	0.167
ω_g	SN	–	0.702	0.699	0.700	0.702	0.702
ω_g	Trawl	–	0.701	0.699	0.699	0.700	0.700
p_g^{obs}	SN	–	0.499	0.498	0.495	0.501	0.496
p_g^{obs}	Trawl	–	0.747	0.748	0.745	0.751	0.748
N_s	–	HDO	14920	14932	14929	14900	14919
N_s	–	HDM	63.335	63.364	63.326	63.181	63.223
$(C_{sg}^{\text{live}})'$	SN	HDO	3.141	3.201	2.963	3.205	3.140
$(C_{sg}^{\text{live}})'$	SN – non- cartilaginous	HDO	–	–	0.203	–	–
$(C_{sg}^{\text{live}})'$	Trawl	HDO	0.008	0.354	0.344	0.338	0.342
$(C_{sg}^{\text{live}})'$	SN	HDM	0.315	0.015	0.002	0.015	0.019
$(C_{sg}^{\text{live}})'$	SN – non- cartilaginous	HDM	–	–	0.010	–	–
$(C_{sg}^{\text{live}})'$	Trawl	HDM	0.004	0.004	0.006	0.006	0.008
$(C_{sg}^{\text{dead}})'$	SN	HDO	12.896	12.785	11.971	12.810	12.746
$(C_{sg}^{\text{dead}})'$	SN – non- cartilaginous	HDO	–	–	0.812	–	–
$(C_{sg}^{\text{dead}})'$	Trawl	HDO	0.030	1.689	1.706	1.688	1.663
$(C_{sg}^{\text{dead}})'$	SN	HDM	1.689	0.071	0.009	0.058	0.069
$(C_{sg}^{\text{dead}})'$	SN – non- cartilaginous	HDM	–	–	0.039	–	–
$(C_{sg}^{\text{dead}})'$	Trawl	HDM	0.016	0.037	0.037	0.036	0.041

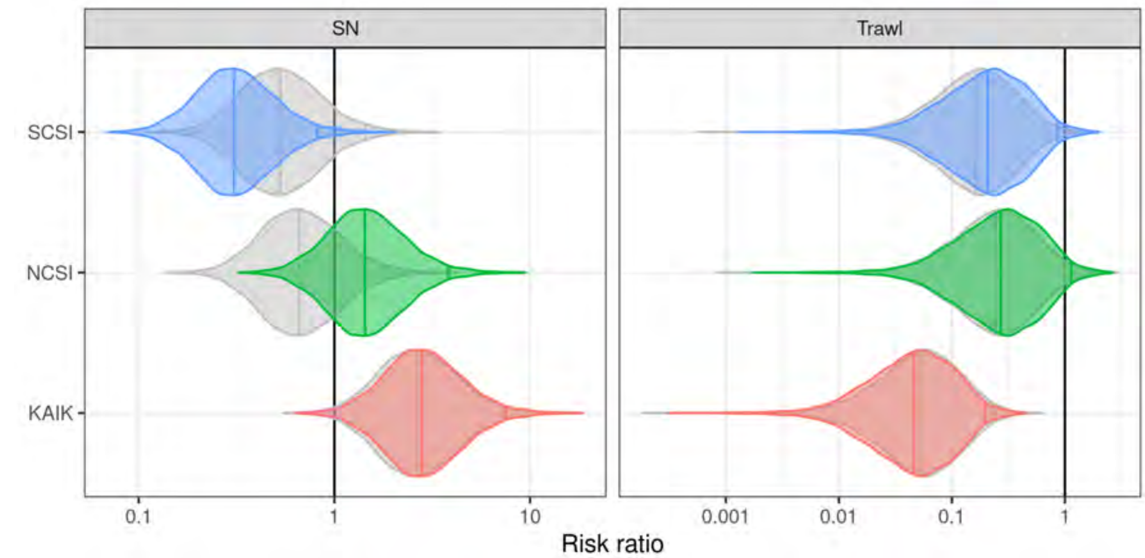

Figure 5: Annual estimated commercial fishery (set net and inshore trawl) risk ratio (plotted using log-scale) for Hector's dolphins across fishing years 2014–15 to 2016–17, by summary area (Figure 1a) from models *update* (coloured violins) and *previous* (grey violins). The median and 97.5% quantiles are indicated as vertical lines within each density. This model run assumed a calibration coefficient (ϕ) of 0.2, consistent with population recovery to at least 90% of carrying capacity when assuming logistic population growth (Darryl Mackenzie unpublished data).

Table 13: **Summary of average annual deaths and risk ratio during the 2017–18 to 2019–20 fishing years, estimated by the *update* and *vuln* model runs. Given the value of ϕ chosen by Fisheries New Zealand (ϕ = 0.2), risk ratios below 1 are consistent with population recovery to at least 90% of carrying capacity when assuming logistic population growth (Darryl Mackenzie unpublished data).**

			Deaths				Risk ratio			
Model	Method	Region	Mean	5%	50%	95%	Mean	5%	50%	95%
update	SN	KAIK	8.473	4.253	7.770	15.190	1.941	0.830	1.712	3.807
		NCSI	1.150	0.577	1.054	2.061	1.219	0.521	1.075	2.391
		SCSI	0.505	0.253	0.463	0.905	0.345	0.147	0.304	0.676
	Trawl	KAIK	0.322	0.055	0.262	0.788	0.078	0.012	0.061	0.201
		NCSI	0.275	0.047	0.224	0.673	0.292	0.045	0.227	0.752
		SCSI	0.316	0.054	0.257	0.774	0.217	0.034	0.168	0.557
vuln	SN	KAIK	7.314	3.287	6.492	13.897	1.619	0.605	1.370	3.421
		NCSI	1.087	0.535	0.994	1.960	1.139	0.477	1.004	2.278
		SCSI	0.494	0.248	0.452	0.874	0.333	0.142	0.294	0.655
	Trawl	KAIK	0.327	0.056	0.263	0.798	0.079	0.012	0.061	0.204
		NCSI	0.280	0.048	0.225	0.682	0.294	0.045	0.227	0.762
		SCSI	0.322	0.055	0.259	0.785	0.218	0.034	0.168	0.565
alt_dist1	SN	KAIK	6.790	3.414	6.202	11.910	1.786	0.776	1.570	3.496
		NCSI	0.932	0.468	0.851	1.634	0.988	0.429	0.868	1.934
		SCSI	0.425	0.214	0.388	0.745	0.290	0.126	0.255	0.568
	Trawl	KAIK	0.316	0.055	0.256	0.775	0.083	0.013	0.064	0.215
		NCSI	0.255	0.044	0.207	0.626	0.270	0.042	0.208	0.702
		SCSI	0.328	0.057	0.266	0.805	0.224	0.035	0.173	0.583
alt_dist2	SN	KAIK	8.021	3.973	7.288	14.460	1.616	0.678	1.423	3.206
		NCSI	1.268	0.628	1.152	2.285	1.343	0.563	1.182	2.664
		SCSI	0.624	0.309	0.567	1.124	0.426	0.179	0.375	0.845
	Trawl	KAIK	0.326	0.058	0.267	0.817	0.067	0.011	0.051	0.172
		NCSI	0.274	0.049	0.224	0.686	0.292	0.048	0.223	0.749
		SCSI	0.229	0.041	0.188	0.575	0.158	0.026	0.121	0.404

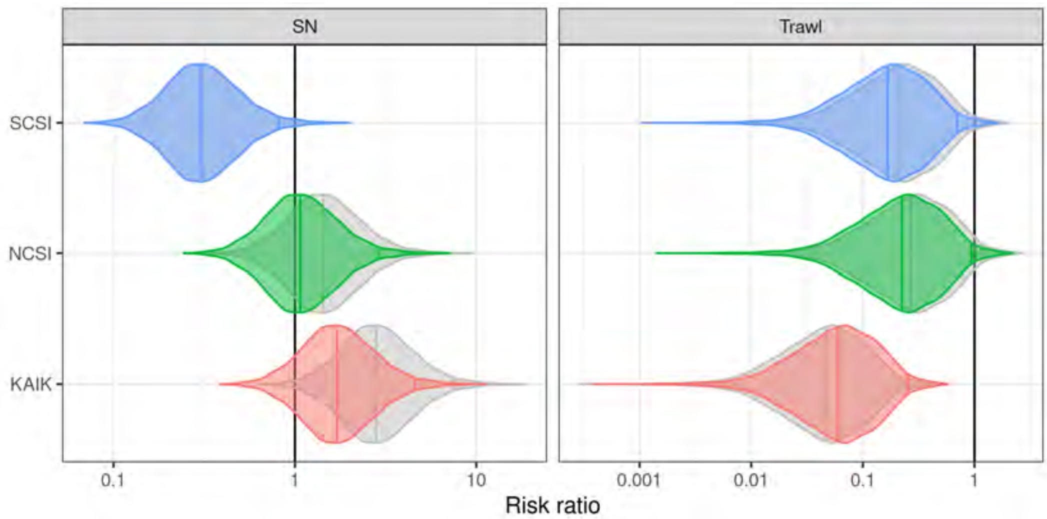

Figure 6: **Annual estimated commercial fishery (set net and inshore trawl) risk ratio (plotted using log-scale) for Hector's dolphins by summary area (Figure 1a) from model *update* for fishing years 2017–18 to 2019–20 (coloured violins) and 2014–15 to 2016–17 (grey violins). The median and 97.5% quantiles are indicated as vertical lines within each density. This model run assumed a calibration coefficient (ϕ) of 0.2, consistent with population recovery to at least 90% of carrying capacity when assuming logistic population growth (Darryl Mackenzie unpublished data).**

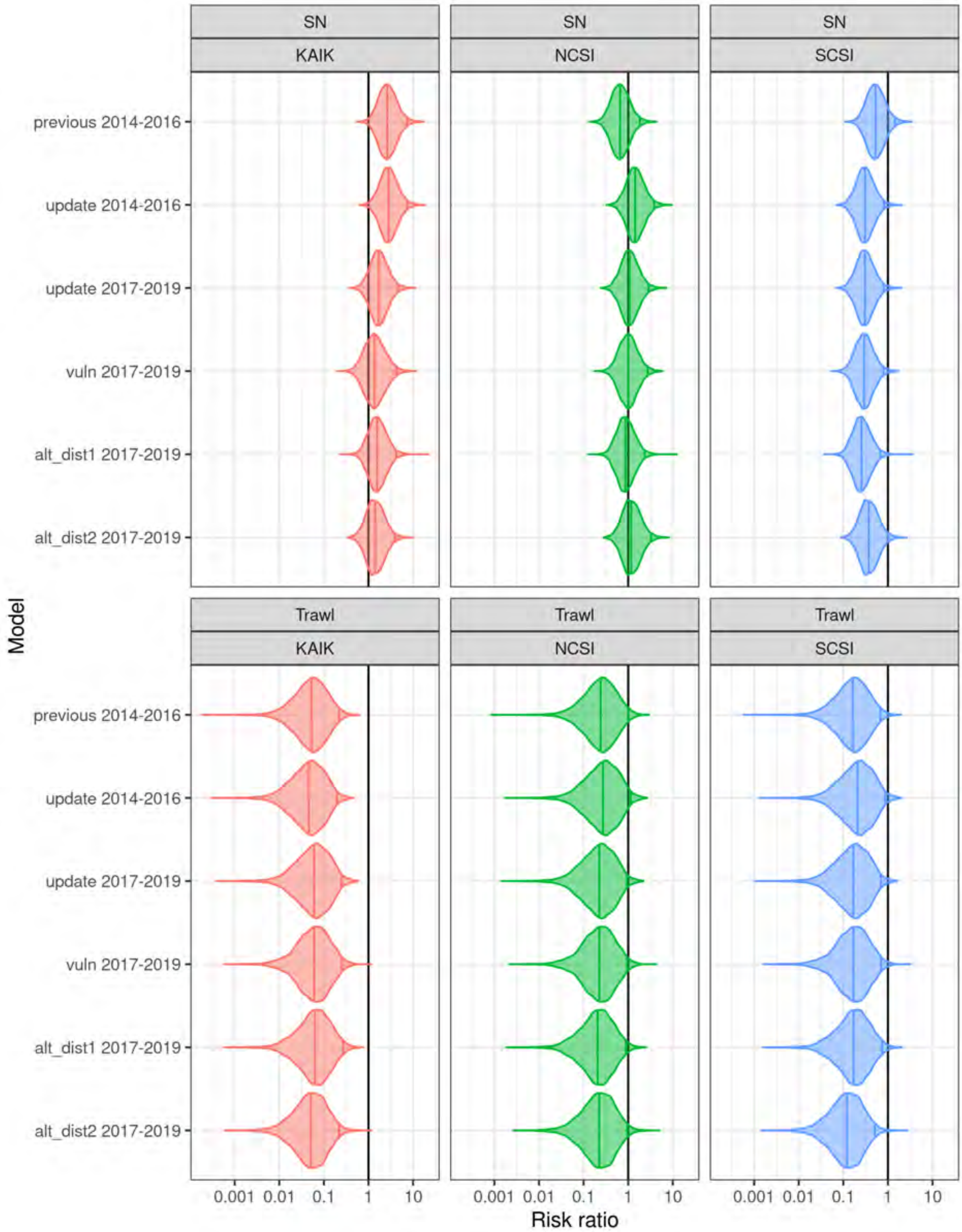

Figure 7: Annual estimated commercial fishery (set net and inshore trawl) risk ratio (plotted using log-scale) for Hector's dolphins by summary area (Figure 1a). The median and 97.5% quantiles are indicated as vertical lines within each density. This model run assumed a calibration coefficient (ϕ) of 0.2. This value of ϕ is consistent with population recovery to at least 90% of carrying capacity when assuming logistic population growth (Darryl Mackenzie unpublished data). Note the years denoted here represent fishing years, i.e., 2014-2016 represents 2014–15 to 2016–17, etc.

Time series plots of the outputs from the **update** model run are shown in Appendix G for commercial set nets (Figure G.5, Figure G.6, and Figure G.7) and the inshore trawl fishery (Figure G.8, Figure G.9 and Figure G.10).

In all three local-scale areas there was a decrease in model estimates of annual deaths and risk in the commercial set net fishery over time since 1992–93 (the first year in the PSC database). Within NCSI, this appears to have primarily been driven by a declining trend in effort over time, which declined by slightly more than half over the past 28 fishing years (Figure G.5). For the KAIK local-scale area, the decline in estimated annual deaths and risk was driven by a decline in fishing effort since the early 2000s and also a decline in spatial overlap per unit of fishing effort, which was particularly pronounced in the final two fishing years (2018–19 and 2019–20) (Figure G.6). Within SCSI, this was driven by an abrupt drop in overlap per unit of fishing effort after the 2007–08 fishing year, which compensated for an increasing trend in overall effort (Figure G.7).

The timing of this change in overlap per unit effort within the SCSI area coincides with the implementation of a ban on commercial set netting within the whole of Te Waewae Bay and a 4-nautical mile offshore strip along the entire SCSI area, beginning at the start of 2008–09 (Department of Conservation 2022b). Prior to this change the mean estimated risk ratio was above a value of 2 for two years (in 2006–07 and 2007–08) and was estimated to be below 0.5 in all years since (Figure G.7).

While the 4-nautical mile coastal ban was also imposed within the KAIK area, the effect on overlap per unit effort was minimal (Figure G.6), perhaps due in part to an exemption on the use of commercial set nets at greater than 100 m depth (Department of Conservation 2022b) (Figure G.6). Note that the NCSI area was not included in the 2008–09 fishing area restrictions imposed on the commercial set net fishery (Department of Conservation 2022b).

For the inshore trawl fishery, the estimated mean risk ratio was well below 1 in all years in all three local-scale areas (Figure G.8, Figure G.9, and Figure G.10).

Observer coverage (i.e., the percent of fishing effort with an observer onboard) was zero in many years in all three areas for both the set net (Figure G.5, Figure G.6, and Figure G.7) and inshore trawl fisheries (Figure G.8, Figure G.9, and Figure G.10). In the NCSI area there was some set net observer coverage during four years from 2005–06 to 2008–09 with a maximum coverage of ~8% for one year (Figure G.5). In the KAIK area there was a period of set net observer coverage from 2006–07 to 2010–11 with a maximum coverage of ~8% for two years and less than 2% coverage in a few other years (Figure G.6). The SCSI set net observer coverage took place from 2005–06 to 2009–10, ceased for two years, and has been relatively high in most years since 2014–15. Observer coverage of inshore trawl fishing events was very light in most years for all three areas (Figure G.8, Figure G.9, and Figure G.10).

Spatial plots of observed captures predicted by model **update** are shown in Appendix H (Figure H.1, Figure H.2, Figure H.3, Figure H.4, Figure H.5, and Figure H.6). The corresponding spatial plots of predicted deaths are shown in the main body of this report (Figure 8, Figure 9, Figure 10, Figure 11, Figure 12, Figure 13). The spatial pattern of estimated deaths is different for inshore trawls versus commercial set nets in all three local-scale areas. However, these patterns were consistent with respect to fishing year between 2014–15 and 2019–20, based on total reported fishing effort (Figure 8 to Figure 13).

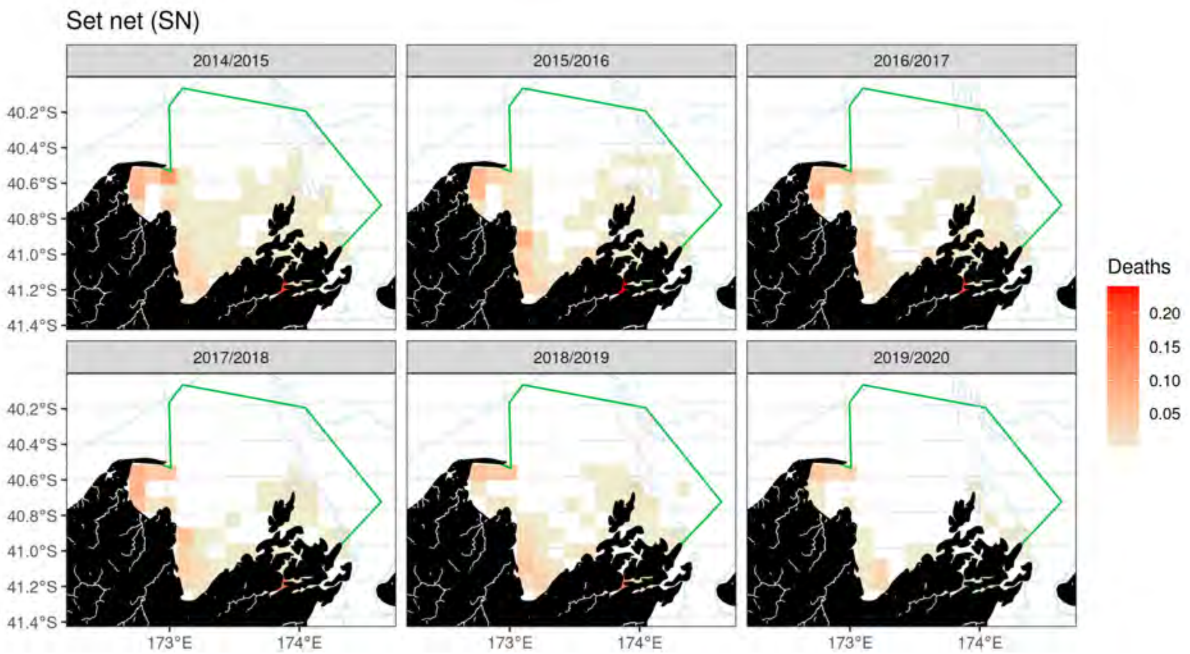

Figure 8: Spatial plot of outputs of model *update*, showing the mean predicted number of Hector's dolphin deaths by set nets (SN) in 10-km cells off the north coast of the South Island (NCSI) by fishing year. The NCSI region is shown in green and the 100-m depth contour in light blue.

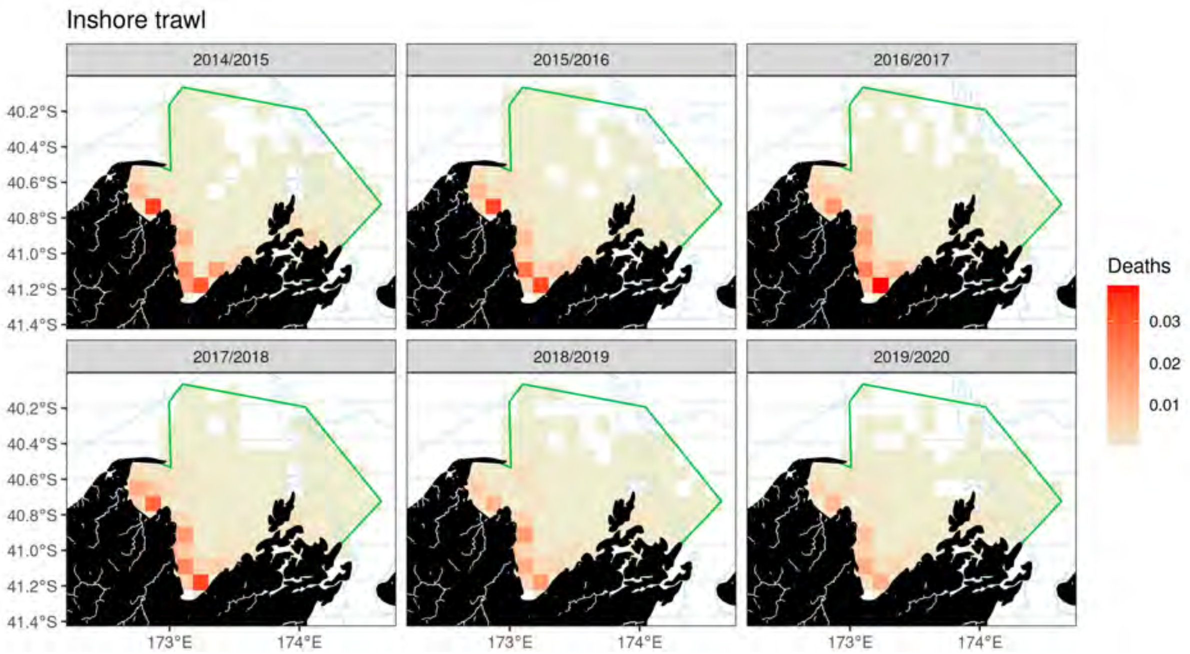

Figure 9: Spatial plot of outputs of model *update*, showing the mean predicted number of Hector's dolphin deaths by inshore trawls in 10-km cells off the north coast of the South Island (NCSI) by fishing year. The NCSI region is shown in green and the 100-m depth contour in light blue.

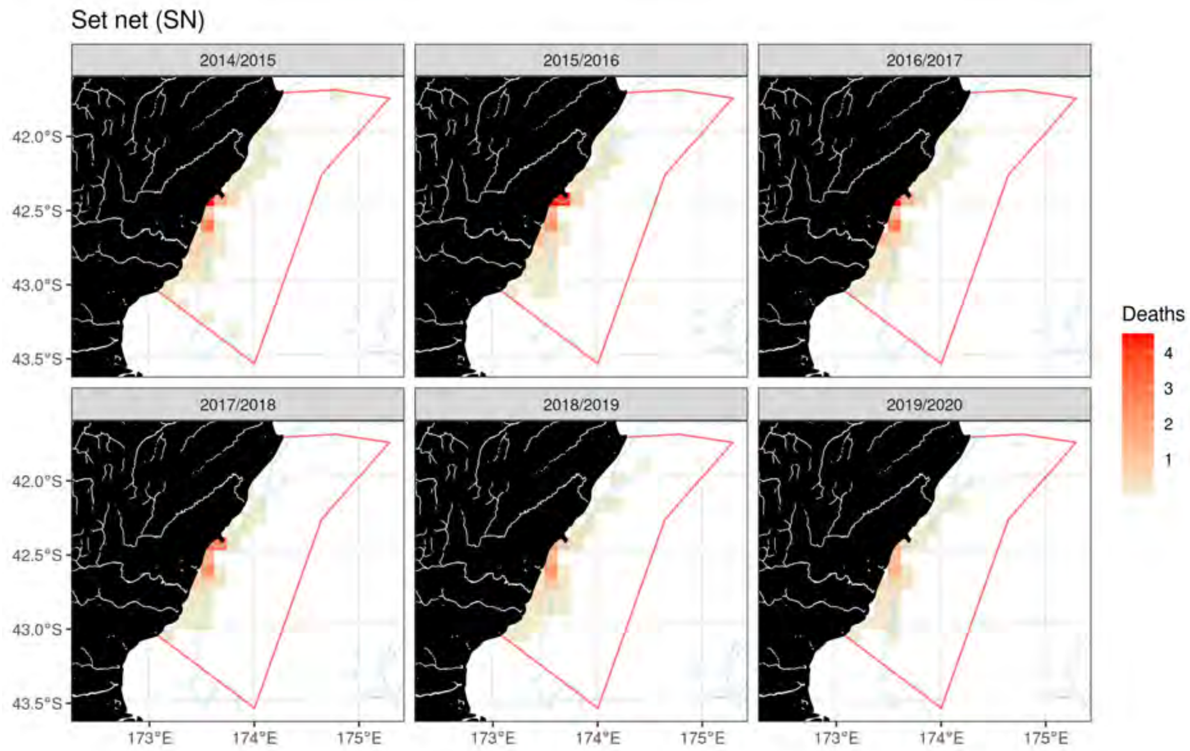

Figure 10: Spatial plot of outputs of model *update*, showing the mean predicted number of Hector's dolphin deaths by set nets (SN) in 10-km cells off Kaikōura (KAIK) by fishing year. The KAIK region is shown in red and the 100-m depth contour in light blue.

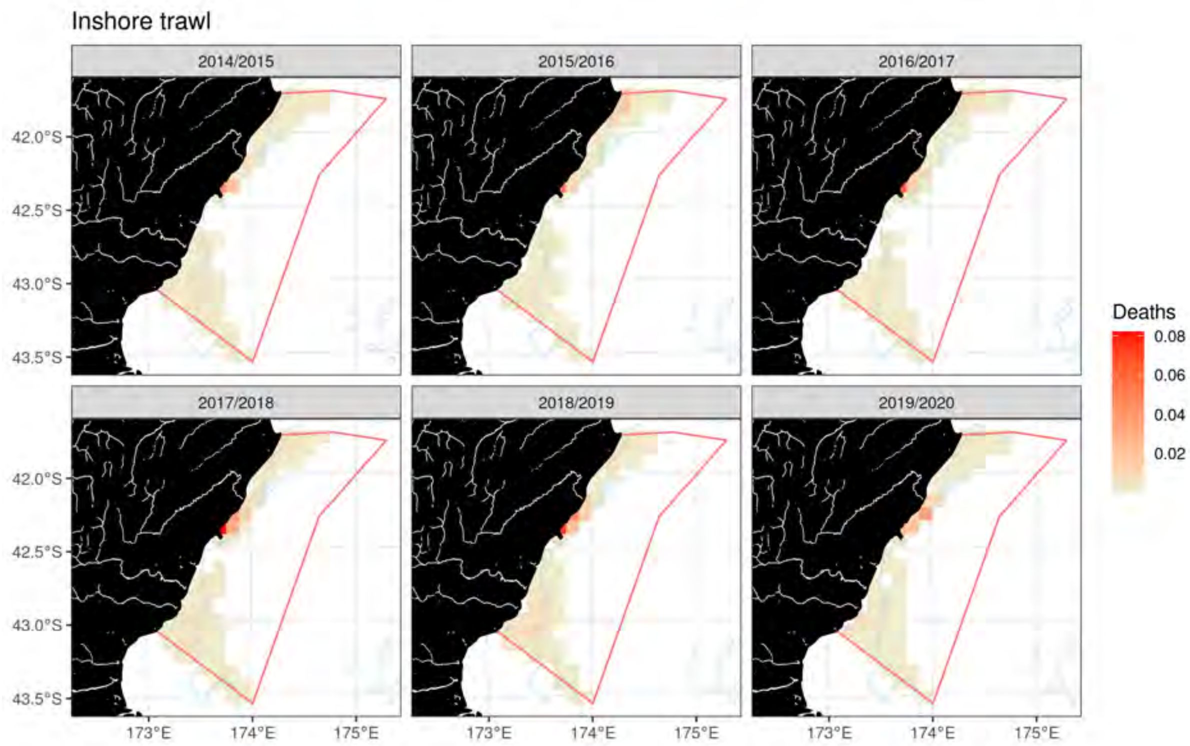

Figure 11: Spatial plot of outputs of model *update*, showing the mean predicted number of Hector's dolphin deaths by inshore trawls in 10-km cells off Kaikōura (KAIK) by fishing year. The KAIK region is shown in red and the 100-m depth contour in light blue.

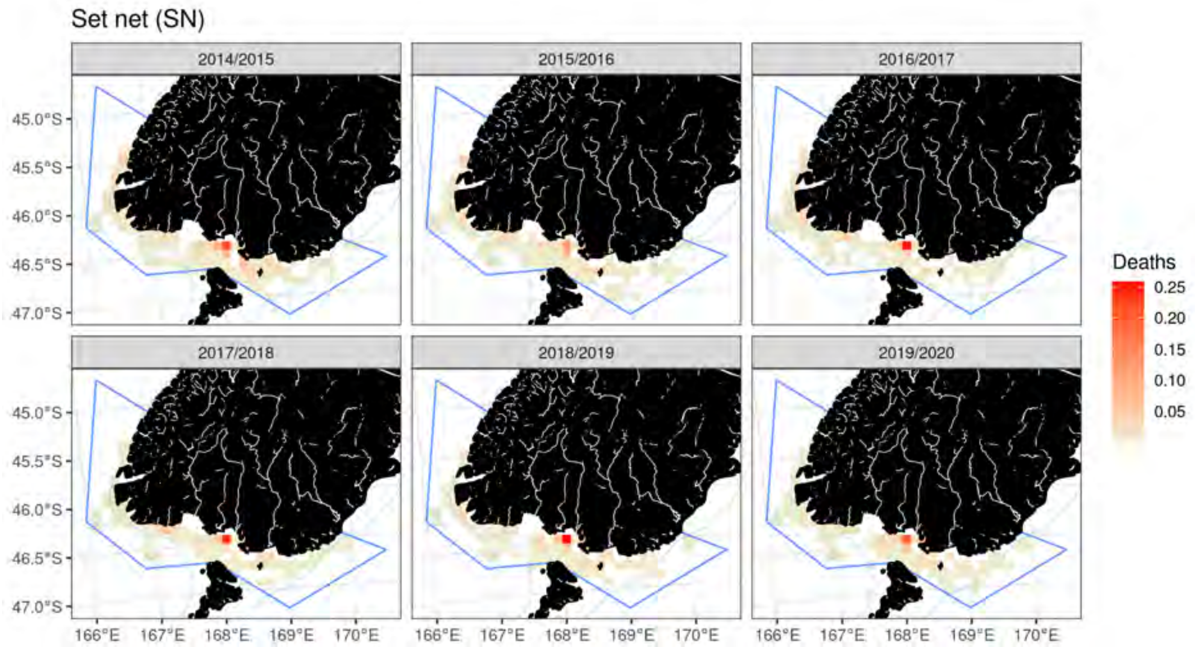

Figure 12: Spatial plot of outputs of model *update*, showing the mean predicted number of Hector's dolphin deaths by set nets (SN) in 10-km cells off the south coast of the South Island (SCSI) by fishing year. The SCSI region is shown in blue and the 100-m depth contour in light blue.

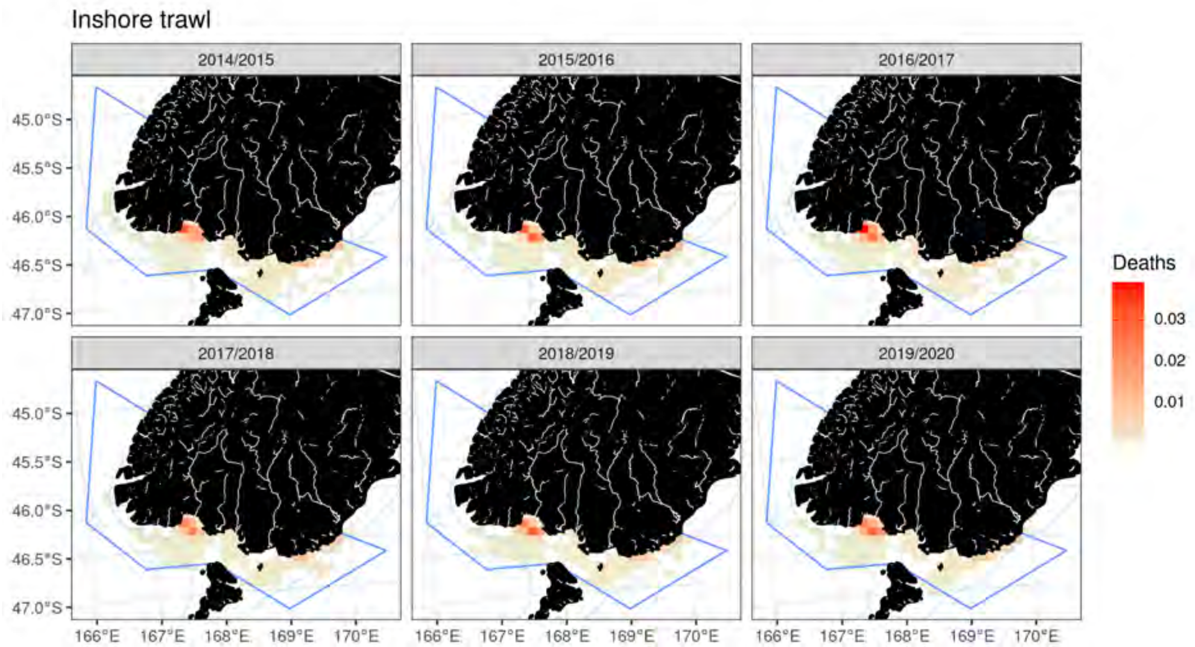

Figure 13: Spatial plot of outputs of model *update*, showing the mean predicted number of Hector's dolphin deaths by inshore trawls in 10-km cells off the south coast of the South Island (SCSI) by fishing year. The SCSI region is shown in blue and the 100-m depth contour in light blue.

4 DISCUSSION

4.1 Limitations of this analysis

The accurate estimation of Hector's dolphin spatial distribution relies on good quality data, ideally with good spatial and temporal coverage. The available data had best spatial coverage within the SCSI area, and poorest coverage within the NCSI area, where data from formal surveys designed for this purpose were limited. The data were also comparatively limited along sections of the Kaikōura coast that are distant from Kaikōura town, with the most spatially comprehensive data coming from a single aerial survey in 2013.

Integrating spatial information across various data sources helped to improve the spatial and temporal coverage of data. However, there was no attempt to explore the sensitivity of model predictions to assuming alternative statistical weightings for different data sources.

There was no attempt to explore alternative effort units for some data sources (e.g., using 10-km instead of 1-km line segments for aerial surveys). However, with this example, the decrease in sample size with using a coarser unit would have been offset to some extent by the counts being summed over a wider area and, therefore, being less noisy.

The exploration of different vulnerability groups used by the SEFRA model (e.g., based on fishery target species) was limited by the small number of events with observed captures. This situation cannot be improved without an increase in the numbers of observed captures across the commercial set net fishery or by assuming that some fishing groups pose no threat to Hector's dolphins (e.g., if a new fishing group is defined with zero observed captures attributed to this group then the SEFRA model will effectively predict no risk for this group and assign more risk to the existing vulnerability groups).

Note that the available time series of fishery data used by this assessment (up to the end of the 2019–20 fishing year) ends immediately prior to the commencement of additional commercial fishing area restrictions (since 1 October 2020) arising from the latest TMP (Department of Conservation & Fisheries New Zealand 2021). Hence, the current assessment does not include any information about changes in annual deaths and risk that might have occurred in response to those changes.

4.2 Drivers of spatial distribution

The initial round of model development, which fitted models separately in each of the three local-scale areas, resulted in model structures that were very different among the three different areas, which did not seem realistic for the same species. This does not appear to have been helped by the modest number of high-density spots in each of these local-scale areas, with only one or two hotspot locations in each area, which probably confounded the identification of the true underlying environmental drivers. The revised approach of fitting a single model across all the available spatial information around the South Island (i.e., including many more regions of high and low density) and integrating across all available sources of spatial information, is likely to have resulted in more relevant models with improved predictive power. Although not done here, this modelling approach could be extended to include the multiple sources of spatial information along the west coast of the North Island, where Māui dolphin occur.

The use of models which combined spatial smoothers and environmental covariates should have accounted for some of the spatial variability in sighting density that was not explained by any of the candidate environmental covariates used by this assessment.

The selection of optimal environmental drivers of Hector's dolphin distribution was highly sensitive to the method used for model comparison. In this case, the standard methods (e.g., comparison using model AIC, or the percentage of null model deviance explained) favoured the models with poorest predictive power (Table 6). Furthermore, the k-fold cross validation would have selected models that were poor at predicting outside the spatial domain of model fitting, as revealed by comparison with the data source-based model cross-validation approach.

The data source-based approach for model cross validation favoured simpler models than the other approaches (Table 6). The three environmental covariates of model *hab3* (used for subsequent model development) were seasonal sea surface turbidity, the presence of *Peltorhamphus* spp. flatfish (key prey species), and the muddiness of benthic sediments. In particular, the summer/winter sea surface turbidity layer appears to be a helpful predictor of Hector's dolphin distribution (also found by Roberts et al. 2019a)—as are the prey presence layers, which were derived from models fitted to trawl survey data (Roberts et al. 2019a). These prey layers were seasonally static, although it has previously been shown that Hector's dolphin distributions are likely to be responsive to the seasonal movements of key prey taxa (Miller 2015). The availability of good quality seasonally disaggregated distributions of key prey taxa would help to refine the estimation of Hector's dolphin spatial distribution. Other plausible drivers of distribution include proximity to river mouths (e.g., Rodda 2016), evident from the plots in Appendix E, and atmospheric/oceanographic factors not explored by this analysis (e.g., Clement 2005).

4.3 Changes to assumed spatial distribution

The previous Hector's dolphin distribution layers indicated a relatively even along-shore distribution in each of the three local-scale areas (see Appendix A). The updated spatial distribution layers suggest that their distribution is much more heterogenous with, in some cases, quite discrete locations of higher density. For example, the dolphins were estimated to be much more abundant in Te Waewae Bay than in other coastal regions of the SCSI (Figure E.5 and Figure E.6), whereas their distribution was previously estimated to be much more dispersed (Figure A.5 and Figure A.6). Similarly, within the NCSI area, the estimated density of Hector's dolphins was much greater in Golden Bay than in Tasman Bay, particularly in turbid waters near to river mouths (Figure E.1 and Figure E.2).

Within the Kaikōura coast area (KAIK), the estimated density of Hector's dolphins was greatest along the coastal stretch north of Kaikōura town, particularly around the Clarence River estuary (Figure E.3 and Figure E.4), contrasting with the previous assumed distributions, which were more dispersed (Figure A.3 and Figure A.4). Hence, the spatial distribution inputs to the SEFRA risk model were altered by this assessment.

4.4 Spatial risk assessment

The SEFRA model estimates of deaths and risk were surprisingly insensitive to the use of alternative spatial distributions in the three local-scale areas, despite the new layers being somewhat different from those used previously by Roberts et al. (2019a). Generally, the revised spatial distributions in all three local-scale areas had a more uneven along-shore distribution than the previous ones (see the previous section). The updated Hector's dolphin layers for NCSI and SCSI were the most different from the previous layers, and SEFRA model estimates in these areas were the most sensitive to updating the spatial distribution, causing an increase in estimated annual risk from commercial set nets in NCSI and a decrease in risk in SCSI (see Figure 5). SEFRA estimates of annual trawl fishery risk were almost totally unaffected by the change in assumed Hector's dolphin spatial distribution in all three local-scale areas (see Figure 5), or with the use of either of the sensitivity spatial distributions (Figure 7).

By comparison, the choice of prior for cryptic mortality for the commercial set net fishery will make a substantial difference. The current assessment used a prior developed by Roberts et al. (2019a), based on literature review, which was specified as the probability that an event is observable (given that an observer is on watch) for each fisheries group (p_g^{obs}). This prior inflates the total deaths by approximately 30–300% above the estimated observable deaths, based on the 95% credible interval of this prior (bottom-left plot of Figure F.2). Improvements to this prior may only be possible with better information about the proportion of dolphins dropping out of nets between the sea surface and being landed on deck. Currently, it is assumed that New Zealand fisheries observers do not include any of these in their capture records.

A decline in estimated risk ratio was estimated through time for all three local-scale areas. However, the estimated mean risk ratio remained above 1 in both NCSI and KAIK across the final three fishing years. Given the value of ϕ that was used by this assessment, this level of mortality would be consistent with population recovery to below 90% of carrying capacity when assuming logistic population growth (Darryl Mackenzie unpublished data) and disregarding other anthropogenic threats.

A set net fishery targets relatively deep aggregations of tarakihi (*Nemadactylus macropterus*) off Kaikōura during summer and autumn (Beentjes et al. 2012). The outputs of model **vuln** are consistent with this fishery having a relatively lower probability of capturing Hector's dolphins per kilometre of set net. Accounting for this had a minor effect on model estimates of annual risk, although these results should be treated with extreme caution, given the very small number of observed capture events for each fishery group (Table 9).

With the change to electronic reporting, which should hasten the processing and delivery of fishing effort data, this application of SEFRA provides an operating model that could be used by management procedures (MPs). For example, cumulative set net and inshore trawl fishing effort could be accessed at regular intervals throughout a fishing year (e.g., monthly) and used to operate a SEFRA-driven MP that could dictate, for example, that if the median risk ratio across a given period (e.g., across the latest years) is close to exceeding 1, then a management intervention could be actioned. Comparable effort-based MPs are used to manage New Zealand sea lion (*Phocarctos hookeri*) deaths associated with commercial fishing around the Auckland Islands.

4.5 Potential research

With respect to spatial distribution modelling of Hector's dolphins:

- Future research could target regions with the poorest quality and coverage of spatial data, including the NCSI and northern and regions of the Kaikōura coast away from Kaikōura town.
- The seasonal movements of Hector's dolphins are likely, in part, to be a response to seasonal changes in prey distribution. The non-availability of spatially comprehensive seasonal layers for key prey taxa is one area for improvement.

With respect to the estimation of population risk from commercial fisheries:

- The benefits of future research seeking to improve estimates of the spatial distribution of Hector's dolphin appear to be minimal.
- The main residual source of uncertainty with respect to the estimation of population risk of commercial fisheries for Hector's and Māui dolphins now appears to be the magnitude of cryptic mortality, which could be refined by future research.
- Measures to increase the number of observed captures may result in improvements in the accuracy of SEFRA estimates of deaths and risk, particularly for the trawl fishery.
- Future assessments could update the SEFRA model with fishing data since the implementation of new fishing area restrictions on 1 October 2020.

5. ACKNOWLEDGEMENTS

We are grateful to the following researchers for providing raw Hector's dolphin sighting and effort data for use by this project: Darryl MacKenzie (Proteus), Judy Rodda (Otago University), Stefan Bräger (formerly of Otago University), Jody Weir (DOC), Hannah Hendriks (DOC), and Mike Ogle (DOC). The authors would like to thank Ben Sharp at Fisheries New Zealand for his guidance with selecting study areas and refining the project methodology. This research project was funded by Fisheries New Zealand (project code PMM2020-09).

6. REFERENCES

Akaike, H. (1974). A new look at the statistical model identification. *IEEE Transactions on Automatic Control 19 (6)*: 716–723.

Baker, C.S.; Chilvers, B.L.; Childerhouse, S.; Constantine, R.; Currey, R.; Mattlin, R.; Van Helden, A.; Hitchmough, R.; Rolfe, J. (2016). Conservation status of New Zealand marine mammals, 2013. *New Zealand Threat Classification Series 14*. 18 p.

Beentjes, M.P.; Parker, S.; Fu, D. (2012). Characterisation of TAR 2 & TAR 3 fisheries and age composition of landings in 2010/11. *New Zealand Fisheries Assessment Report 2012/25*. 68 p.

Bräger, S.H.-J. (1998). Behavioural ecology and population structure of Hector's dolphin (*Cephalorhynchus hectori*). (PhD Thesis, University of Otago.) 223 p. Retrieved from http://hdl.handle.net/10523/3507

Clement, D.M. (2005). Distribution of Hector's dolphin (*Cephalorhynchus hectori*) in relation to oceanographic features. (PhD Thesis, University of Otago.) 270 p.

Clement, D.; Mattlin, R.; Torres, L. (2011). Abundance, distribution and productivity of Hector's (and Māui's) dolphins. Final Research Report, PRO2009-01A. (Unpublished report held by Fisheries New Zealand, Wellington.)

Department of Conservation (2005). Hector's dolphin (*Cephalorhynchus hectori hectori*) satellite tagging, health and genetic assessment project. URL https://www.doc.govt.nz/about-us/science-publications/conservation-publications/native-animals/marine-mammals/hectors-dolphin-cephalorhynchus-hectori-hectori-satellite-tagging-health-and-genetic-assessment-project/. Accessed 4 July 2022.

Department of Conservation (2021). Māui and Hector's dolphin sightings database. URL https://www.doc.govt.nz/our-work/our-work-with-Māui-dolphin/Māui-dolphin-sightings/. Accessed 5 April 2021.

Department of Conservation (2022a). Māui and Hector's dolphin sightings database. URL https://www.doc.govt.nz/our-work/our-work-with-Māui-dolphin/Māui-dolphin-sightings/. Accessed 1 May 2022.

Department of Conservation (2022b). Timeline of protection for Māui and Hector's dolphins. URL https://www.doc.govt.nz/nature/native-animals/marine-mammals/dolphins/maui-dolphin/timeline-of-research-and-protection-events/. Accessed 16 July 2022.

Department of Conservation and Fisheries New Zealand (2021). Hector's and Māui Dolphin Threat Management Plan 2020. New Zealand Department of Conservation & Fisheries New Zealand. 17 p. URL: https://www.doc.govt.nz/globalassets/documents/conservation/native-animals/marine-mammals/maui-tmp/hectors-and-maui-dolphin-threat-management-plan-2020.pdf

Edwards, C.T.T.; Roberts, J.; Doonan, I. (2018). Estimation of the maximum rate of intrinsic growth for Hector's dolphin. (Final Research Report available from Fisheries New Zealand.) 22 p.

Fisheries New Zealand (2022). *Aquatic Environment and Biodiversity Annual Review 2021*. Compiled by the Fisheries Science Team, Ministry for Primary Industries, Wellington New Zealand. 779 p.

Hartill, B.; Vaughan, M.; Rush, N. (2011). Recreational harvest estimate for SNA 8 in 2006–07. *New Zealand Fisheries Assessment Report 2011/51*. 48 p.

MacKenzie, D.I. (2022). An updated assessment of historical impact of setnet fisheries on Māui dolphin. *New Zealand Aquatic Environment and Biodiversity Report No. 293*. 43 p.

MacKenzie, D.I.; Clement, D.M. (2014). Abundance and distribution of ECSI Hector's dolphin. *New Zealand Aquatic Environment and Biodiversity Report No. 123*. 79 p.

MacKenzie, D.I.; Clement, D.M. (2016). Abundance and distribution of WCSI Hector's dolphin. *New Zealand Aquatic Environment and Biodiversity Report No. 168*. 67 p + supplemental material.

MacKenzie, D.I.; Clement, D.M. (2018). PRO2016 09: Abundance and distribution of South Coast South Island Hector's dolphins. (Presentation to Aquatic Environment Working Group, 6 September 2018.)

Miller, E.J. (2015). Ecology of Hector's dolphin (*Cephalorhynchus hectori*): Quantifying diet and investigating habitat selection at Banks Peninsula. (PhD Thesis, University of Otago.) 168 p.

Mormede, S.; Webber, D.; Edwards, E. (2022). Creating standardised grids for New Zealand marine science outputs. *New Zealand Aquatic Environment and Biodiversity Report No. 283*. 7 p.

Pichler, F. (2001). Population structure and genetic variation in Hector's dolphin (*Cephalorhynchus hectori*). (Ph.D. Thesis, University of Auckland.) 169 p.

Pinkerton, M.H.; Gall, M.; Wood, S.; Zeldis, J. (2018). Measuring the effects of bivalve mariculture on water quality in northern New Zealand using MODIS-Aqua satellite observations. *Aquaculture Environment Interactions 10*: 529–545.

Rayment, W.; Dawson, S.; Slooten, E. (2009). Use of T-PODs for acoustic monitoring of Cephalorhynchus dolphins: a case study with Hector's dolphins in a marine protected area. *Endangered Species Research 10*: 333–339.

Richard, Y.; Abraham, E.; Berkenbusch, K. (2020). Counts of seabirds around commercial fishing vessels within New Zealand waters, 2007–08 to 2018–19. (Report prepared for the Department of Conservation.) 43 p.

Roberts, J.; Constantine, R.; Baker, C.S. (2019b). Population Effects of Commercial Fishery and Non-Fishery Threats on Māui Dolphins (*Cephalorhynchus hectori maui*). *New Zealand Aquatic Environment and Biodiversity Report No. 215*. 18 p.

Roberts, J.O.; Webber, D.N.; Roe, W.T.; Edwards, C.T.T.; Doonan, I.J. (2019a). Spatial risk assessment of threats to Hector's/Māui dolphins (*Cephalorhynchus hectori*). *New Zealand Aquatic Environment and Biodiversity Report No. 214*. 168 p.

Rodda, J.L. (2016). Analysis and geovisualisation of Hector's dolphin abundance and distribution patterns in space and time. (PhD Thesis, University of Otago.) 241 p. Retrieved from http://hdl.handle.net/10523/6320.

Sharp, B.R. (2018). Spatially-explicit fisheries risk assessment (SEFRA): a framework for quantifiying and managing incidental commercial fisheries impacts on non-target species. In: *Aquatic Environment and Biodiversity Annual Review 2017*. Ministry for Primary Industries. pp. 20–56. URL https://www.mpi.govt.nz/dmsdocument/34854-aquatic-environment-and-biodiversity-annual-review-aebar-2018-a-summary-of-environmental-interactions-between-the-seafood-sector-and-the-aquatic-environment

Slooten, E.; Dawson, S.M. (2010). Assessing the effectiveness of conservation management decisions: likely effects of new protection measures for Hector's dolphin (*Cephalorhynchus hectori*). *Aquatic Conservation Marine and Freshwater Ecosystems 20*: 334–347.

Wade, P.R. (1998). Calculating Limits to the Allowable Human-Caused Mortality of Cetaceans and Pinnipeds. *Marine Mammal Science 14*: 1–37.

Weir, J. S.; Sagnol, O. (2015). Distribution and abundance of Hector's dolphins (*Cephalorhynchus hectori*) off Kaikoura, New Zealand. *New Zealand Journal of Marine and Freshwater Research 49 (3)*: 376–389.

Wood, S.N. (2017). *Generalized Additive Models: An Introduction with R*. Chapman and Hall, New York. 496 p.

APPENDIX A. PREVIOUS HECTOR'S DOLPHIN DISTRIBUTION LAYERS

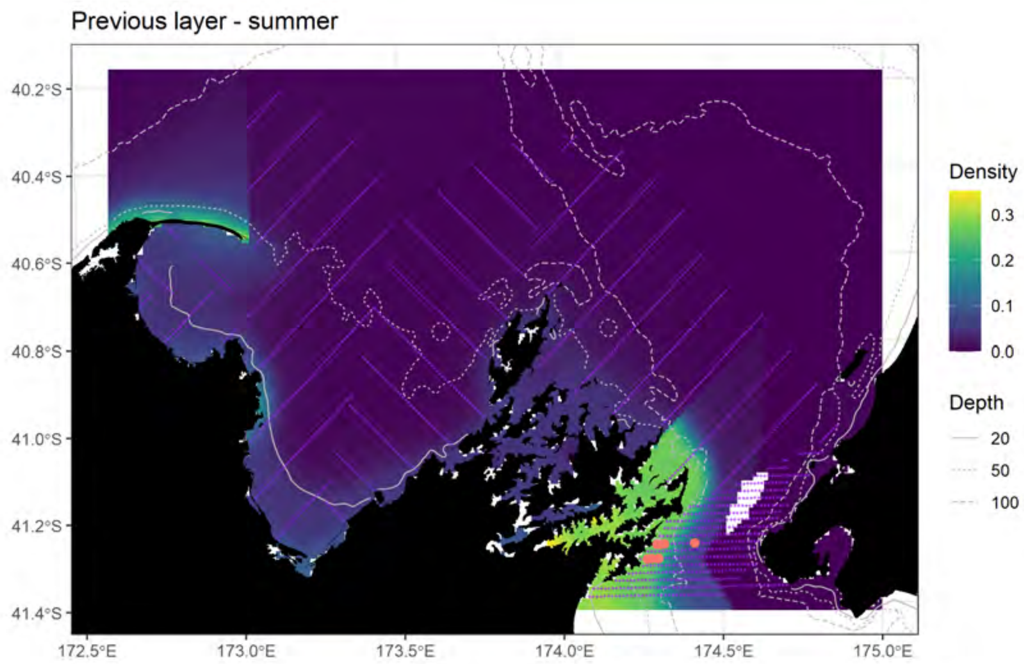

Figure A.1: Previous Hector's dolphin distribution layers for the <u>north coast of the South Island in summer</u>. Red points are locations where dolphins were observed by the 2013 aerial survey, small purple points are the associated effort.

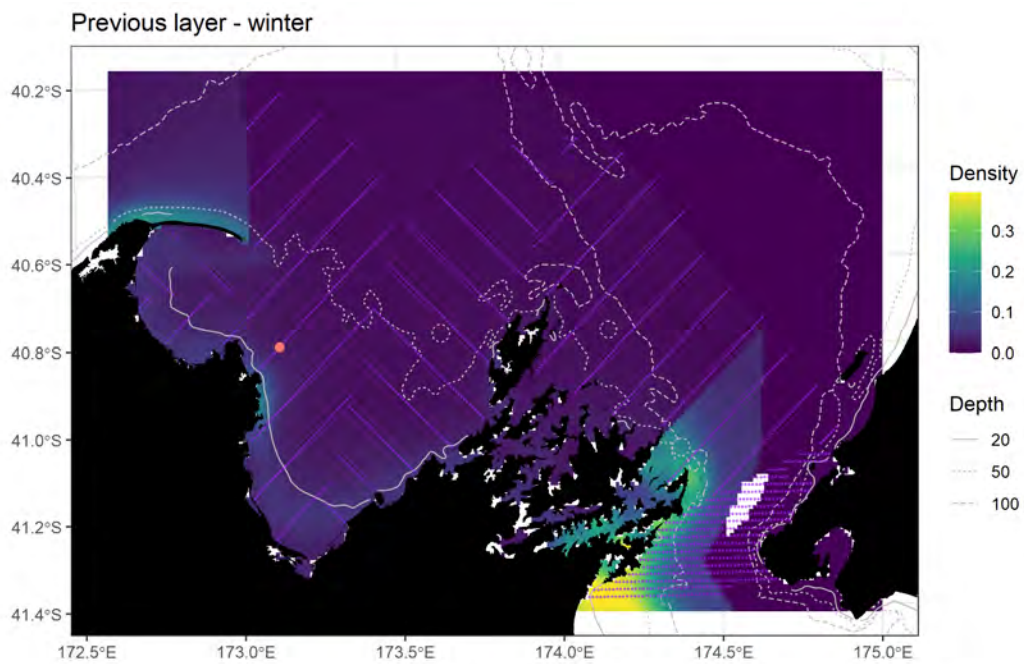

Figure A.2: Previous Hector's dolphin distribution layers for the <u>north coast of the South Island in winter</u>. Red points are locations where dolphins were observed by the 2013 aerial survey, small purple points are the associated effort.

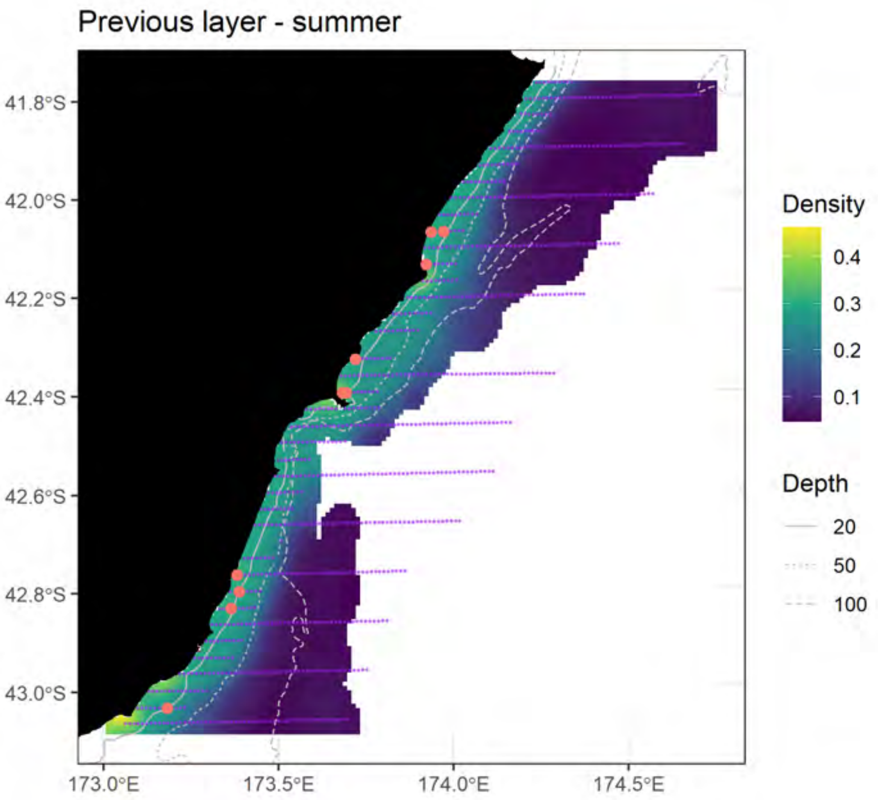

Figure A.3: **Previous Hector's dolphin distribution layers for the <u>Kaikōura coast in summer</u>. Red points are locations where dolphins were observed by the 2013 aerial survey, small purple points are the associated effort.**

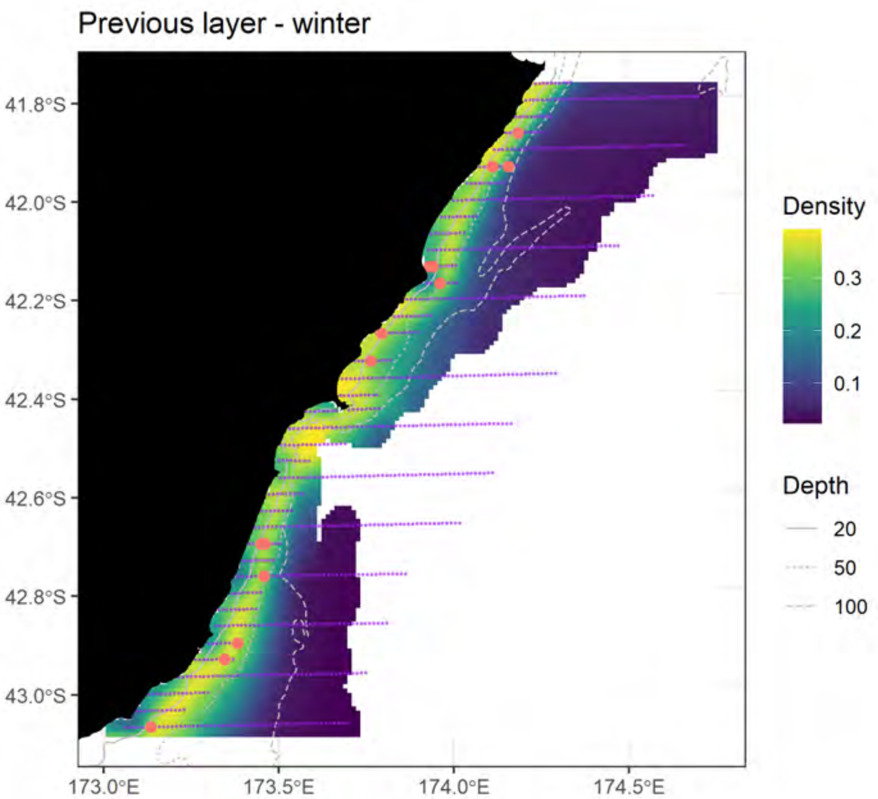

Figure A.4: **Previous Hector's dolphin distribution layers for the <u>Kaikōura coast in winter</u>. Red points are locations where dolphins were observed by the 2013 aerial survey, small purple points are the associated effort.**

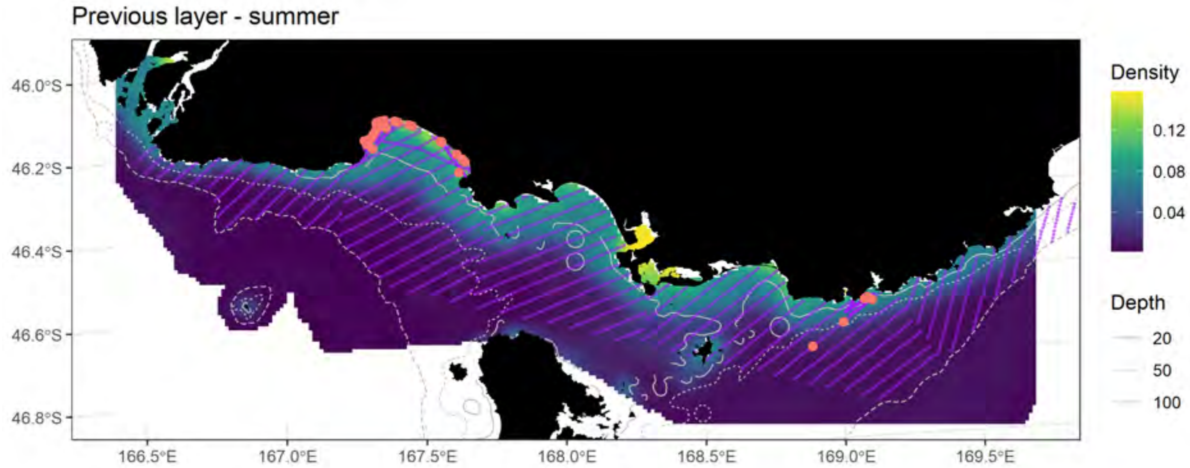

Figure A.5: **Previous Hector's dolphin distribution layers for the south coast of the South Island in summer. Red points are locations where dolphins were observed by the 2010 aerial survey, small purple points are the associated effort.**

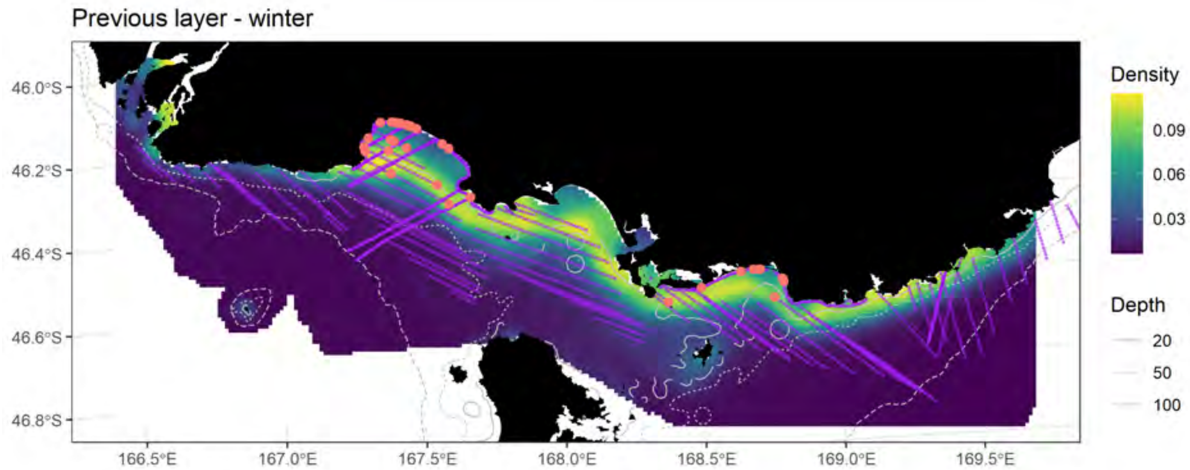

Figure A.6: **Previous Hector's dolphin distribution layers for the south coast of the South Island in winter. Red points are locations where dolphins were observed by the 2010 aerial survey, small purple points are the associated effort.**

APPENDIX B. SPATIAL COVARIATES

All candidate environmental covariates offered to Hector's dolphin distribution models are summarised in Table B.1. These covariates were either monthly (Figure B.1 to Figure B.4), quarterly (Figure B.5 and Figure B.7), summer/winter (Figure B.6), or temporally static (Figure B.8 to Figure B.10).

Table B.1: Summary of all spatial environmental covariates offered to spatial predictive models of Hector's dolphin sighting rate.

Covariate	Spatial resolution	Temporal resolution	Source
Mean sea surface temperature (sst, °C)	~0.25 degree	Monthly, 1979-2020	ERA5 climate data re-analysis (https://cds.climate.copernicus.eu/cdsapp#!/dataset/reanalysis-era5-single-levels-monthly-means?tab=overview)
Mean SST gradient (sst_gradient, °C)	~0.25 degree	Monthly, 1979-2020	Calculated from SST data
Mean wind speed (wind, metres s^{-1})	~0.25 degree	Monthly, 1979-2020	ERA5 climate data re-analysis (https://cds.climate.copernicus.eu/cdsapp#!/dataset/reanalysis-era5-single-levels-monthly-means?tab=overview)
Sea level anomaly (sla, cm)	0.25 degree	Monthly, 1993-2020	Satellite altimetry data processed and provided by Copernicus Climate Change Service (C3S) (https://cds.climate.copernicus.eu/cdsapp#!/dataset/satellite-sea-level-global?tab=overview)
Surface chlorophyll-a concentration (chl, mg m^{-3})	4 km	Quarterly climatology, 2003-2020	Satellite ocean colour data processed and provided by NASA GIOVANNI (https://giovanni.gsfc.nasa.gov/giovanni/)
Surface turbidity proxy 1 (turbidity1, Nephelometric Turbidity Units)	1 km	Summer/winter climatology, 2007-2018	Satellite ocean colour data derived using method described by Pinkterton et al. (2018). Layers originally produced for MPI project PRO2017-12 (Roberts et al. 2019a)
Surface turbidity proxy 2 (turbidity2, diffuse attenuation coefficient at 490 nm)	4 km	Quarterly climatology, 2003-2020	Satellite ocean colour data product (Kd490) processed and provided by NASA GIOVANNI (https://giovanni.gsfc.nasa.gov/giovanni/)
Bathymetric depth (depth, m)	250 m	Static	NIWA (https://niwa.co.nz/our-science/oceans/bathymetry/download-the-data)
Bathymetric slope (slope, m)	1 km	Static	Derived from bathymetry
Distance from shore (distance_to_shore, km)	1 km	Static	Derived from bathymetry
Tidal current speed (current, ms^{-1})	1 km	Static	Leathwick et al. (2012), processed by Stephenson et al. (2020).
Probability of presence of selected key prey species	1 km	Static	Derived from spatial model fitted to research trawl survey catch data. Layers originally produced for MPI project PRO2017-12 (Roberts et al. 2019a). Only species with positive correlation with dolphins sighting rate were used here, these being red cod (*Pseudophycis bachus*), flounder species (*Peltorhamphus* spp.), ahuru (*Auchenoceros punctatus*), and sprat sp. (*Sprattus* spp.).
% sand of benthic sediments (sand)	1 km	Static	Bostock et al. (2018) https://nzodn.nz/
% mud of benthic sediments (mud)	1 km	Static	Bostock et al. (2018) https://nzodn.nz/
% gravel of benthic sediments (gravel)	1 km	Static	Bostock et al. (2018) https://nzodn.nz/

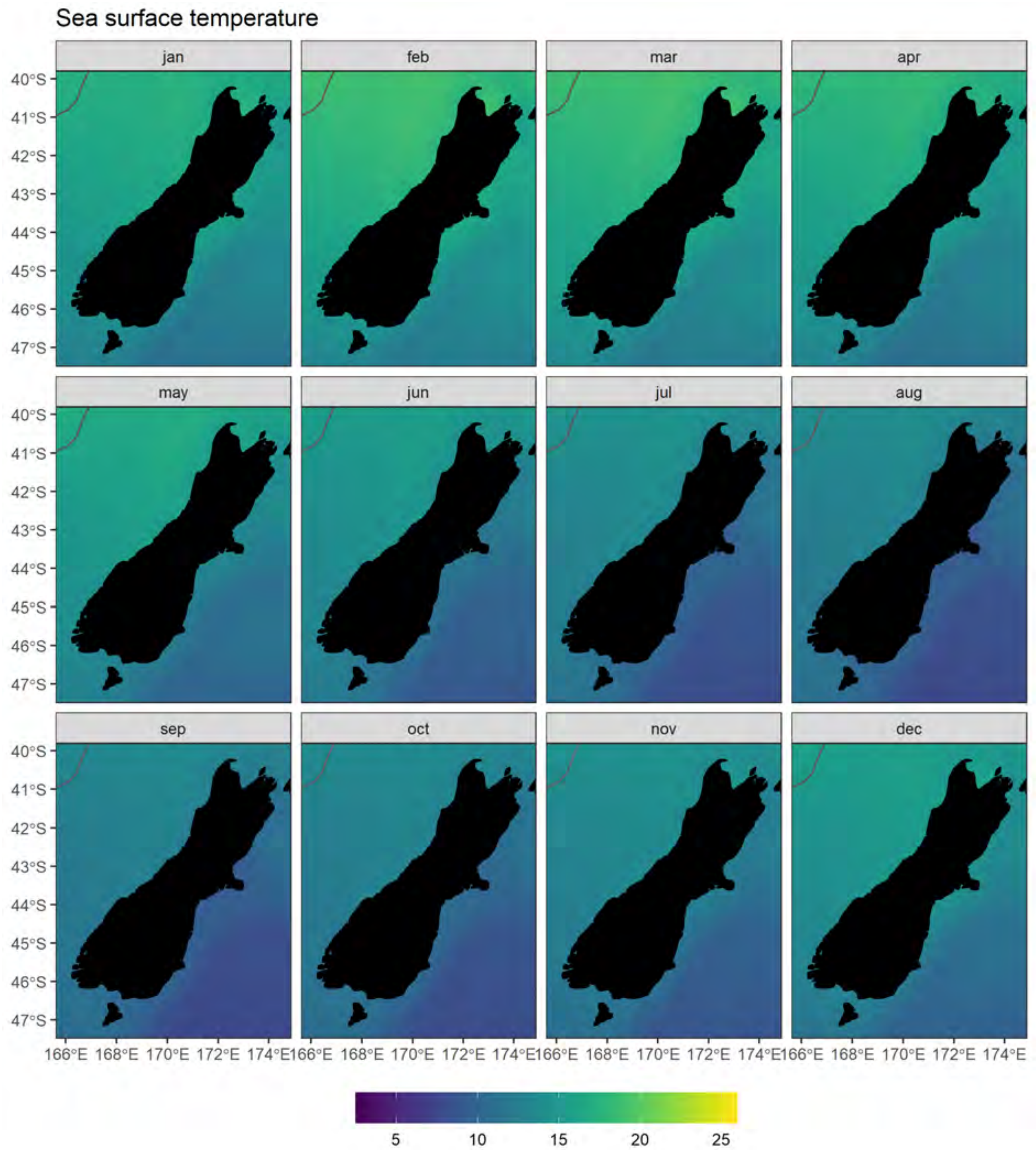

Figure B.1: **Mean sea surface temperature by month (sst, °C). Note that monthly climatologies are shown here, which were used for model predictions, although models were fitted to monthly data in the respective year of observation.**

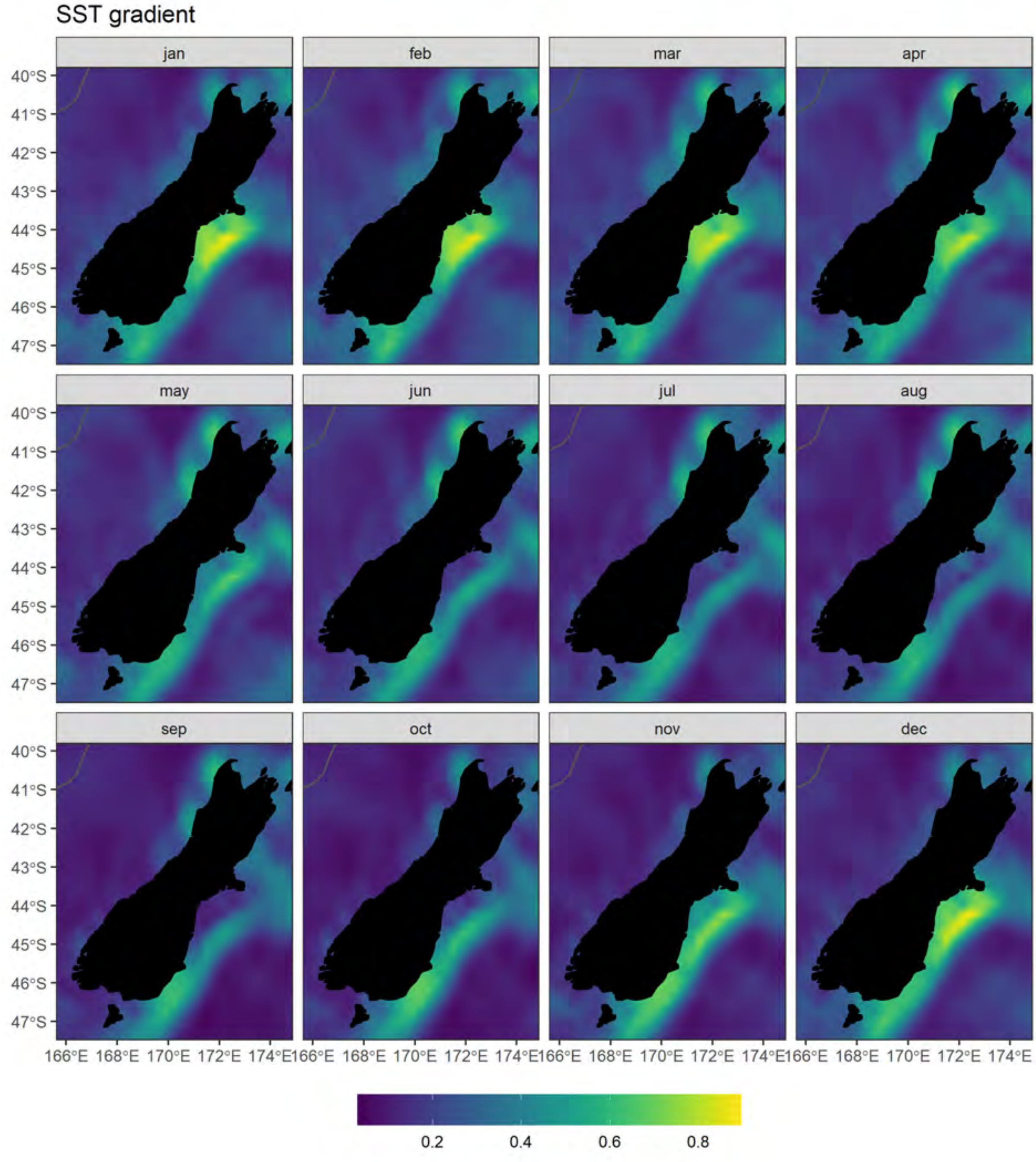

Figure B.2: **Mean sea surface temperature gradient by month (sst_gradient, °C). Note that monthly climatologies are shown here, which were used for model predictions, although models were fitted to monthly data in the respective year of observation.**

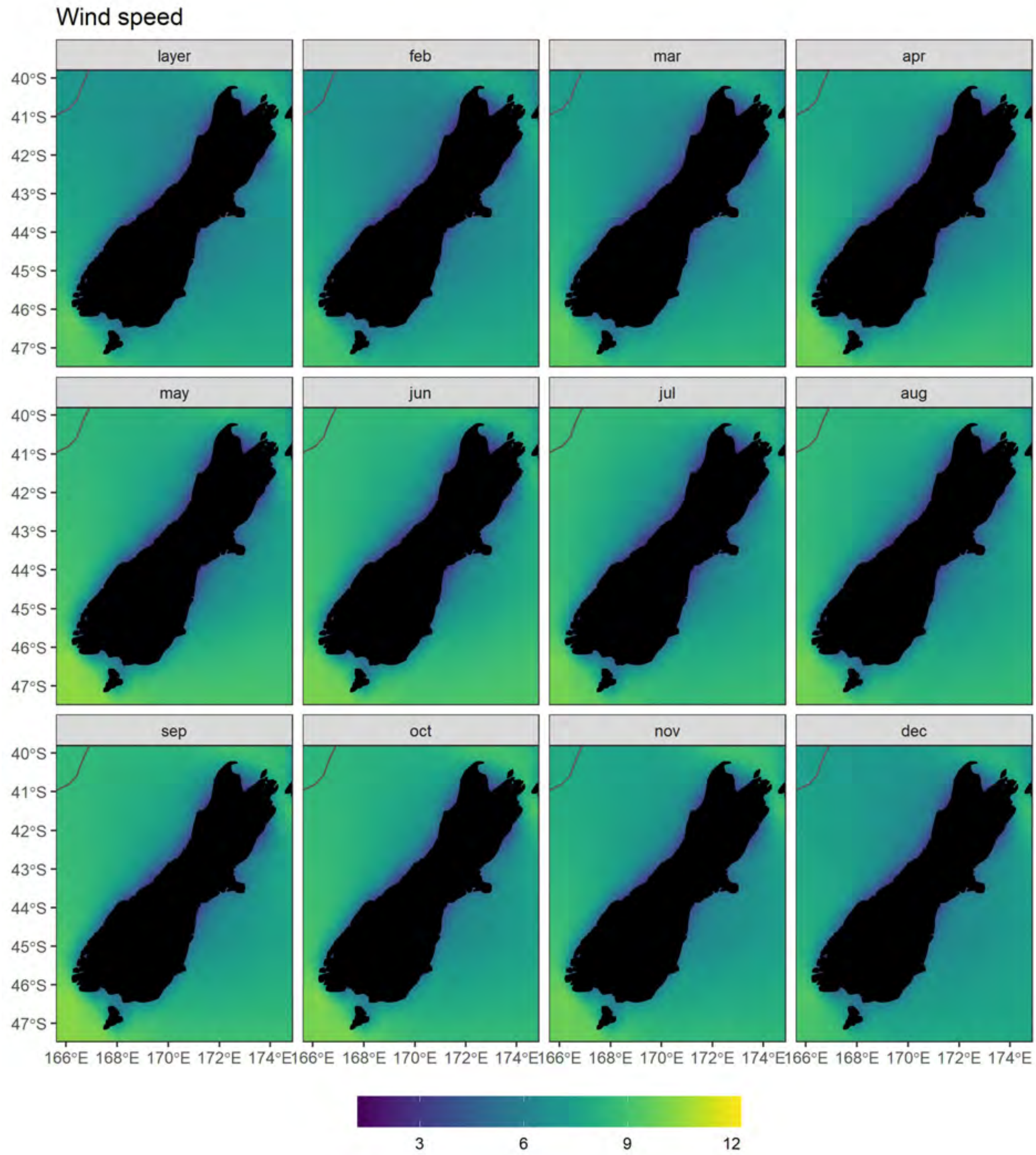

Figure B.3: **Mean wind speed by month (wind, metres s^{-1}). Note that monthly climatologies are shown here, which were used for model predictions, although models were fitted to monthly data in the respective year of observation.**

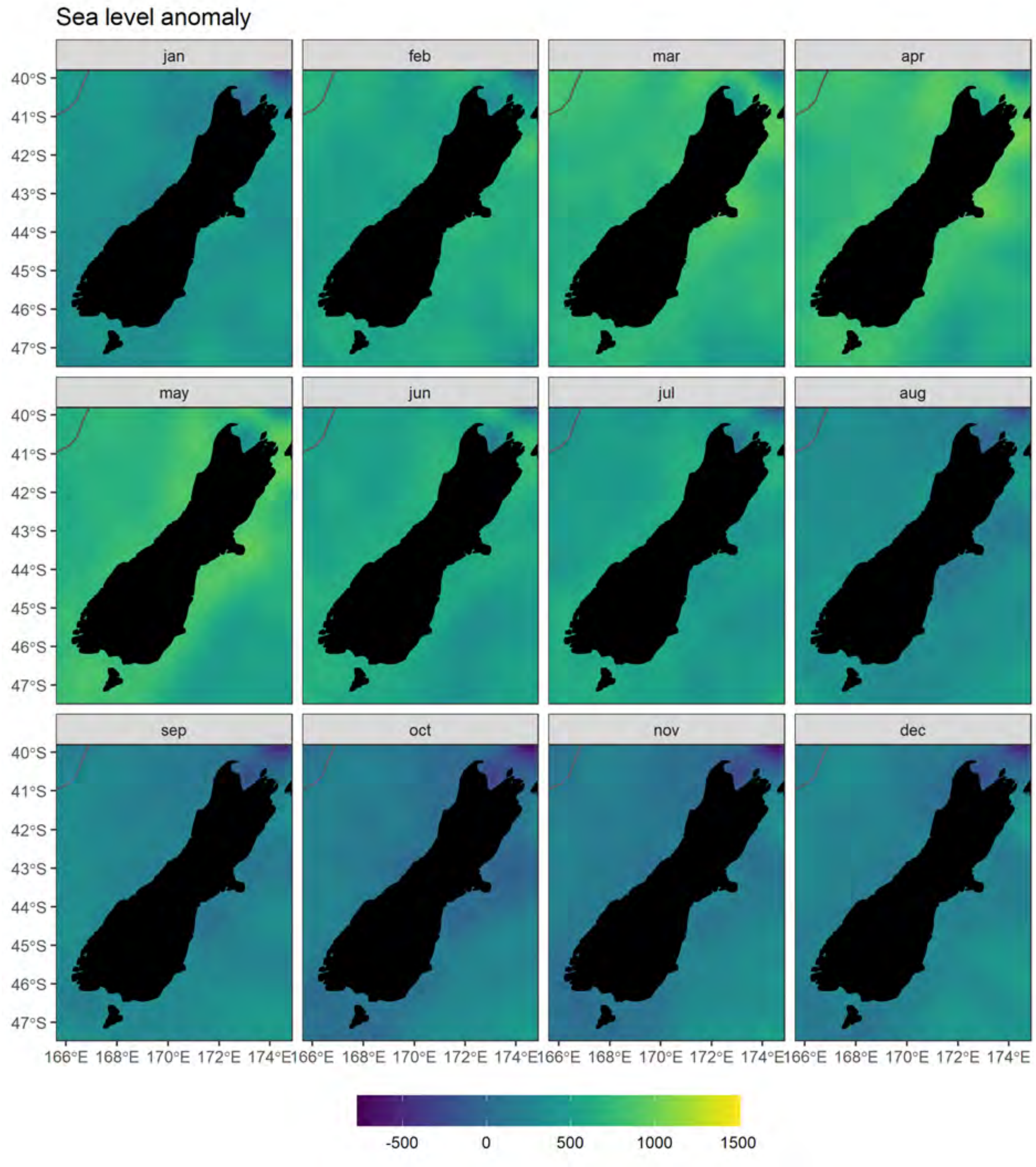

Figure B.4: Mean sea level anomaly by month (sla, cm). Note that monthly climatologies are shown here, which were used for model predictions, although models were fitted to monthly data in the respective year of observation.

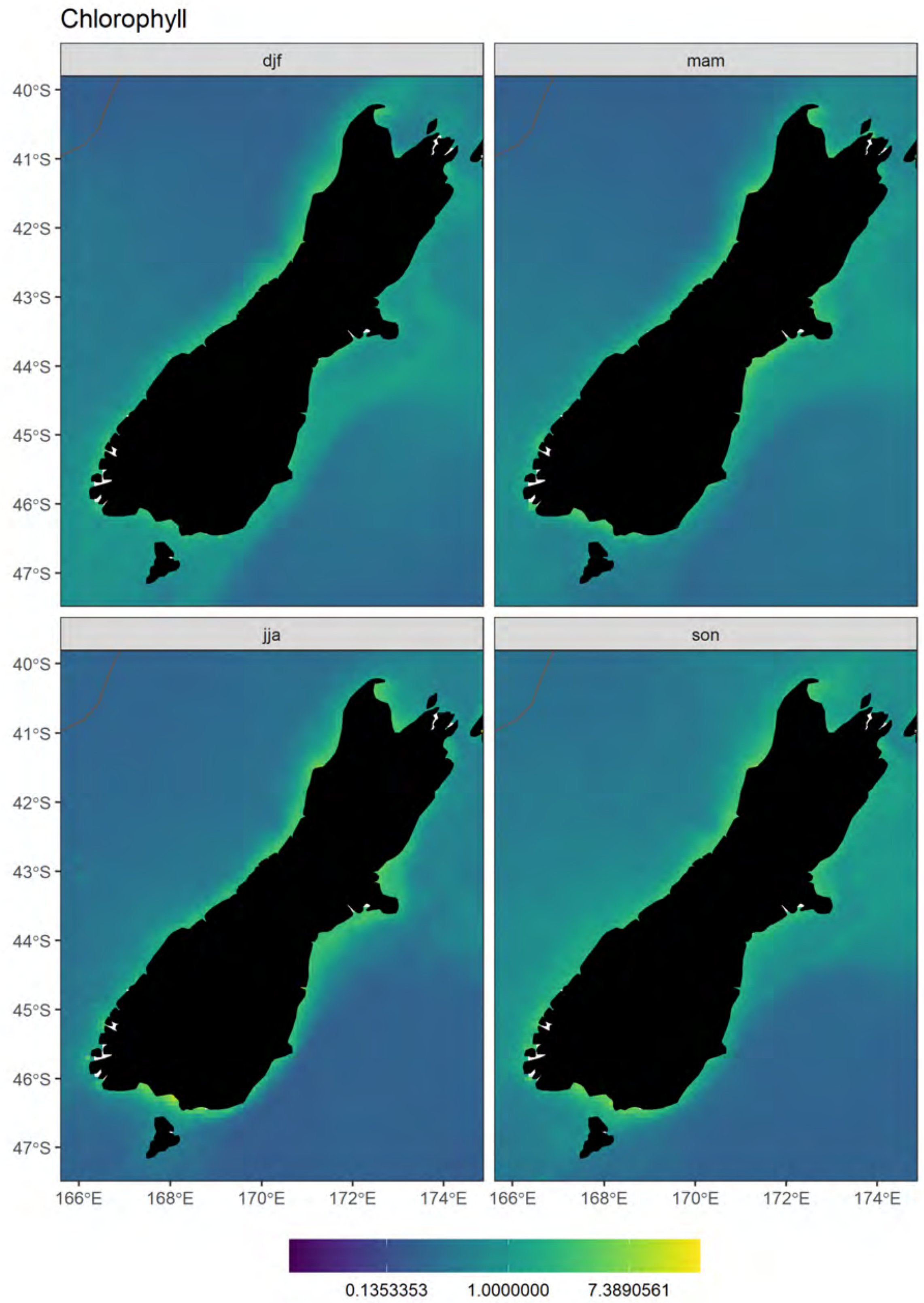

Figure B.5: Mean sea surface chlorophyll-a concentration by quarter (chla, mg m^{-3}) ('djf' = December-February, 'mam' = March-May, 'jja' = June-August, 'son' = September-November). These quarterly climatologies were used for both model fitting and prediction.

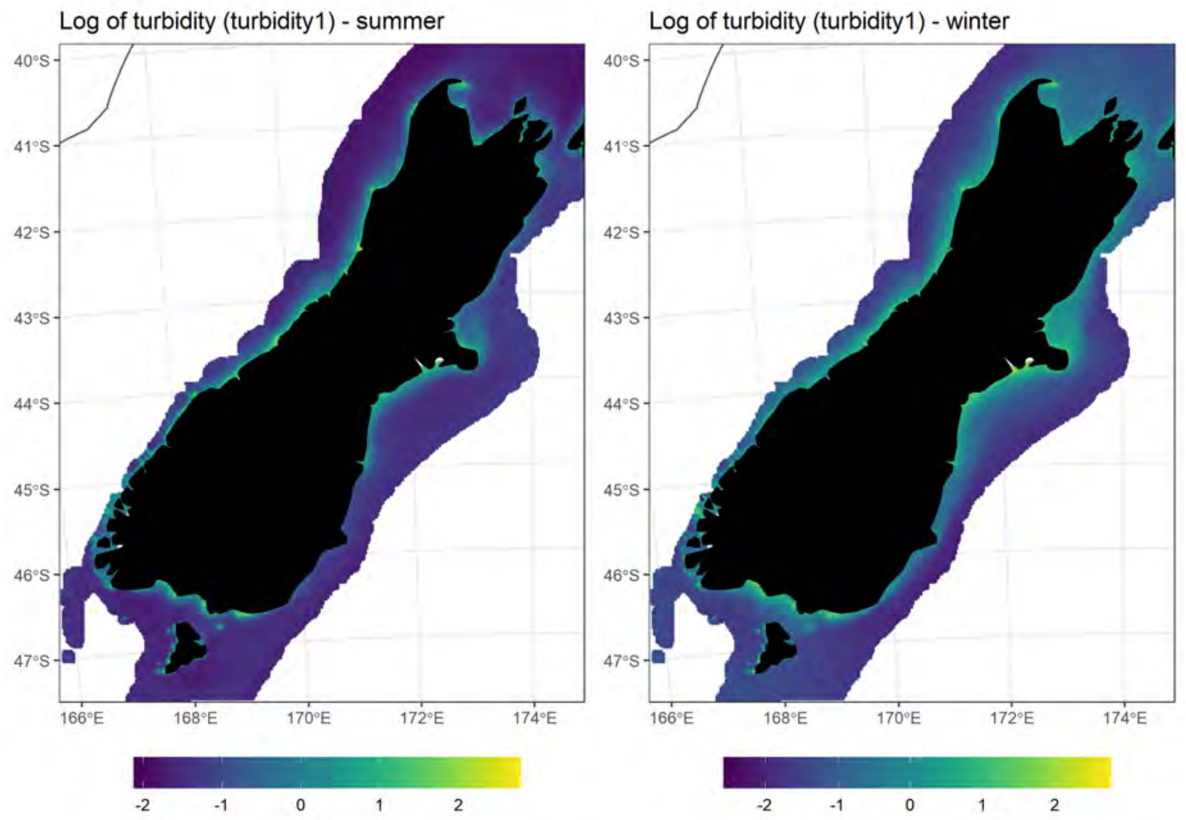

Figure B.6: **Mean sea surface turbidity for summer and winter seasons (turbidity1, Nephelometric Turbidity Units). These summer/winter climatologies were used for both model fitting and prediction and are log-transformed in these plots.**

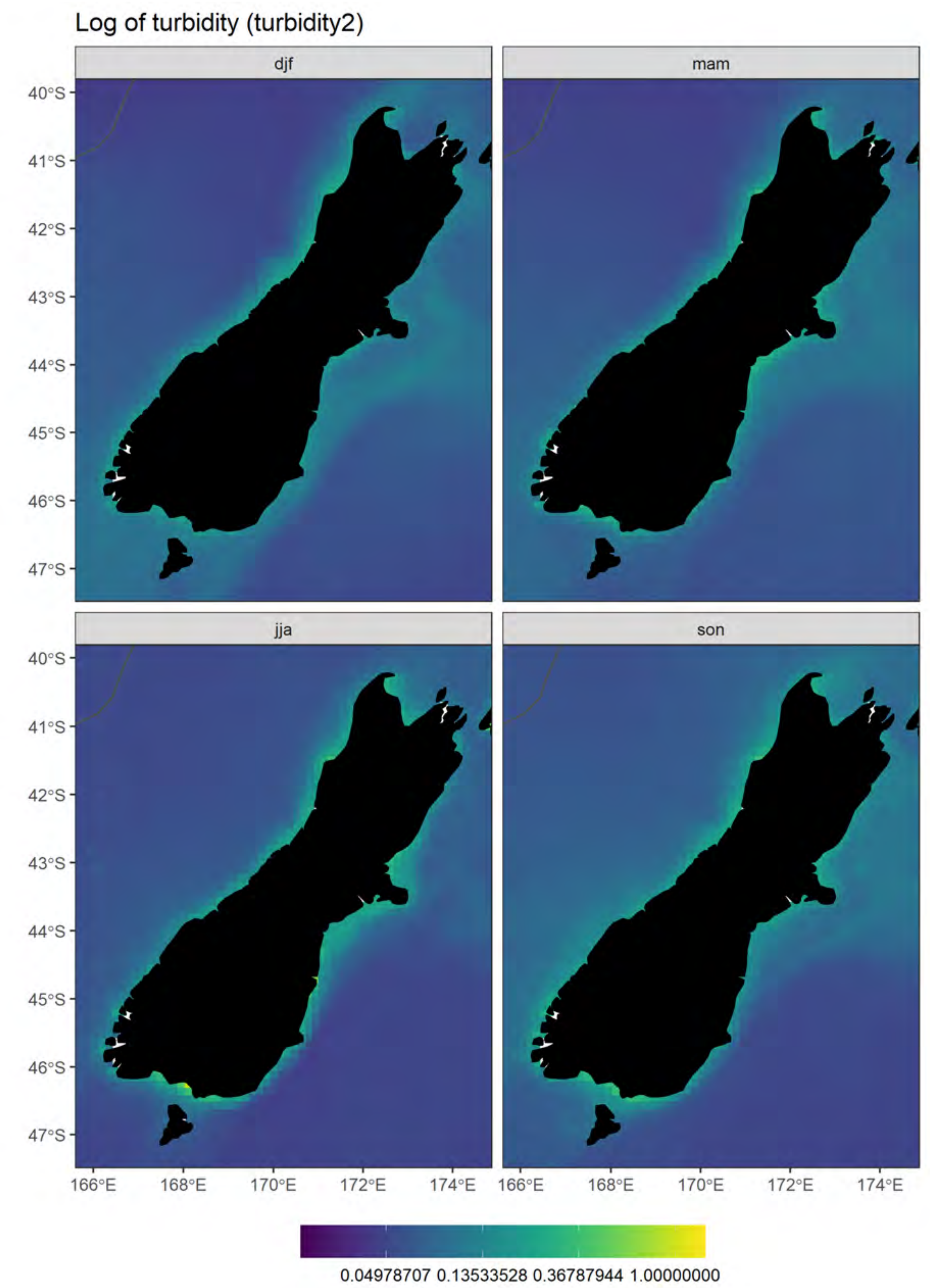

Figure B.7: Mean sea surface turbidity by quarter (turbidity2, diffuse attenuation coefficient at 490 nm) ('djf' = December–February, 'mam' = March–May, 'jja' = June–August, 'son' = September–November). These quarterly climatologies were used for both model fitting and prediction are log-transformed in these plots.

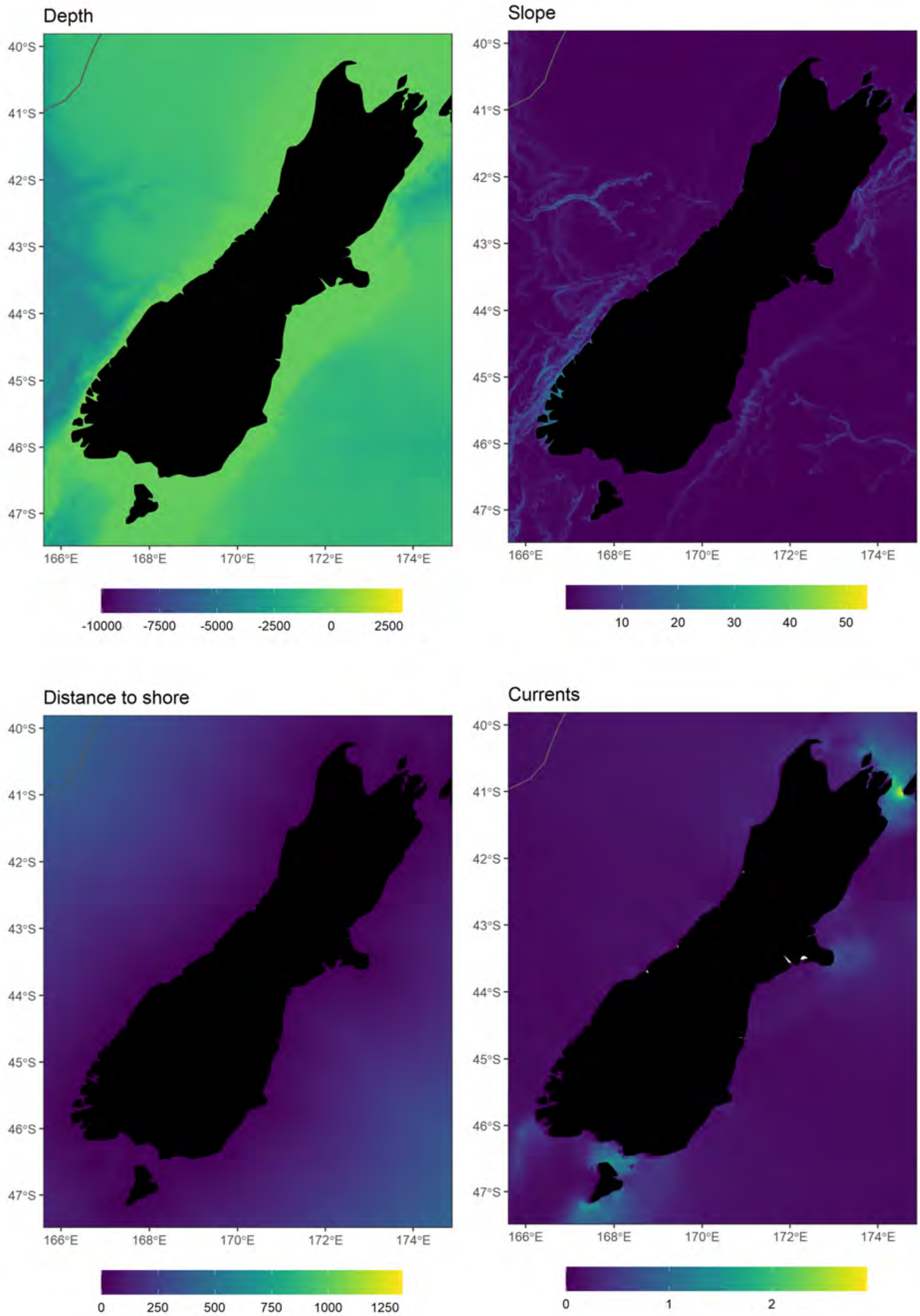

Figure B.8: Bathymetric depth (depth, m), bathymetric slope (slope, m), distance to shore (shore, km), and tidal current speed (currents, m s^{-1}).

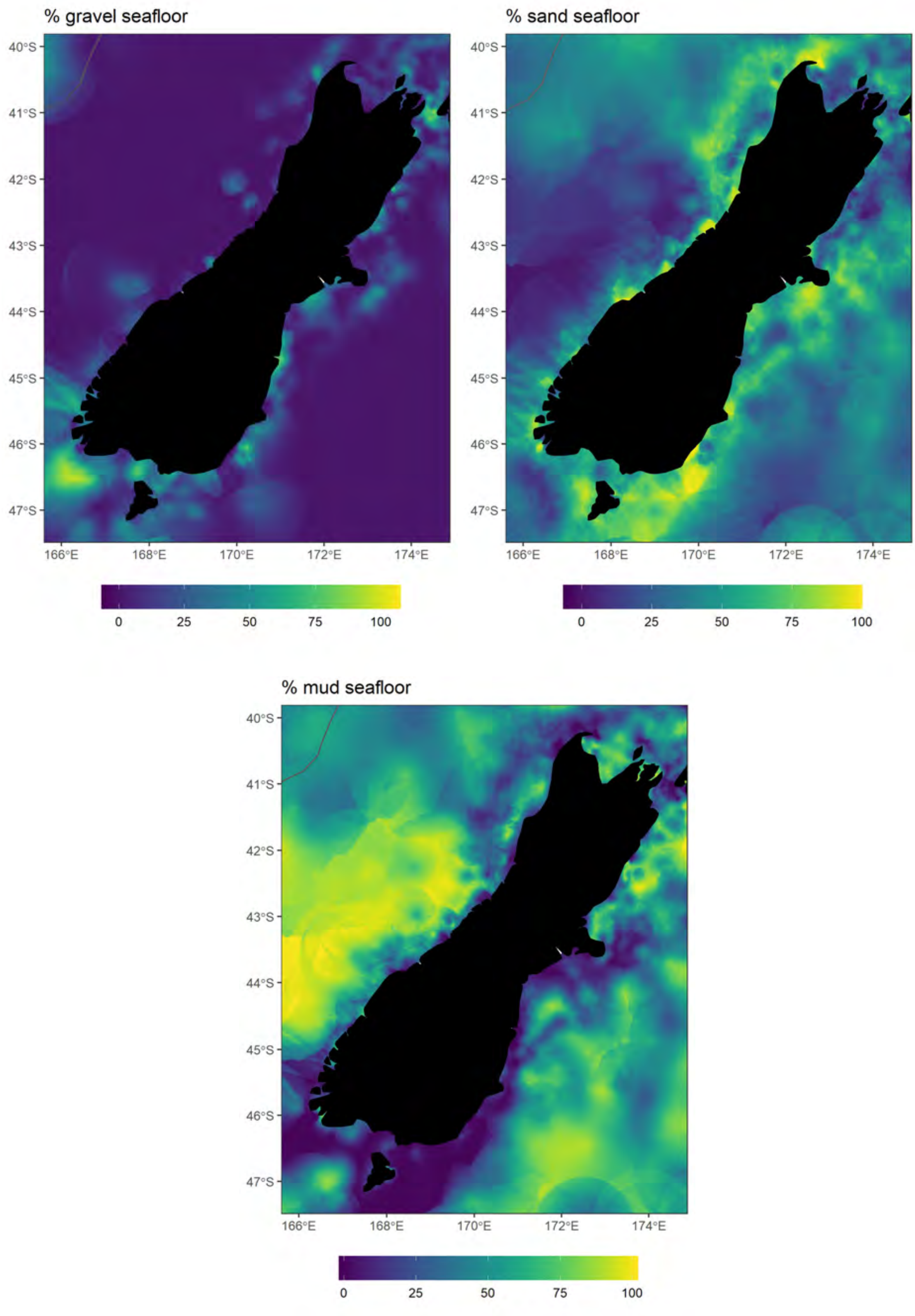

Figure B.9: Percentage sand, gravel, and mud in benthic surface sediments.

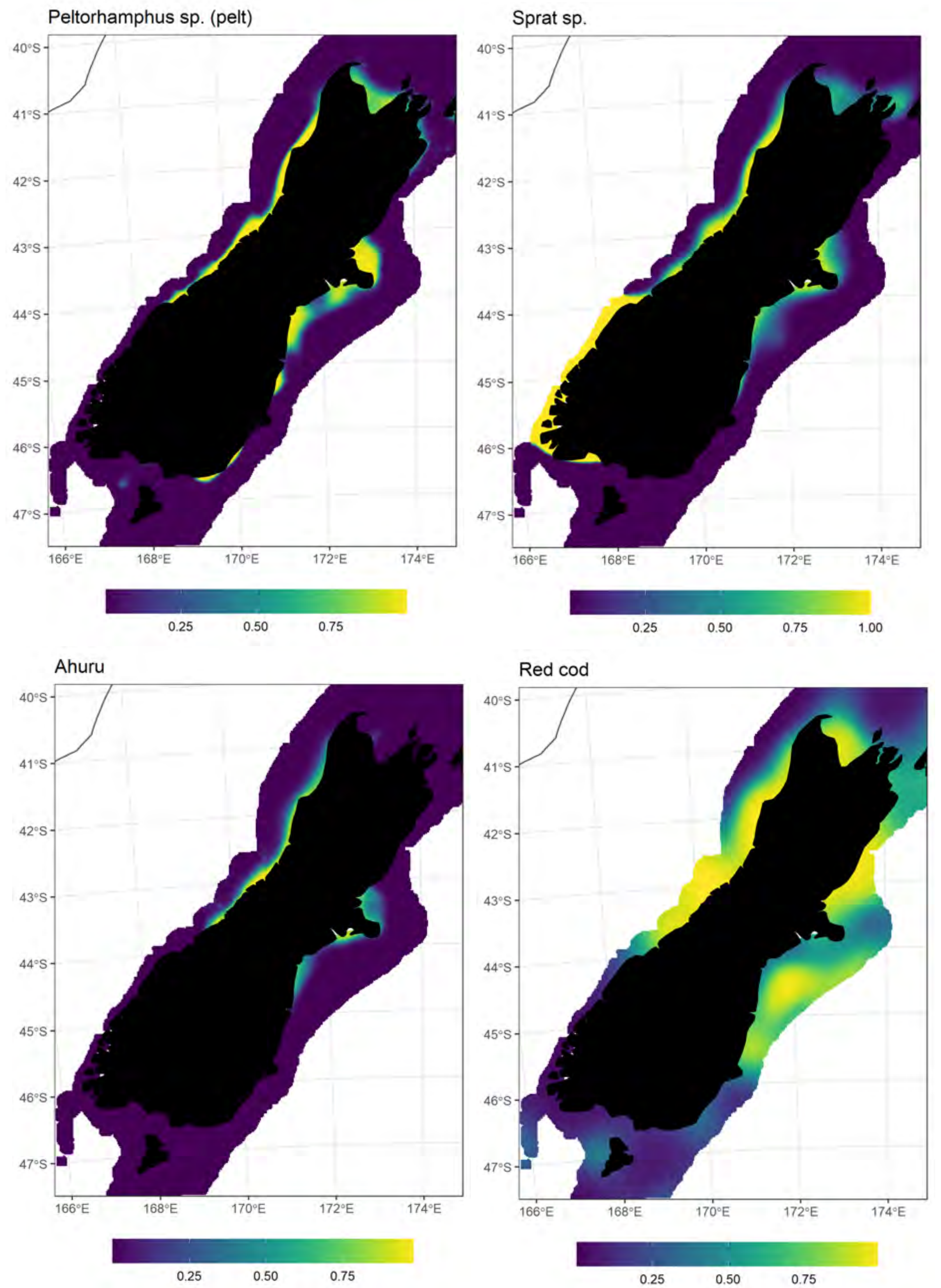

Figure B.10: Probability of presence of key Hector's dolphin prey taxa: *Peltorhamphus* spp. (flounder genus) (pelt), sprat species (sprat), red cod (red cod), and ahuru (ahuru).

APPENDIX C. HECTOR'S DOLPHIN SPATIAL DATA SUMMARIES

Spatial distribution models were fitted to sightings-based spatial information from multiple sources. See Section 2.1 for an overview of data sources and Section 2.2 for methods used to process these data prior to spatial model fitting. A temporal summary of the data used for spatial distribution modelling is shown in Table C.1.

Table C.1: The temporal distribution of sighting events used to model the spatial distribution of Hector's dolphins.

	Season		Year																							
Source	Summer	Winter	1993	1994	1995	1996	1997	2004	2005	2006	2007	2008	2009	2010	2011	2012	2013	2014	2015	2016	2017	2018	2019	2020	2021	2022
aerial_ecsi	7 040	7 854	0	0	0	0	0	0	0	0	0	0	0	0	0	0	14 894	0	0	0	0	0	0	0	0	0
aerial_wcsi	3 685	4 185	0	0	0	0	0	0	0	0	0	0	0	0	0	0	0	0	7 870	0	0	0	0	0	0	0
aerial_scsi_2012_esw	493	1 236	0	0	0	0	0	0	0	0	0	0	0	1 729	0	0	0	0	0	0	0	0	0	0	0	0
aerial_scsi_2012_line	1 675	1 599	0	0	0	0	0	0	0	0	0	0	0	3 274	0	0	0	0	0	0	0	0	0	0	0	0
aerial_scsi_2018	2 784	0	0	0	0	0	0	0	0	0	0	0	0	0	0	0	0	0	0	0	0	2 784	0	0	0	0
nomad	6 741	3 971	0	0	0	0	0	0	0	0	0	0	699	530	4	92	1 211	306	1 172	2 534	4 123	41	0	0	0	0
rodda	1 598	1 333	0	0	0	0	0	46	1 677	1 208	0	0	0	0	0	0	0	0	0	0	0	0	0	0	0	0
weir1	783	41	0	0	0	0	0	0	0	0	0	0	0	0	0	0	0	94	121	123	250	236	0	0	0	0
weir2	356	228	0	0	0	0	0	0	0	0	0	0	0	0	0	0	0	0	0	0	0	115	239	230	0	0
brager	2 280	470	194	713	718	719	406	0	0	0	0	0	0	0	0	0	0	0	0	0	0	0	0	0	0	0
public	2 208	605	0	0	0	0	0		349	2 381	0	0	0	0	0	0	0	14	12	15	6	14	7	15	0	0
public_update	2 477	660	0	0	0	0	0		367	2 544	0	0	0	0	0	15	12	16	8	16	8	16	9	25	38	87

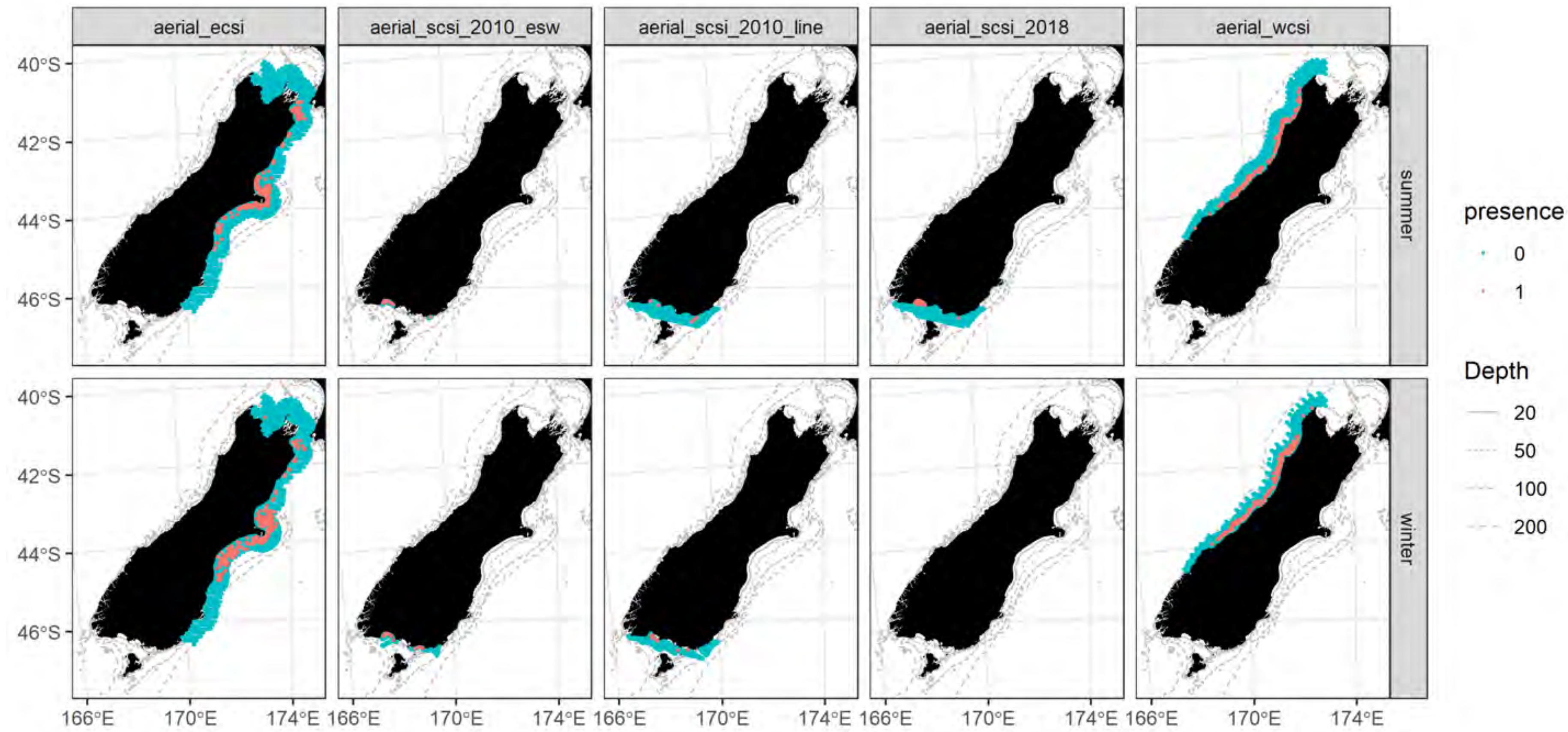

Figure C.1: **Spatial plot of sighting effort data used to model the spatial distribution of Hector's dolphins, including all aerial survey data. Blue circles and pink circles indicate negative and positive sighting events, respectively. Depth contours are shown for 20–200 m.**

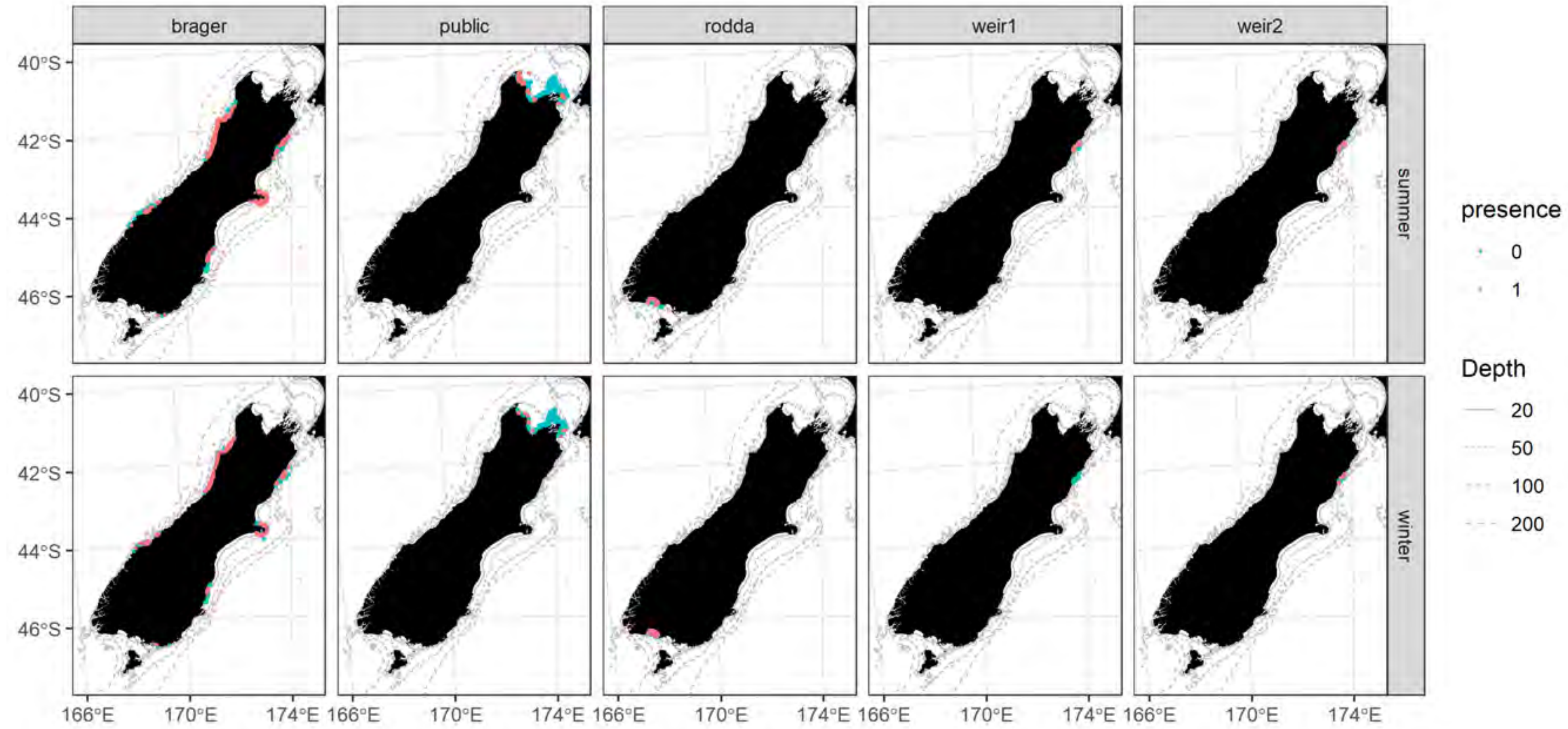

Figure C.2: Spatial plot of sighting effort data used to model the spatial distribution of Hector's dolphins, excluding all aerial survey data. Blue circles and pink circles indicate negative and positive sighting events, respectively. Note that fisheries observer data were excluded from this plot as per the conditions of data sharing. Depth contours are shown for 20–200 m.

North coast South Island

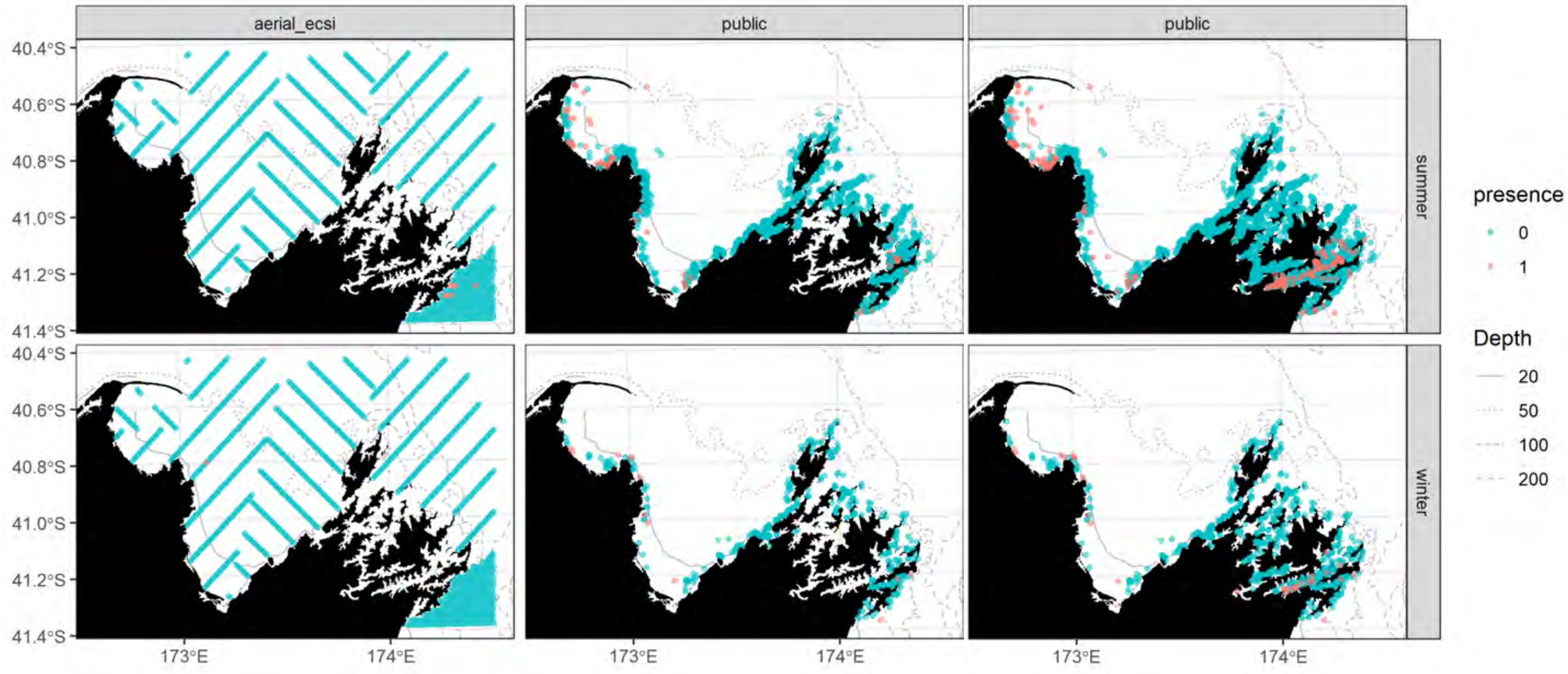

Figure C.3: Spatial plot of sighting effort data used to model the spatial distribution of Hector's dolphins along the north coast of the South Island. Blue circles and pink circles indicate negative and positive sighting events, respectively. The right-hand plots display the 2022 update of the public sightings data shown in the central column. Depth contours are shown for 20–200 m.

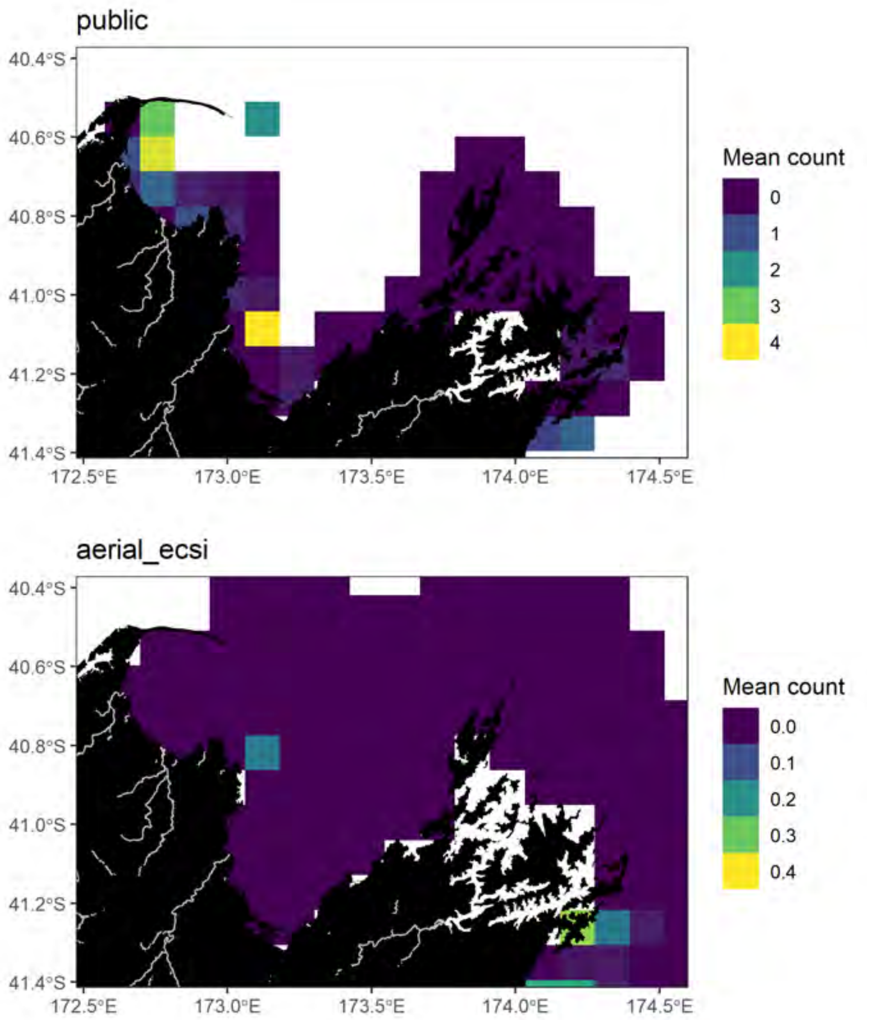

Figure C.4: **Spatial plot of mean count of Hector's dolphins by data source along the north coast of the South Island. Counts are summarised by 10-km grid cell.**

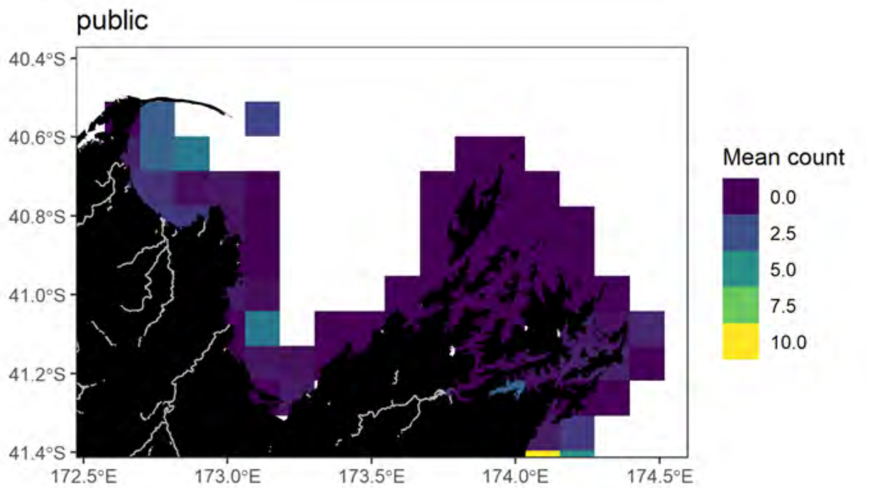

Figure C.5: **Spatial plot of mean count of Hector's dolphins along the north coast of the South Island from public sightings using updated records up to 2022. Counts are summarised by 10-km grid cell.**

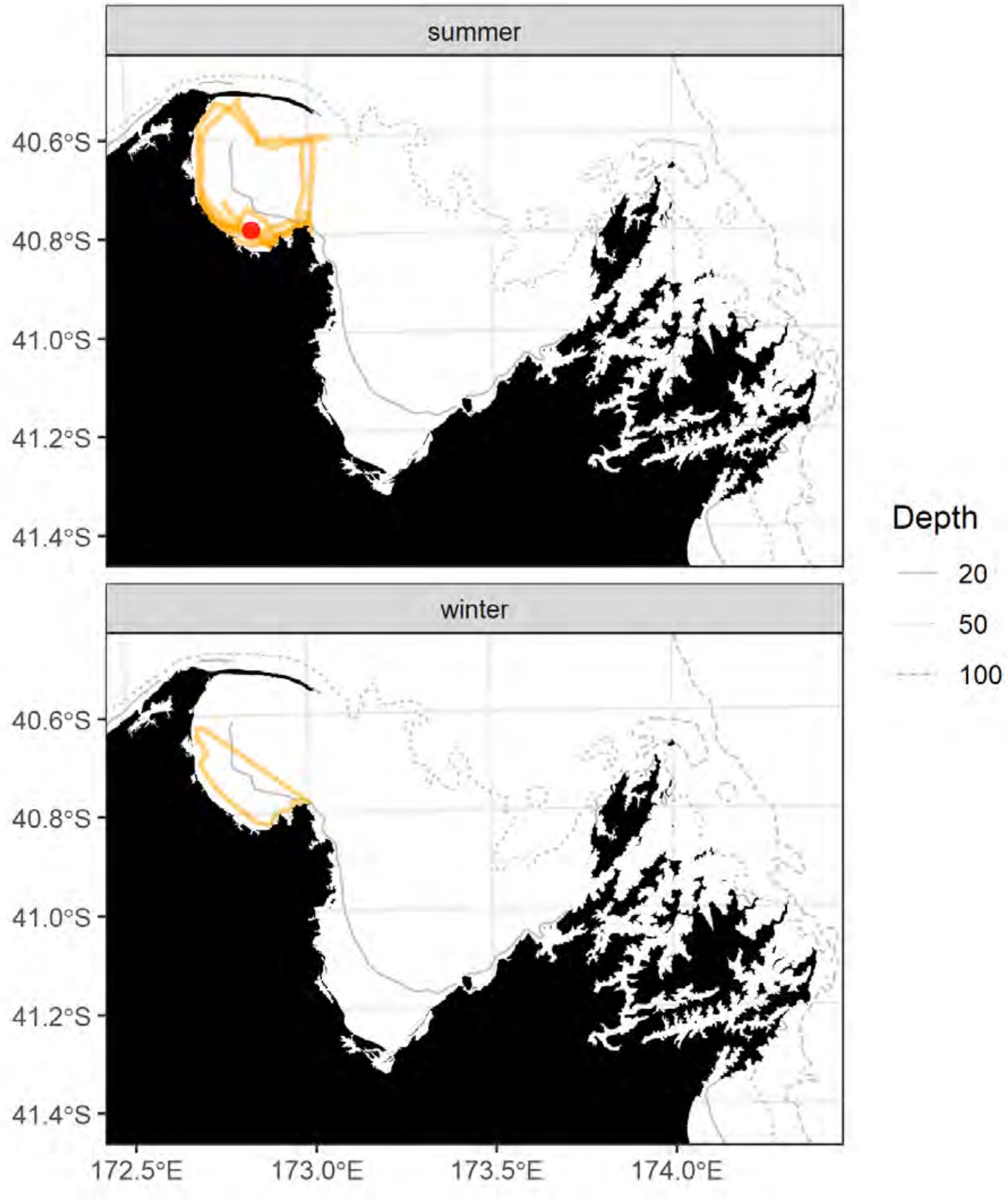

Figure C.6: **Spatial plot of Golden Bay DOC boat survey track lines (orange lines) and solitary on-effort sighting of a pair of Hector's dolphins (red point), by season. Depth contours are shown for 20–100 m. Data source: Mike Ogle (DOC).**

Kaikōura coast

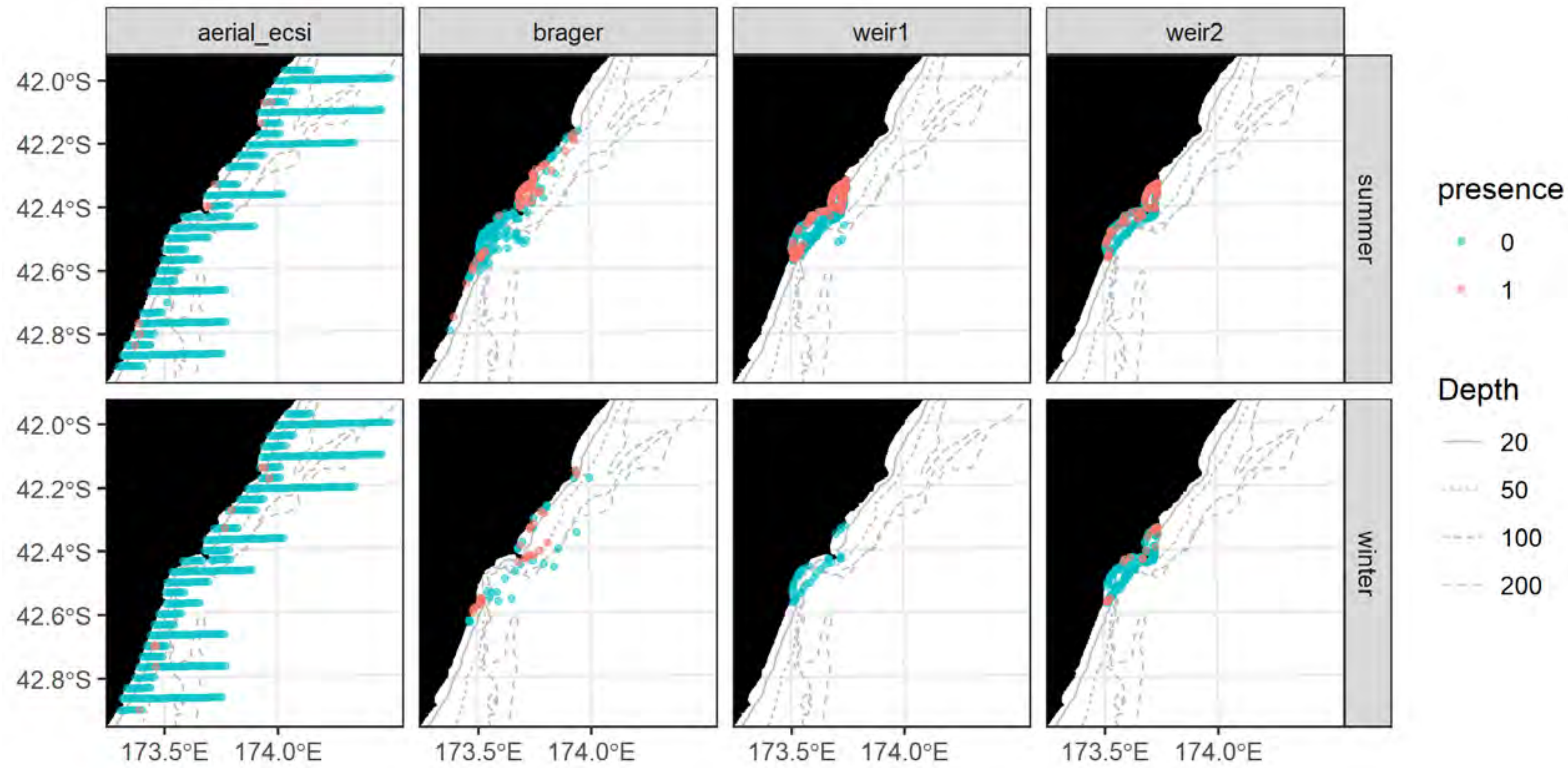

Figure C.7: Spatial plot of sighting effort data used to model the spatial distribution of Hector's dolphins along the Kaikōura coast. Blue circles and pink circles indicate negative and positive sighting events, respectively. Fisheries observer data (nomad) were omitted from this plot because high resolution plots of these data were not permitted under the data sharing agreement. Depth contours are shown for 20–200 m.

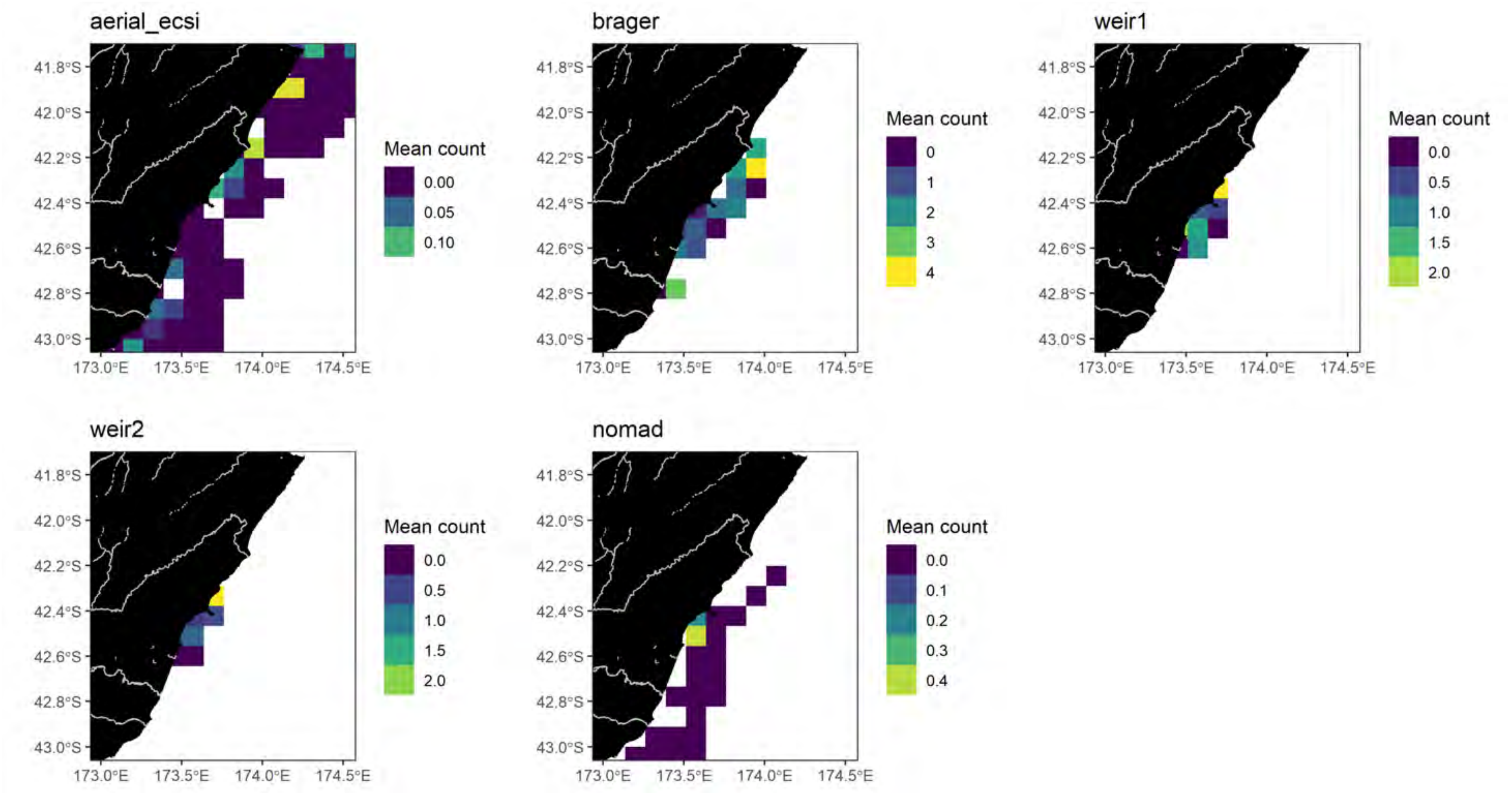

Figure C.8: Spatial plot of mean count of Hector's dolphins by data source along the Kaikōura coast. Counts are summarised by 10-km grid cell.

South coast of the South Island

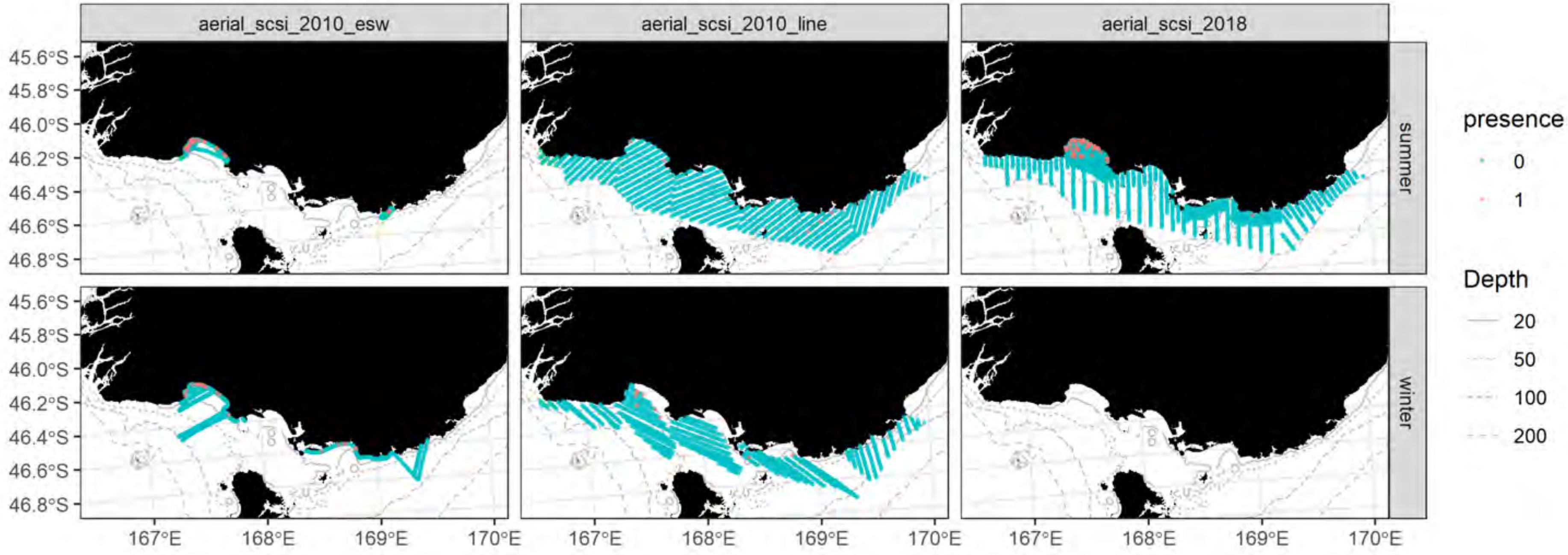

Figure C.9: **Spatial plot of sighting effort data used to model the spatial distribution of Hector's dolphins along the South coast of the South Island, including all aerial survey data. Blue circles and pink circles indicate negative and positive sighting events, respectively. Depth contours are shown for 20–200 m.**

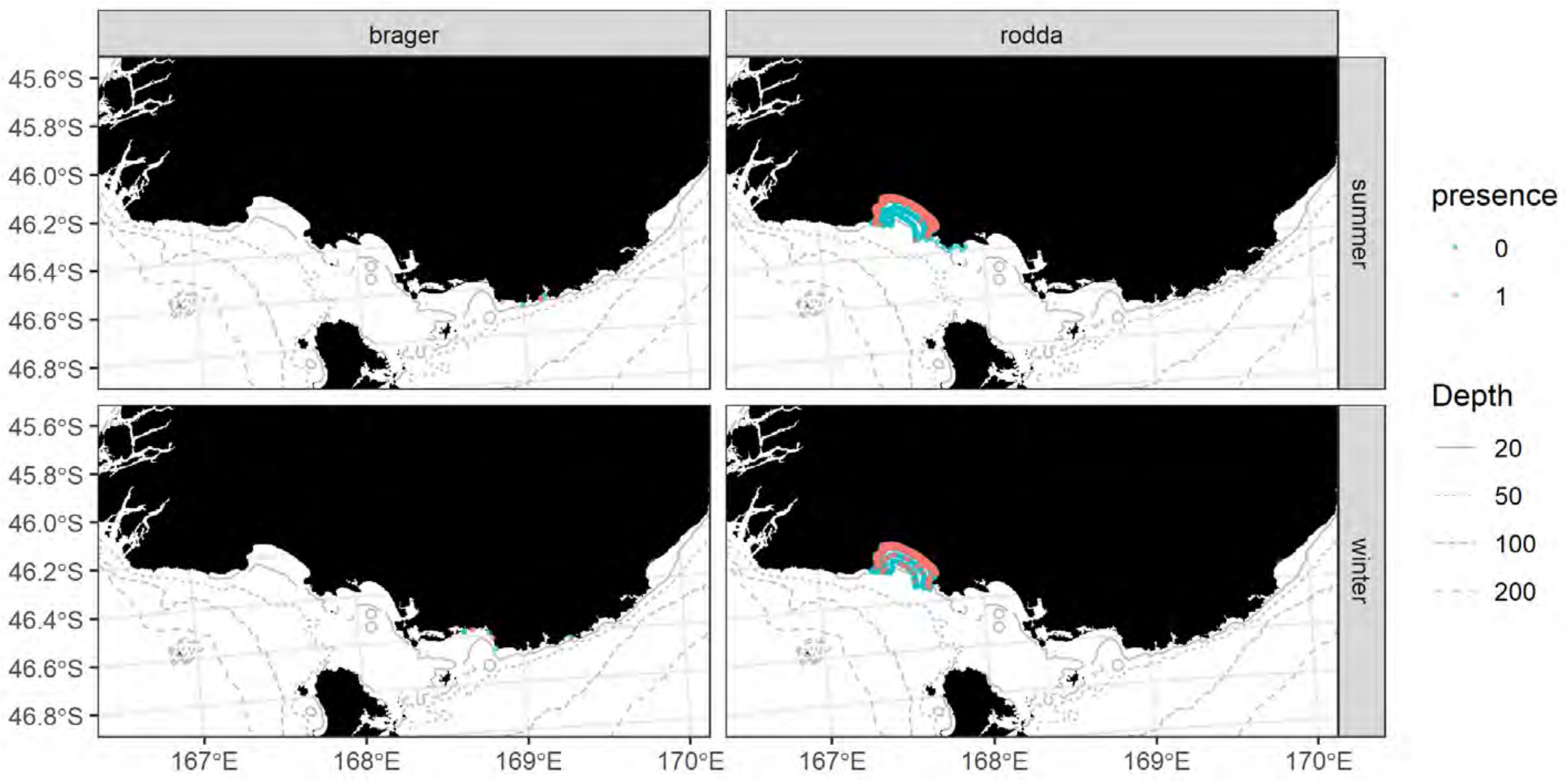

Figure C.10: **Spatial plot of sighting effort data used to model the spatial distribution of Hector's dolphins along the south coast of the South Island, excluding all aerial survey data. Blue circles and pink circles indicate negative and positive sighting events, respectively. Note that fisheries observer data are not shown here, as per the data sharing agreement for these data. Depth contours are shown for 20–200 m.**

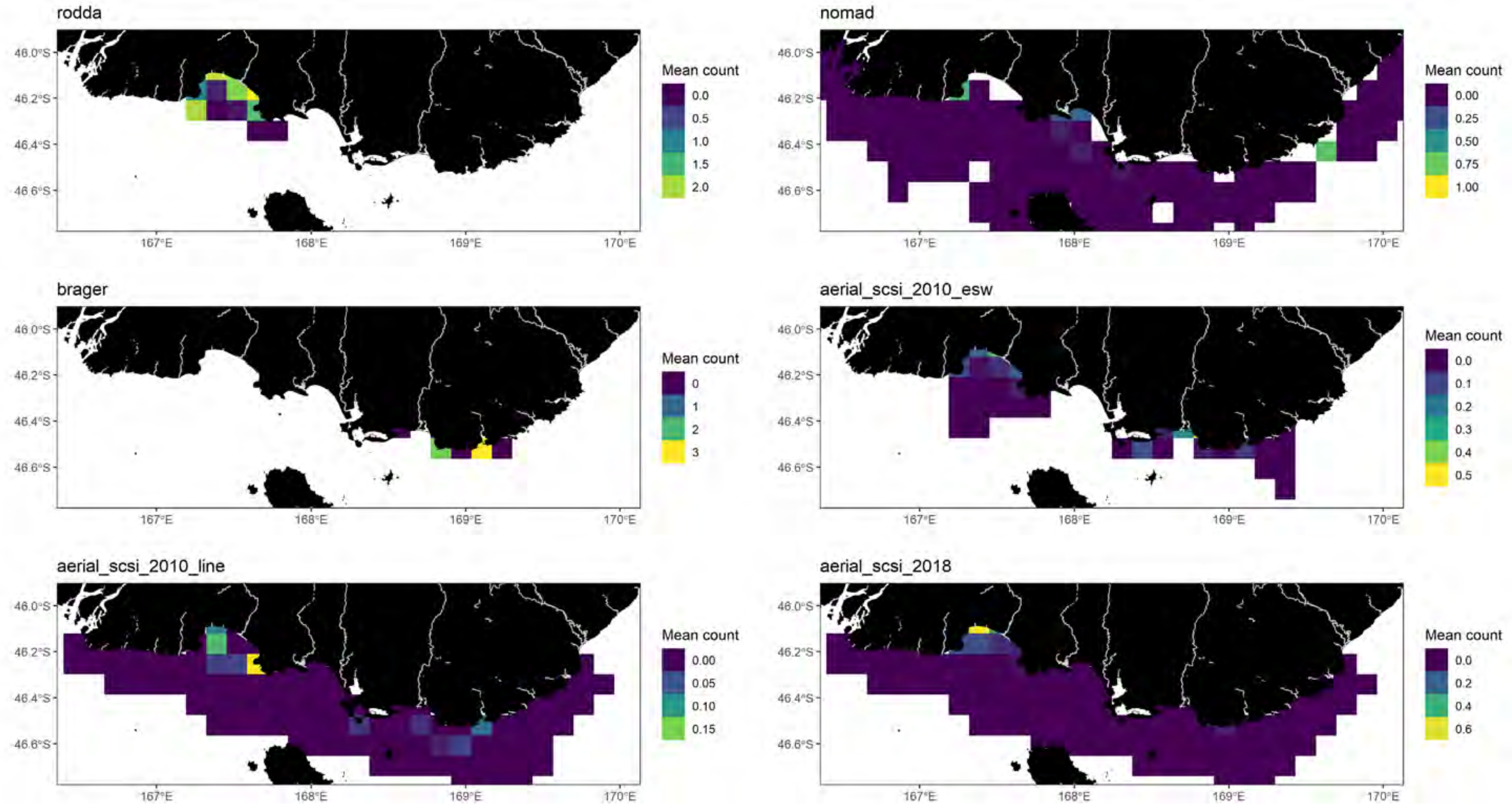

Figure C.11: Spatial plot of mean count of Hector's dolphins by data source along the south coast of the South Island. Counts are summarised by 10-km grid cell.

APPENDIX D. SPATIAL DISTRIBUTION MODEL DIAGNOSTIC PLOTS

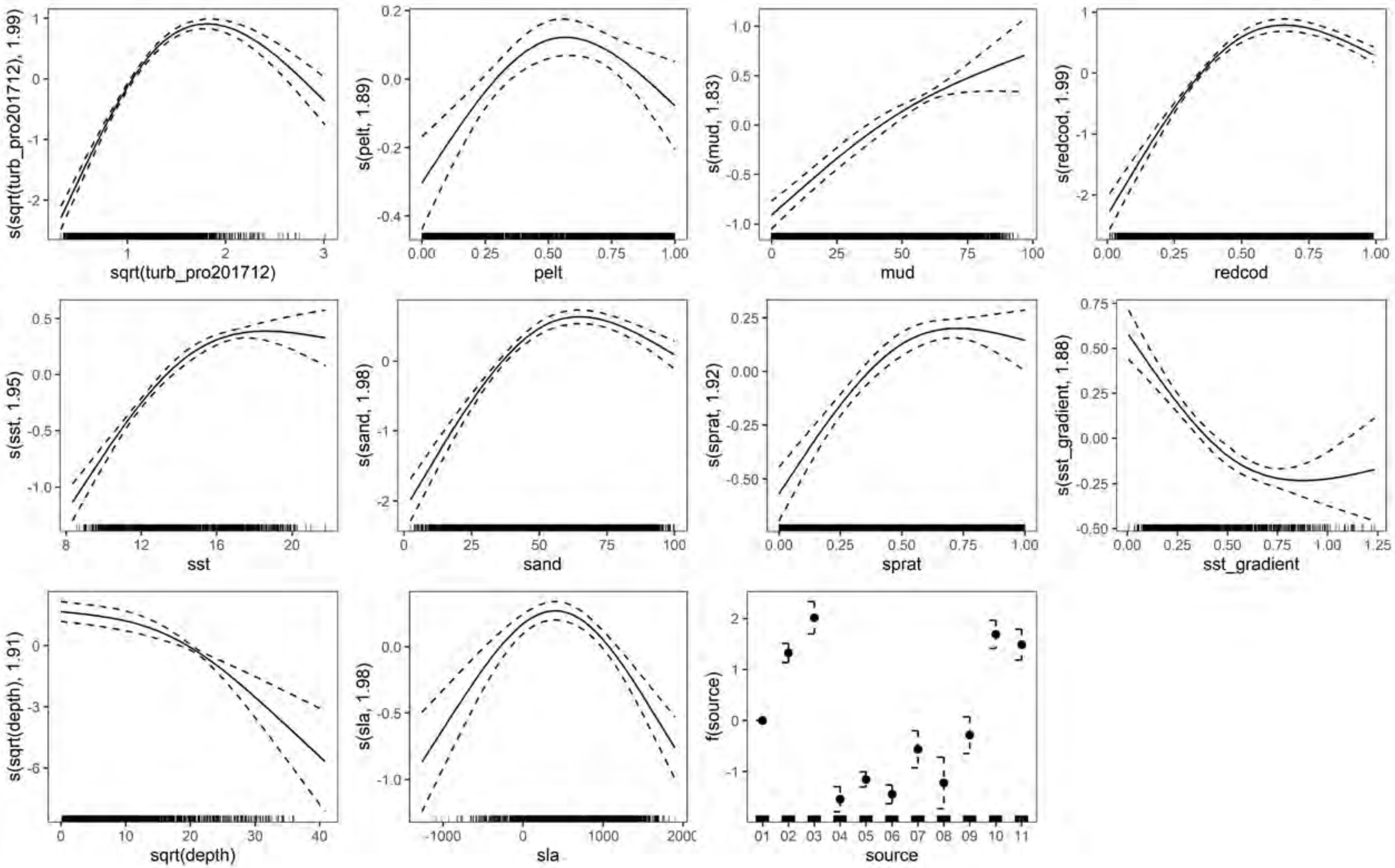

Figure D.1: Term plots for the model *hab10*. Model sources were: '01' = nomad, '02' = brager, '03' = rodda, '04' = public, '05' = aerial_ecsi, '06' = aerial_wcsi, '07' = aerial_scsi_2010_esw, '08' = aerial_scsi_2010_line, '09' = aerial_scsi_2018, '10' = weir1, '11' = weir2.

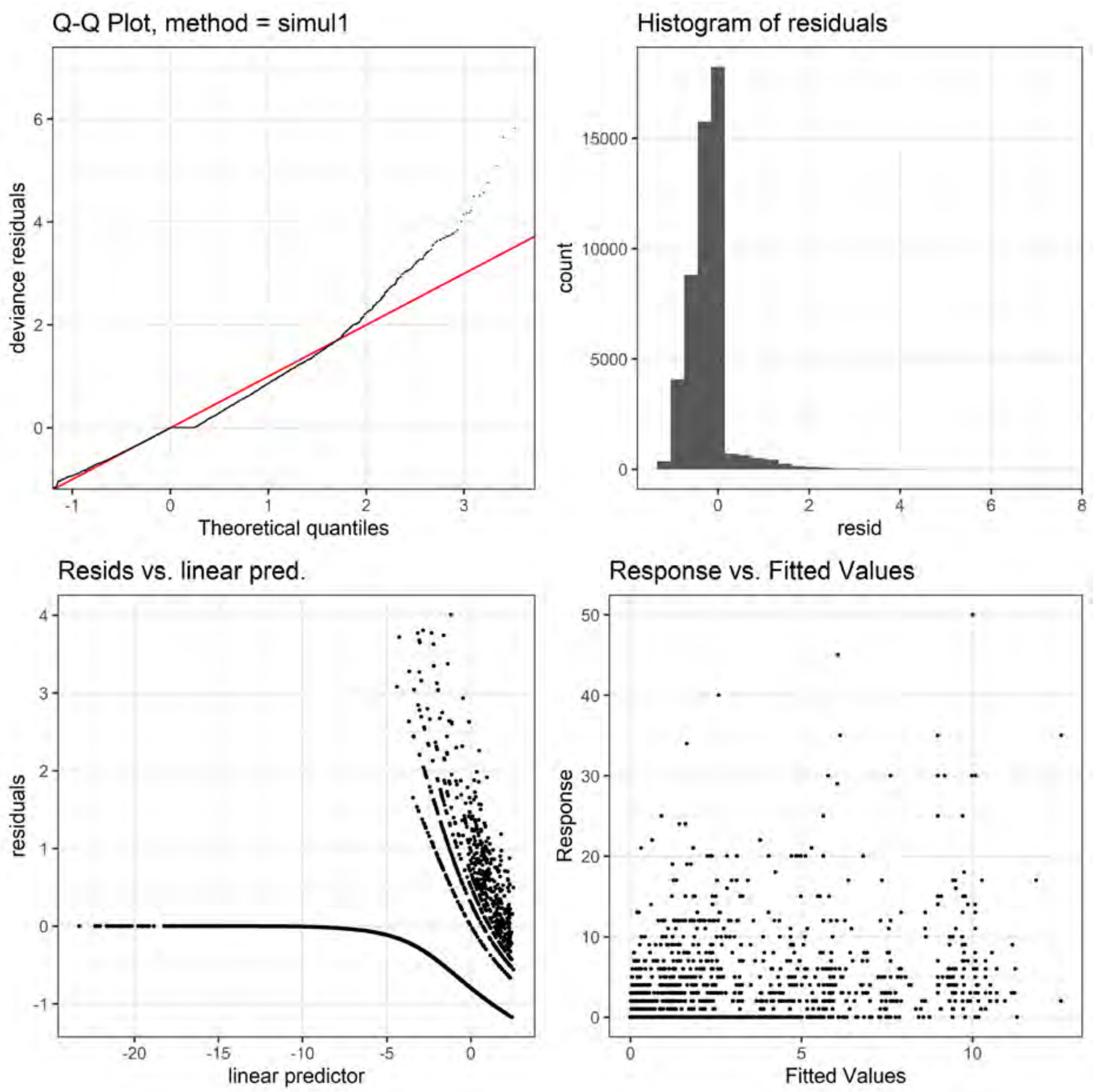

Figure D.2: Diagnostic plots for model *hab2_s50_season* used to estimate the spatial distribution of Hector's dolphins around the South Island, including the three local-scale areas.

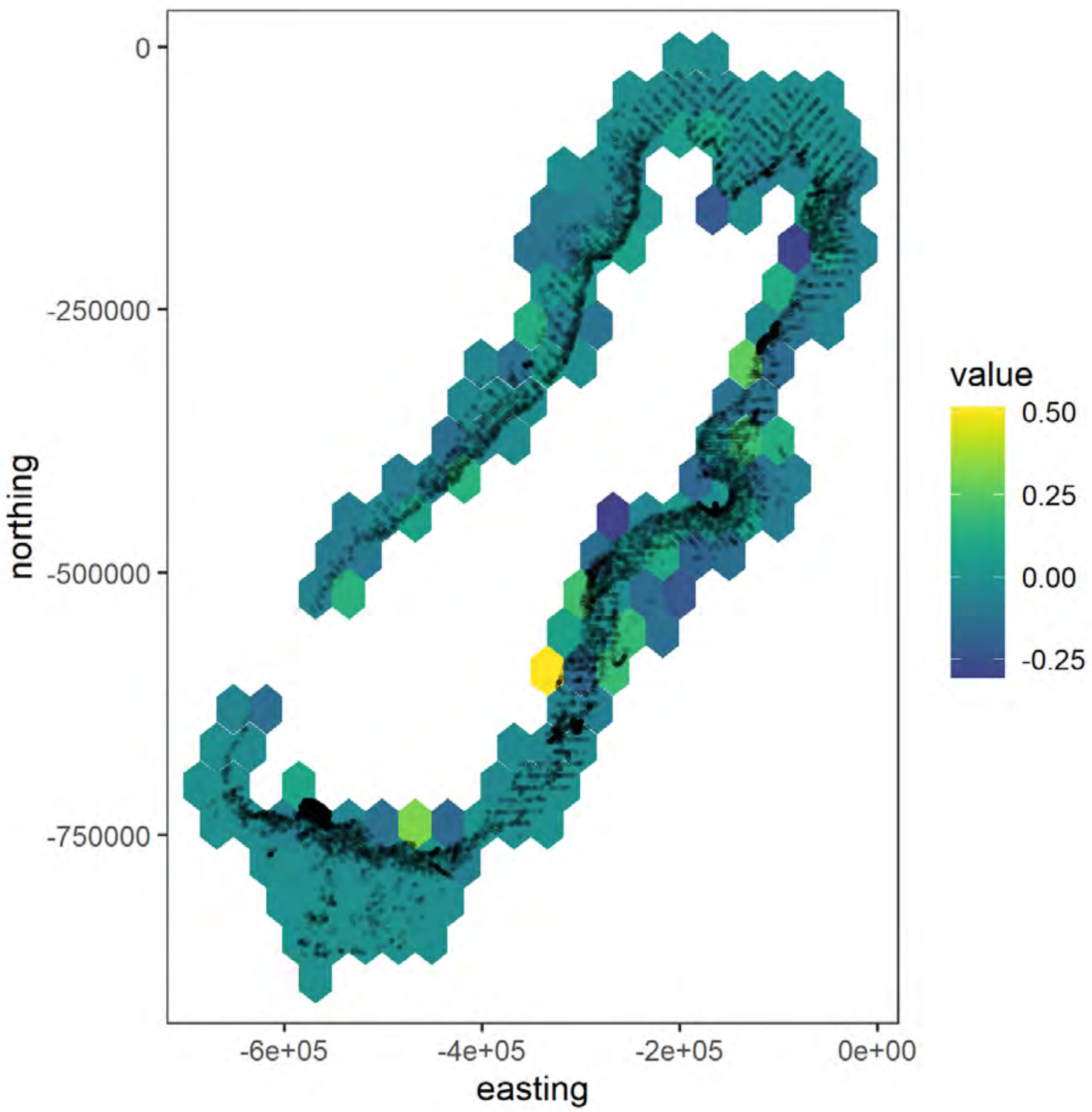

Figure D.3: Spatial plot of Pearson residuals for model *hab2_s50_season* used to estimate the spatial distribution of Hector's dolphins around the South Island, including the three local-scale areas. Colours are the mean of the Pearson residuals by hexagonal grid cell. Black points show the locations of sighting effort data.

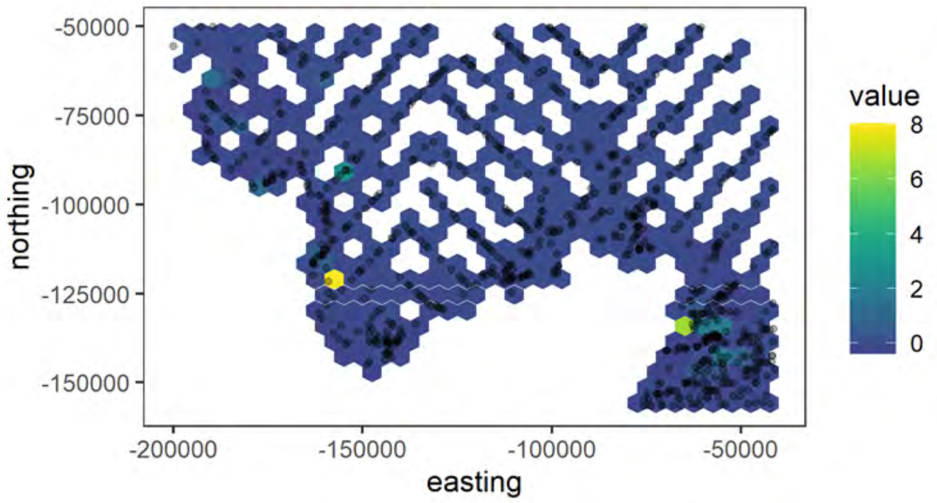

Figure D.4: **Spatial plot of Pearson residuals for model *hab2_s50_season* used to estimate the spatial distribution of Hector's dolphins around the South Island, showing only the north coast of the South Island. Colours are the mean of the Pearson residuals by hexagonal grid cell. Black points show the locations of sighting effort data.**

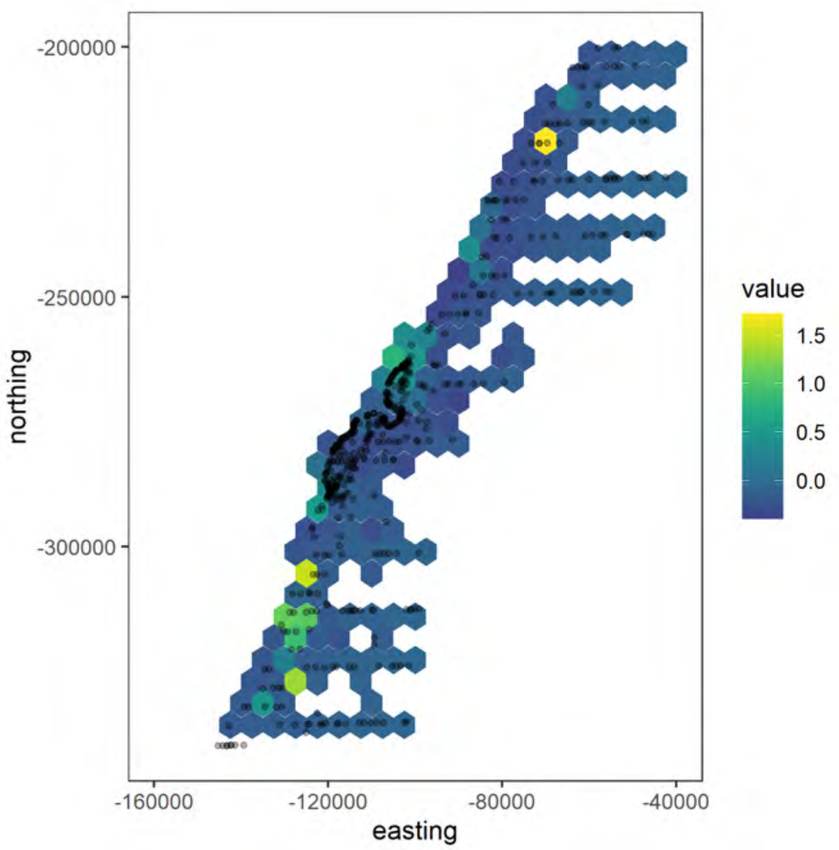

Figure D.5: **Spatial plot of Pearson residuals for model *hab2_s50_season* used to estimate the spatial distribution of Hector's dolphins around the South Island, showing only the Kaikōura coast. Colours are the mean of the Pearson residuals by hexagonal grid cell. Black points show the locations of sighting effort data.**

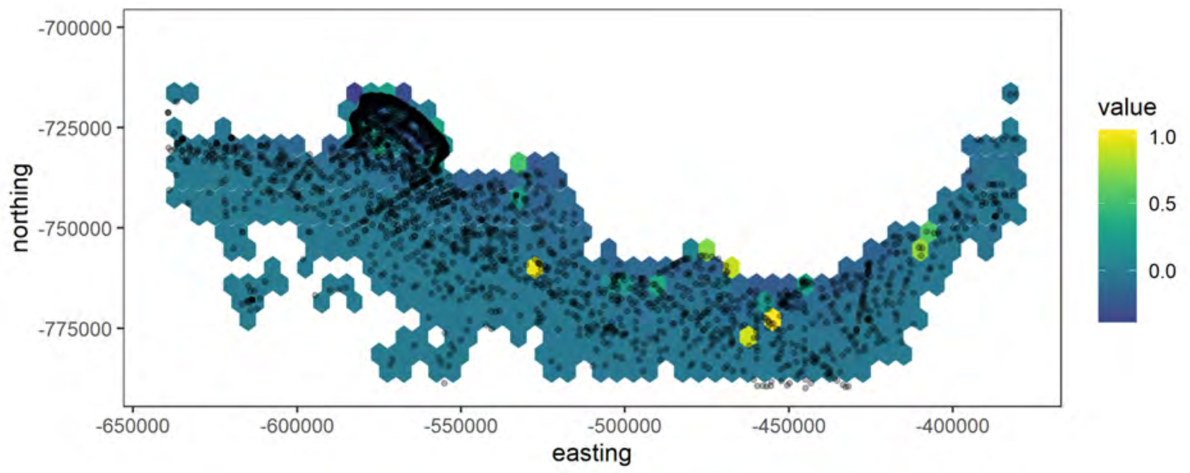

Figure D.6: **Spatial plot of Pearson residuals for model *hab2_s50_season*, used to estimate the spatial distribution of Hector's dolphins around the South Island, showing only the south coast of the South Island. Colours are the mean of the Pearson residuals by hexagonal grid cell. Black points show the locations of sighting effort data.**

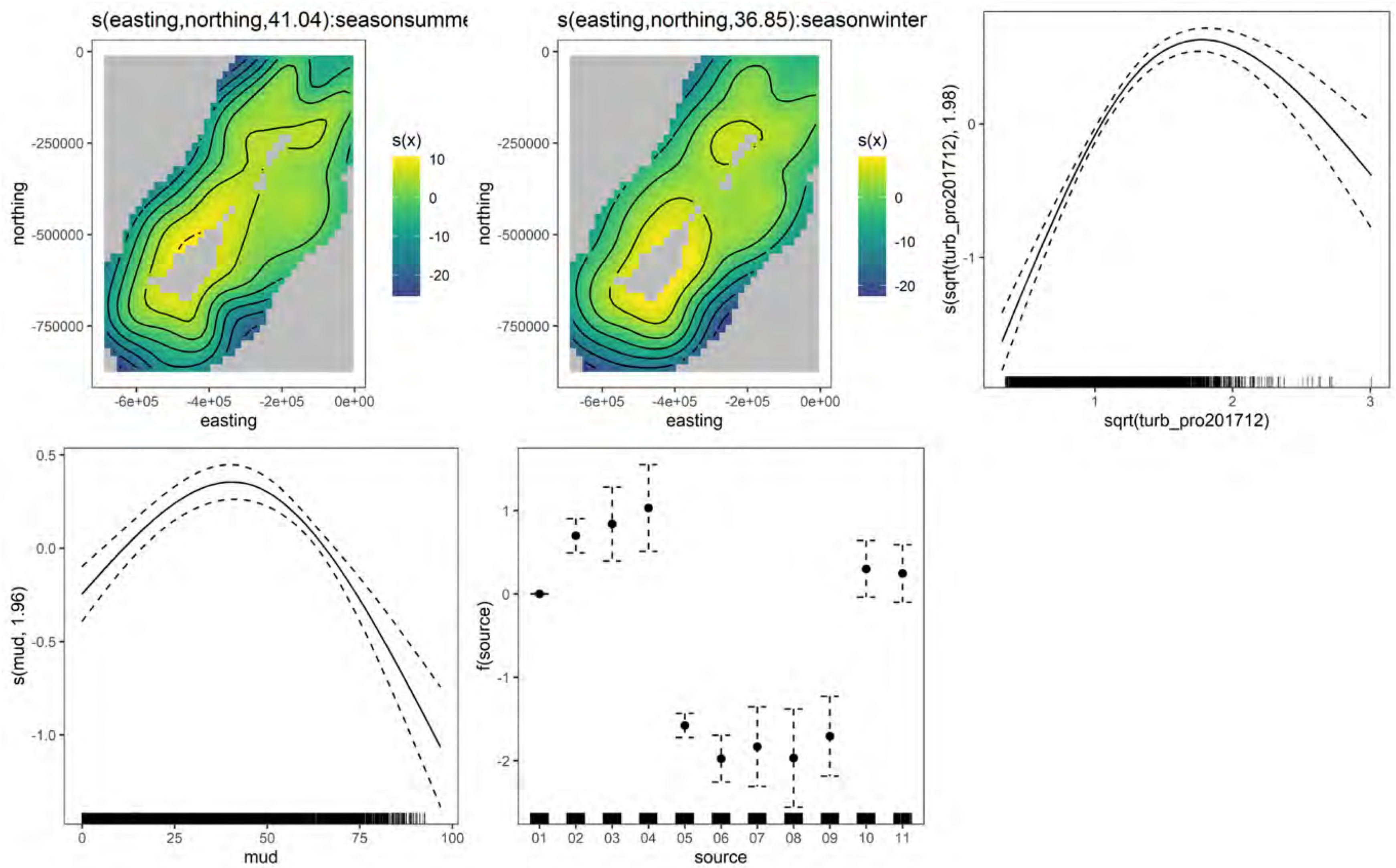

Figure D.7: **Term plots for the model *hab2_s50_season*. Model sources were: '01' = nomad, '02' = brager, '03' = rodda, '04' = public, '05' = aerial_ecsi, '06' = aerial_wcsi, '07' = aerial_scsi_2010_esw, '08' = aerial_scsi_2010_line, '09' = aerial_scsi_2018, '10' = weir1, '11' = weir2.**

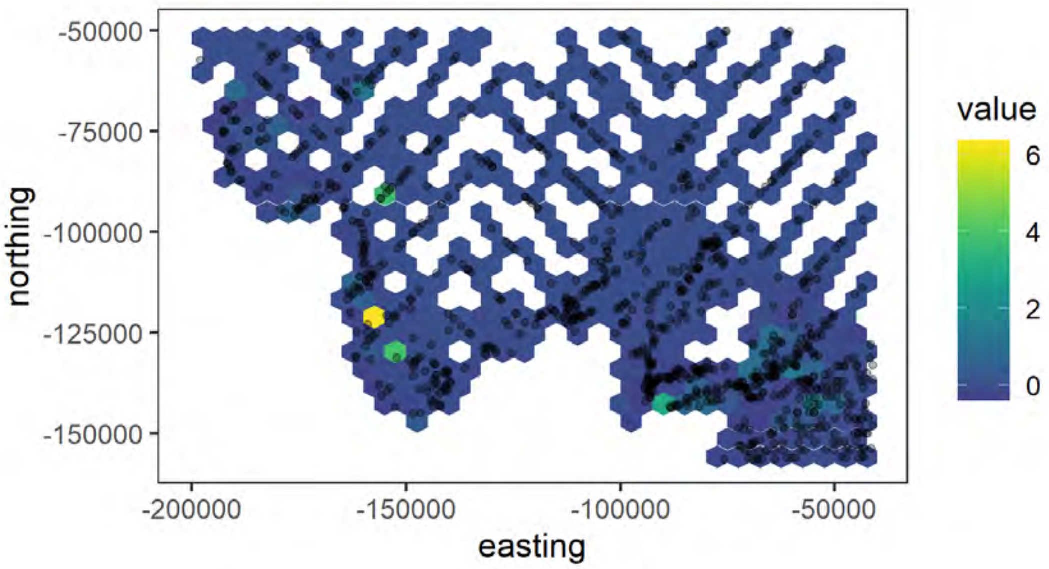

Figure D.8: Spatial plot of Pearson residuals for model *hab2_s50_season_ncsi* used to estimate the spatial distribution of Hector's dolphins around the South Island, showing only the <u>north coast of the South Island</u>. Colours are the mean of the Pearson residuals by hexagonal grid cell. Black points show the locations of sighting effort data.

APPENDIX E. SPATIAL DISTRIBUTION MODEL PREDICTIONS

Predictions from model *hab2_s50_season*

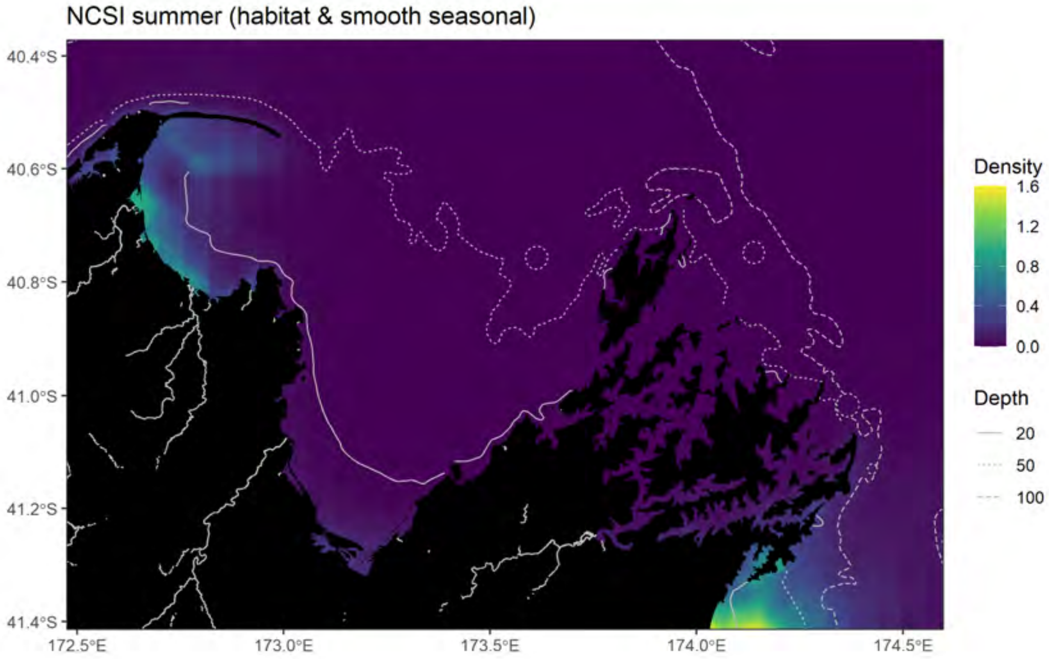

Figure E.1: Summer spatial prediction from model *hab2_s50_season*, showing the north coast of the South Island and depth contours 20–100 m.

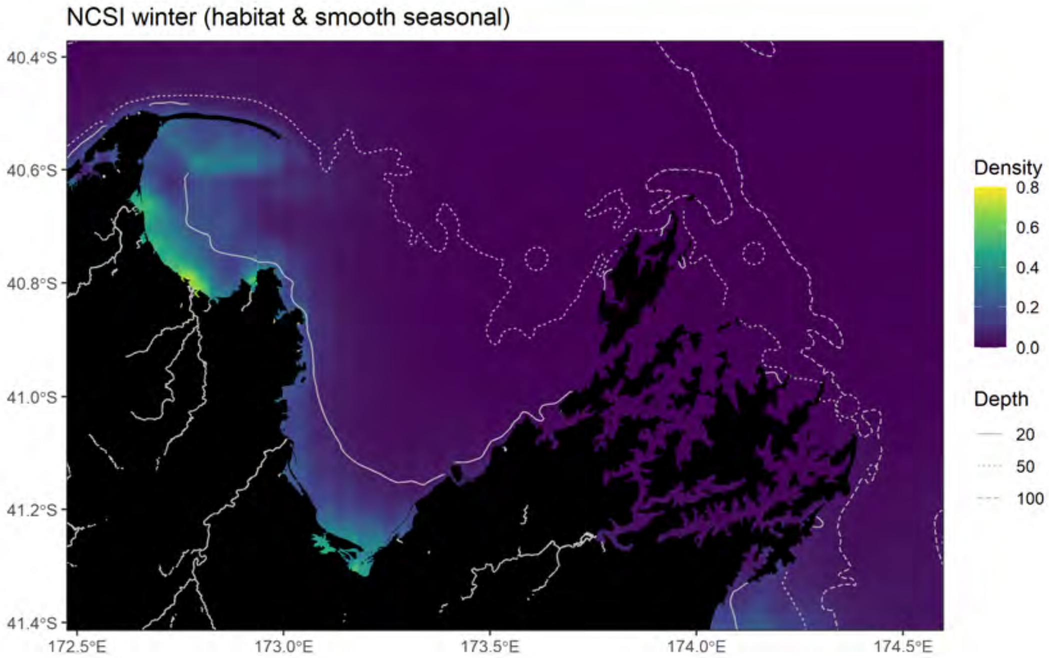

Figure E.2: Winter spatial prediction from model *hab2_s50_season*, showing the north coast of the South Island and depth contours 20–100 m.

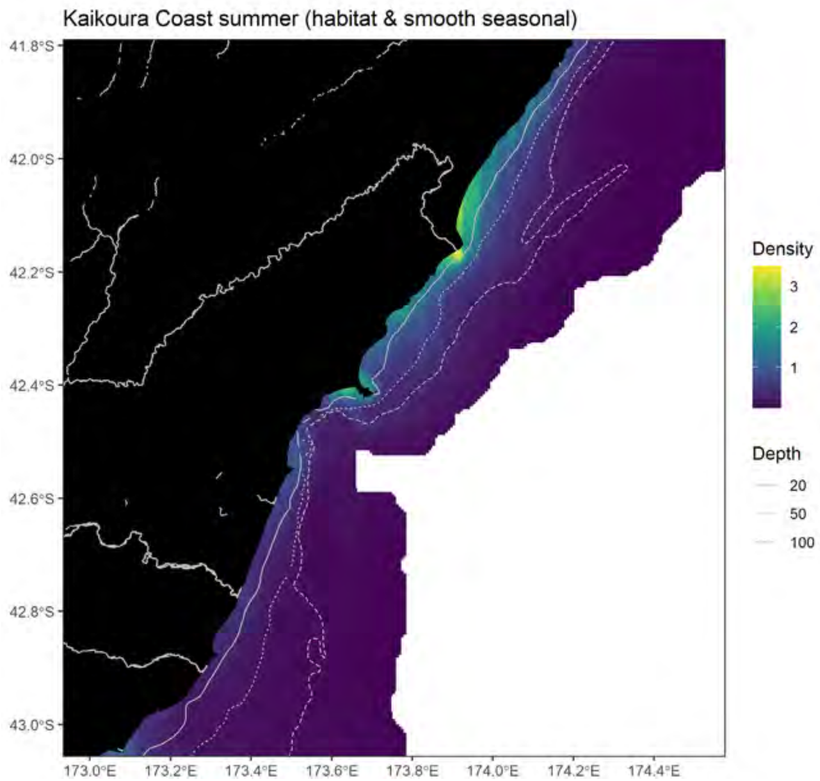

Figure E.3: Summer spatial prediction from model *hab2_s50_season*, showing the Kaikōura coast and depth contours 20–100 m.

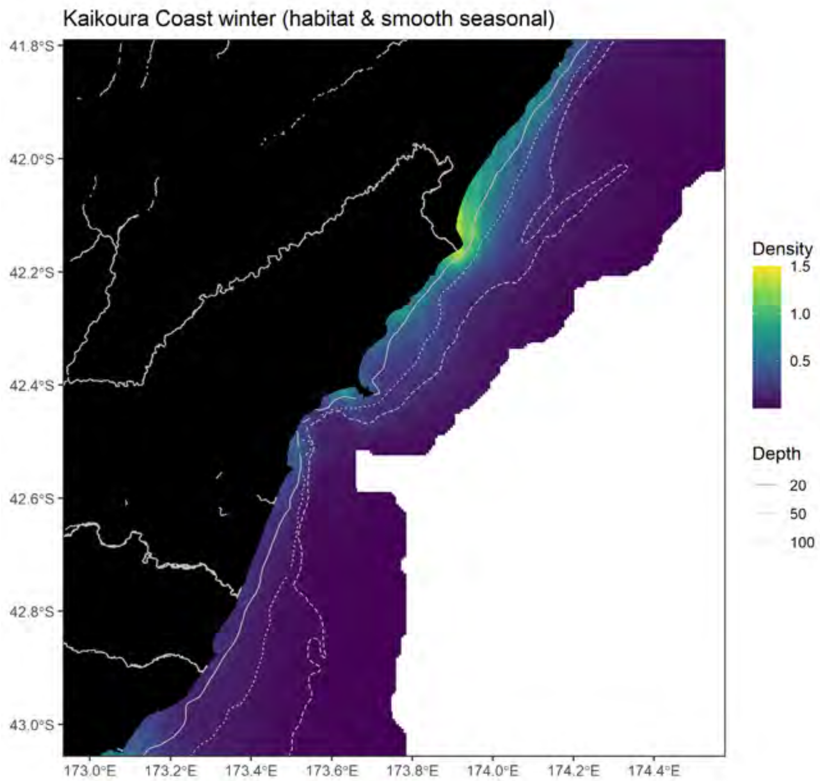

Figure E.4: Winter spatial prediction from model *hab2_s50_season*, showing the Kaikōura coast and depth contours 20–100 m.

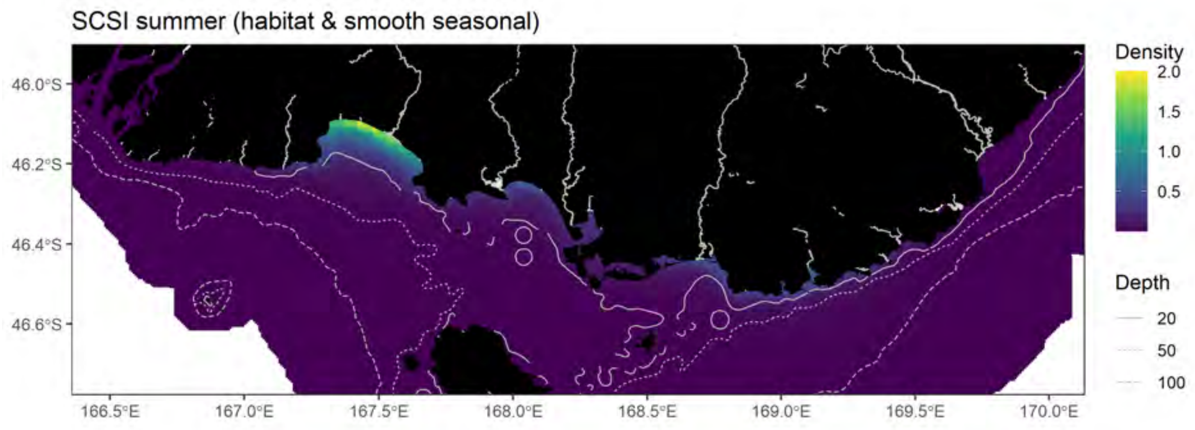

Figure E.5: **Summer spatial prediction from model *hab2_s50_season*, showing the south coast of the South Island and depth contours 20–100 m.**

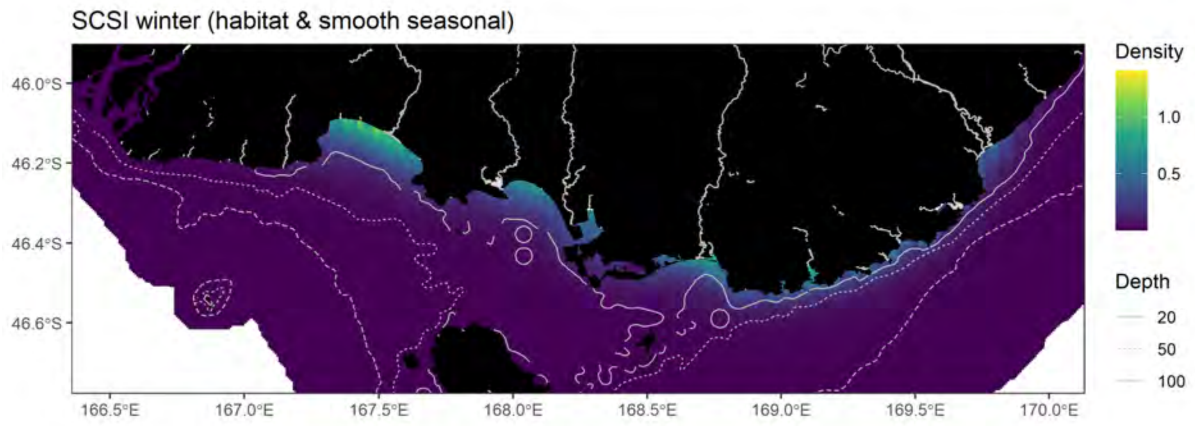

Figure E.6: **Winter spatial prediction from model *hab2_s50_season*, showing the south coast of the South Island and depth contours 20–100 m.**

Predictions from model *hab2_s50*

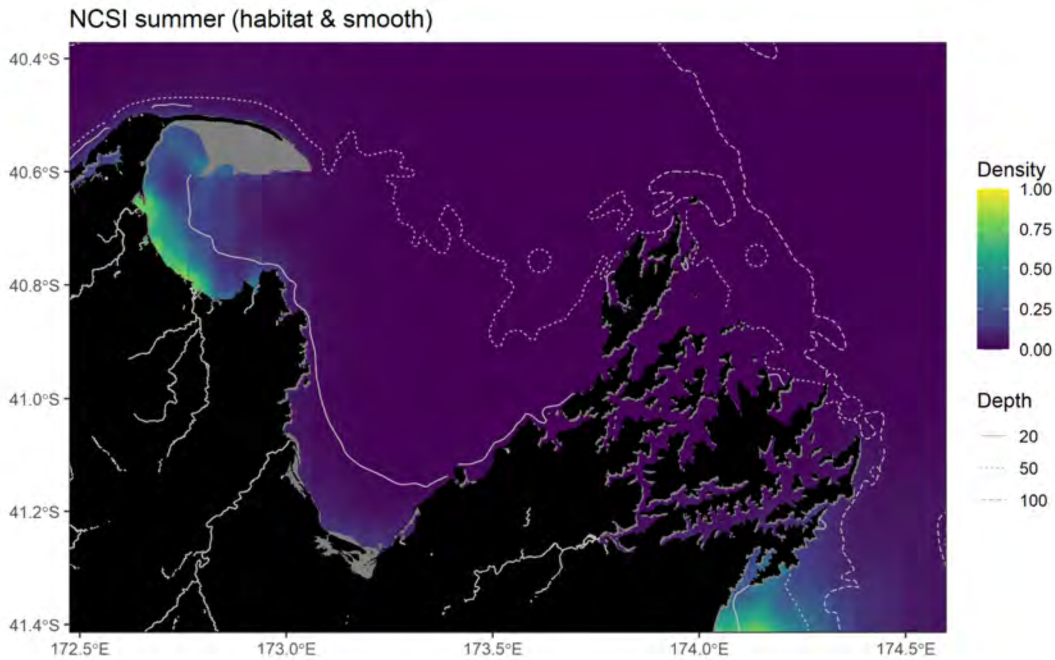

Figure E.7: Summer spatial prediction from model *hab2_s50*, showing the north coast of the South Island and depth contours 20–100 m.

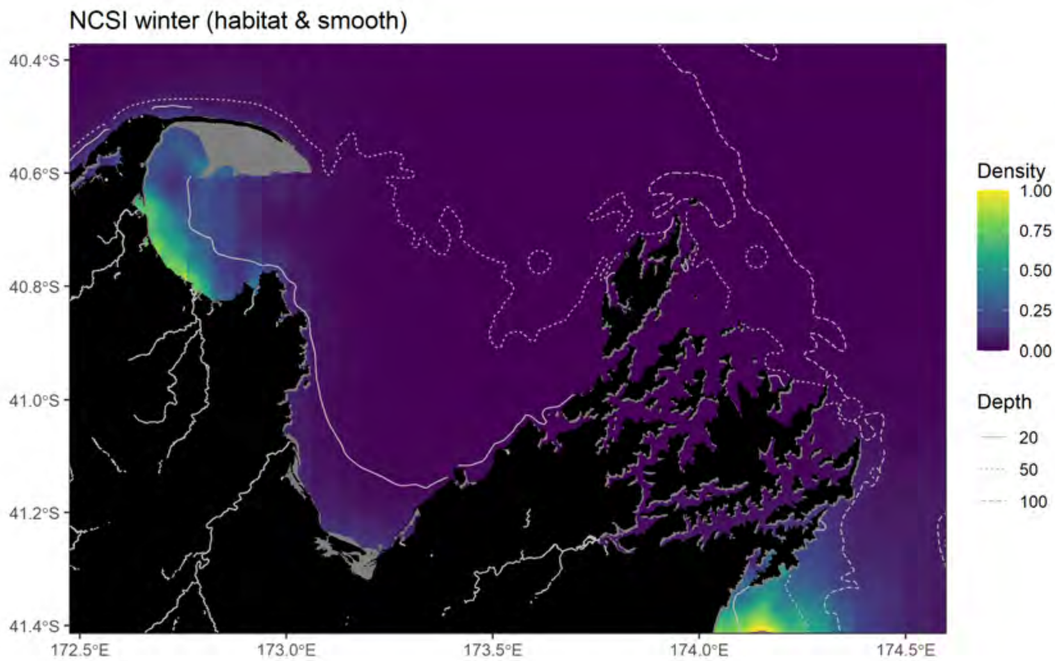

Figure E.8: Winter spatial prediction from model *hab2_s50*, showing the north coast of the South Island and depth contours 20–100 m.

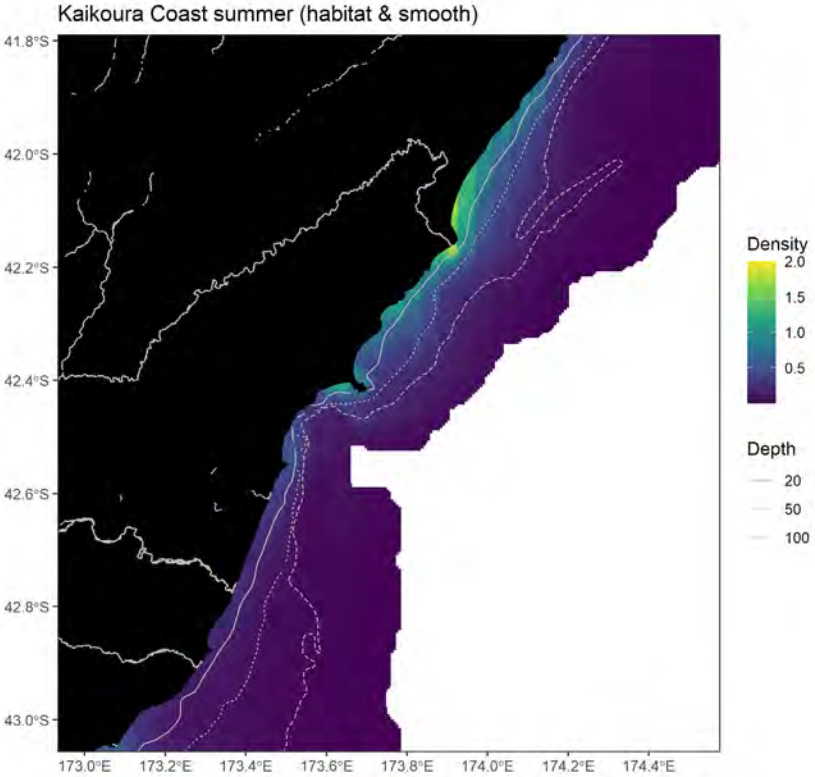

Figure E.9: Summer spatial prediction from model *hab2_s50*, showing the Kaikōura coast and depth contours 20–100 m.

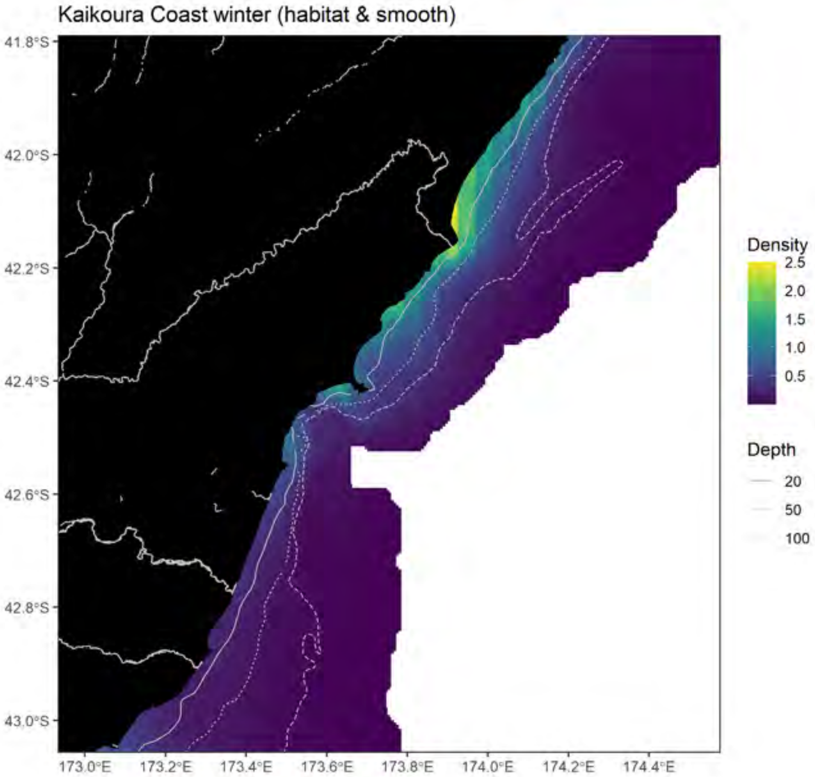

Figure E.10: Winter spatial prediction from model *hab2_s50*, showing the Kaikōura coast and depth contours 20–100 m.

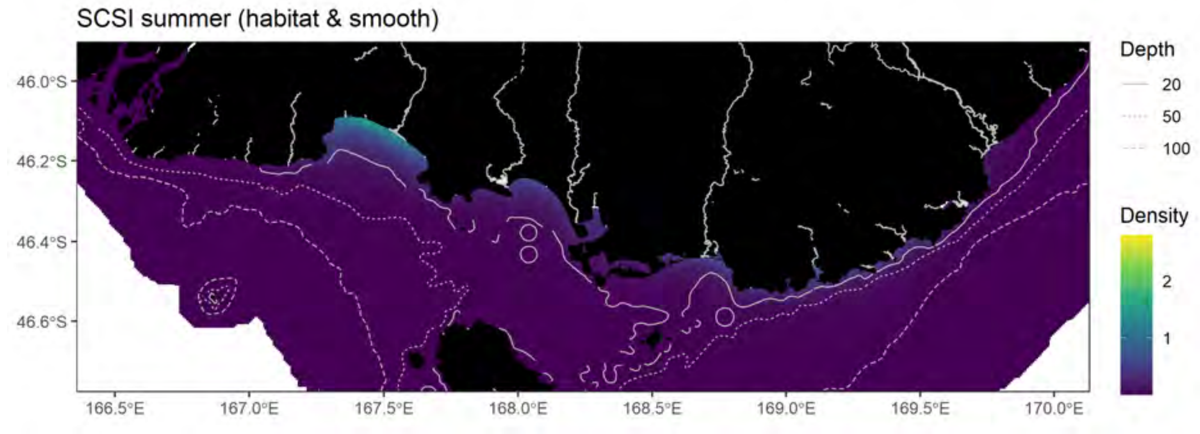

Figure E.11: Summer spatial prediction from model *hab2_s50*, showing the south coast of the South Island and depth contours 20–100 m.

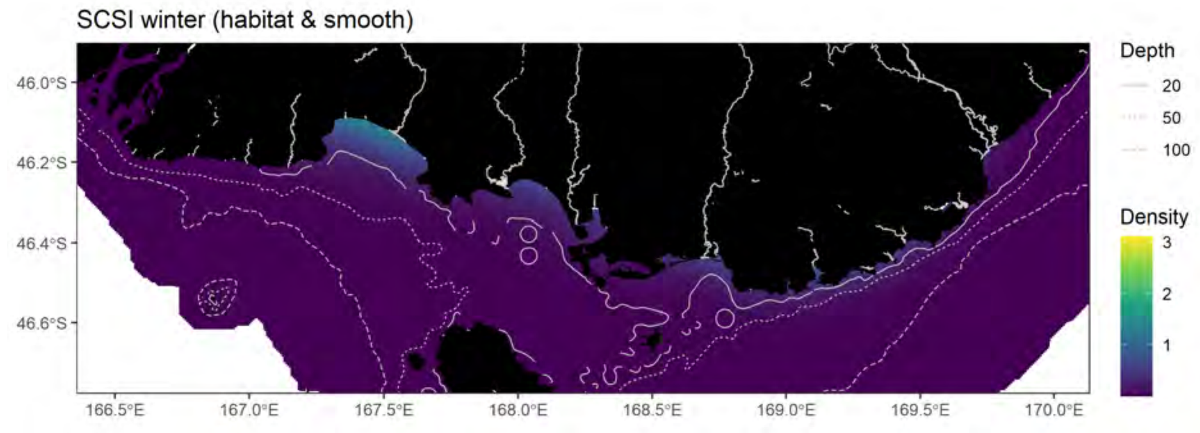

Figure E.12: Winter spatial prediction from model *hab2_s50*, showing the south coast of the South Island and depth contours 20–100 m.

Predictions from model *hab2_s50_season_ncsi*

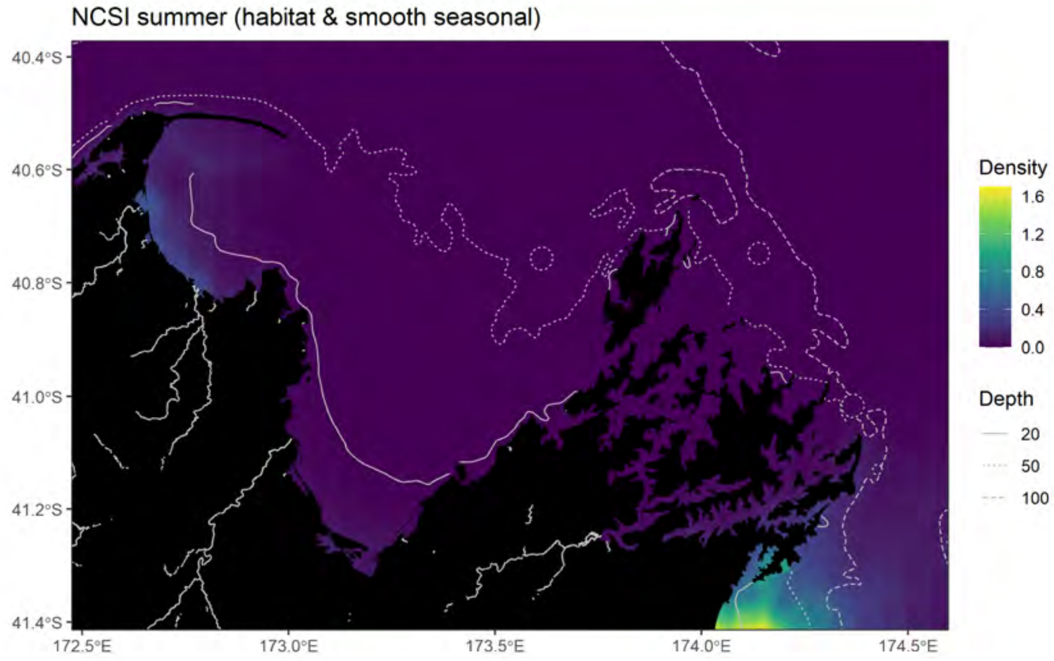

Figure E.13: Summer spatial prediction from model *hab2_s50_season_ncsi*, showing the north coast of the South Island and depth contours 20–100 m.

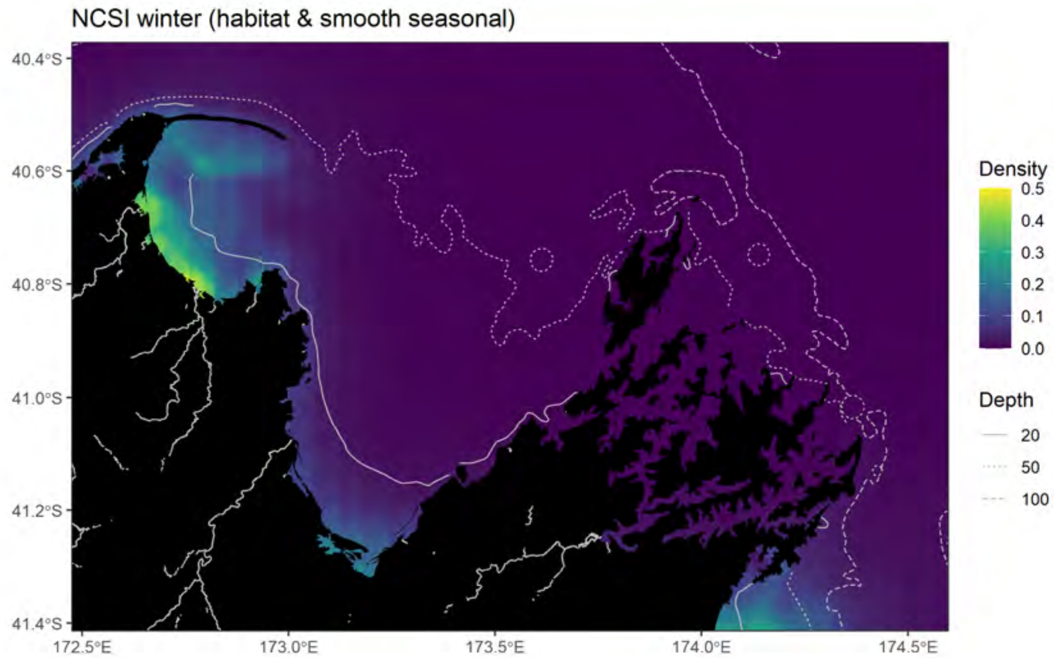

Figure E.14: Winter spatial prediction from model *hab2_s50_season_ncsi*, showing the north coast of the South Island and depth contours 20–100 m.

APPENDIX F. SEFRA DIAGNOSTIC PLOTS

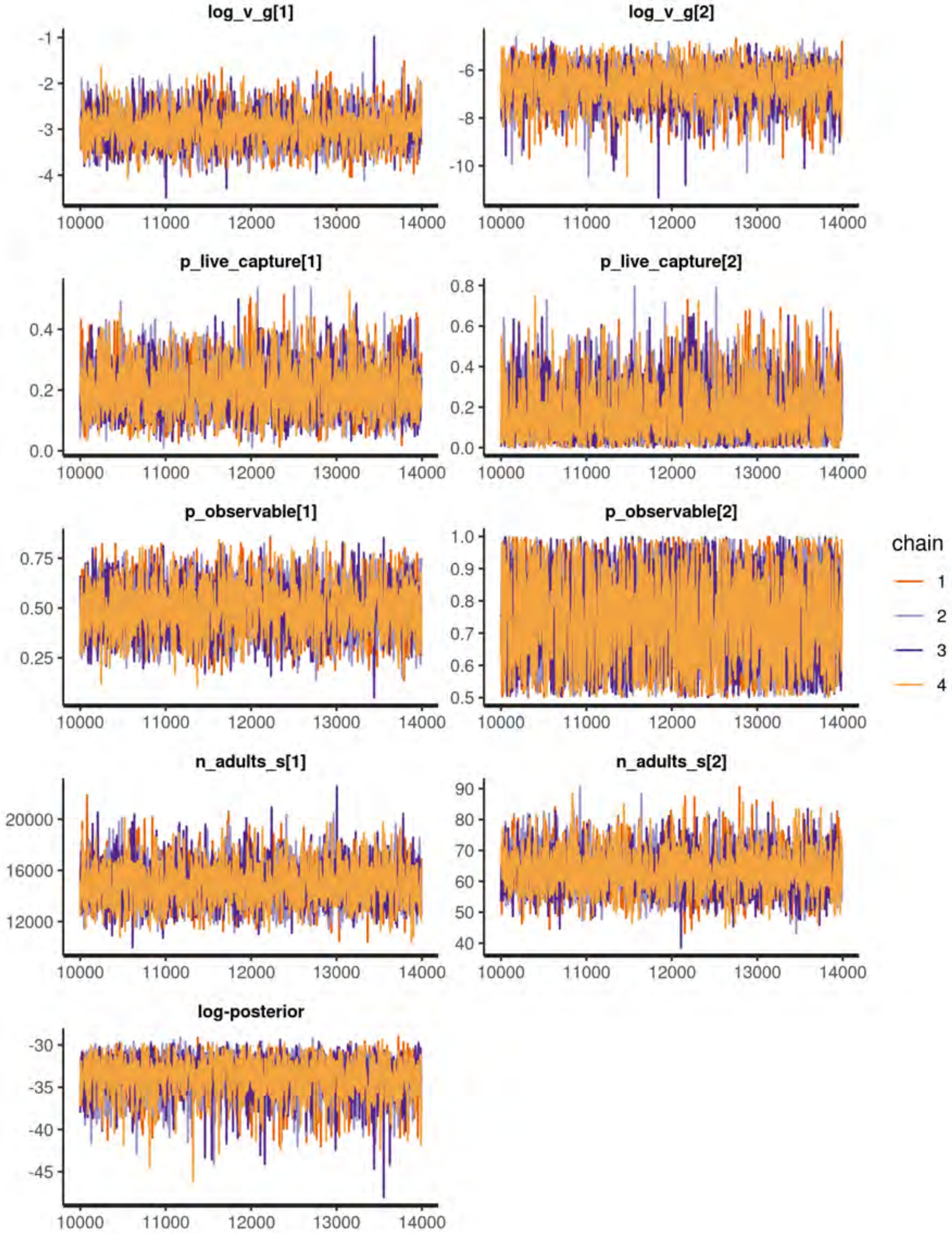

Figure F.1: Markov chain Monte Carlo (MCMC) trace plots for all estimated model parameters of model *update* (log_v_g[1] and log_v_g[2] = set net and trawl vulnerability, n_adults_s[1] and n_adults_s[2] = HDO and HDM population size, p_live_capture[1] and p_live_capture[2] = probability of live capture for set net and inshore trawl, p_observable[1] and p_observable[2] = probability that a set net or trawl event is observable) and the log-posterior density (i.e., the objective function).

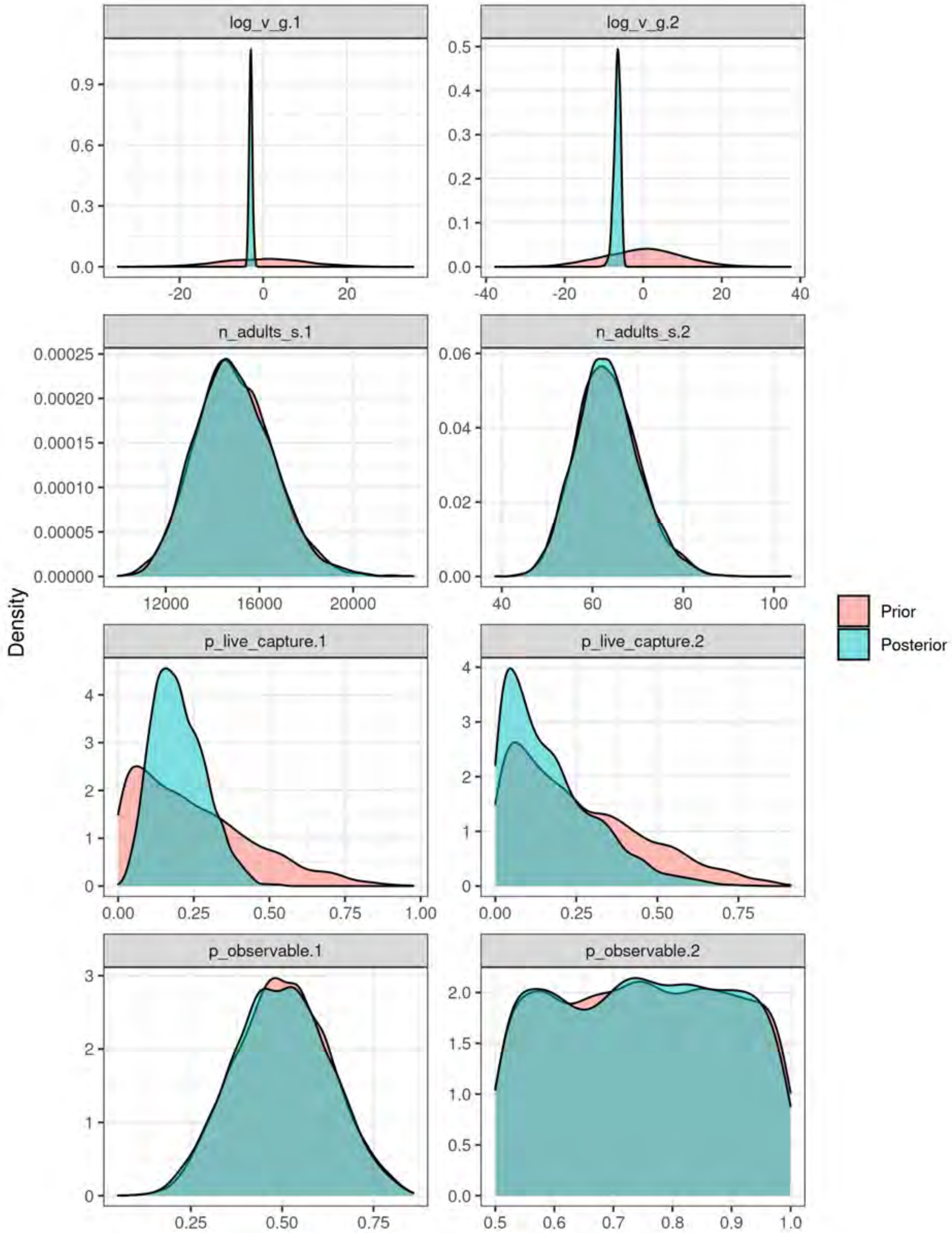

Figure F.2: Prior and posterior distributions of all estimated model parameters of model *update* (log_v_g.1 and log_v_g.2 = set net and trawl vulnerability, n_adults_s.1 and n_adults_s.2 = HDO and HDM population size, p_live_capture.1 and p_live_capture.2 = probability of live capture for set net and trawl, p_observable.1 and p_observable.2 = probability that a setnet or trawl event is observable).

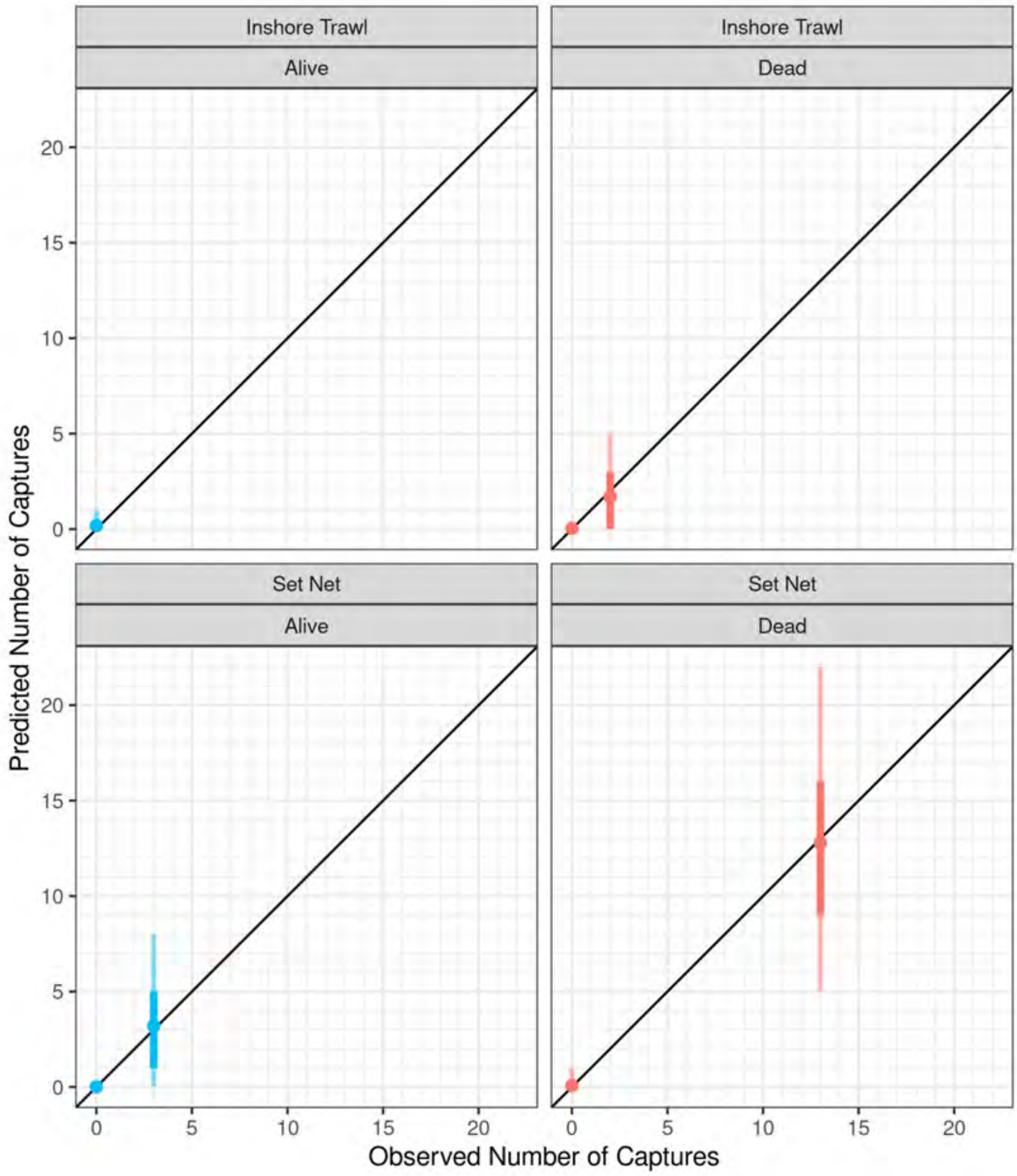

Figure F.3: Observed versus predicted number of Hector's/Māui dolphin captures from 1995–96 to 2019–20 that are alive (blue) or dead (red) in inshore trawl or set nets (model *update*). The 2.5%, 25%, median, 75%, and 97.5% quantiles of the predicted number of captures are provided.

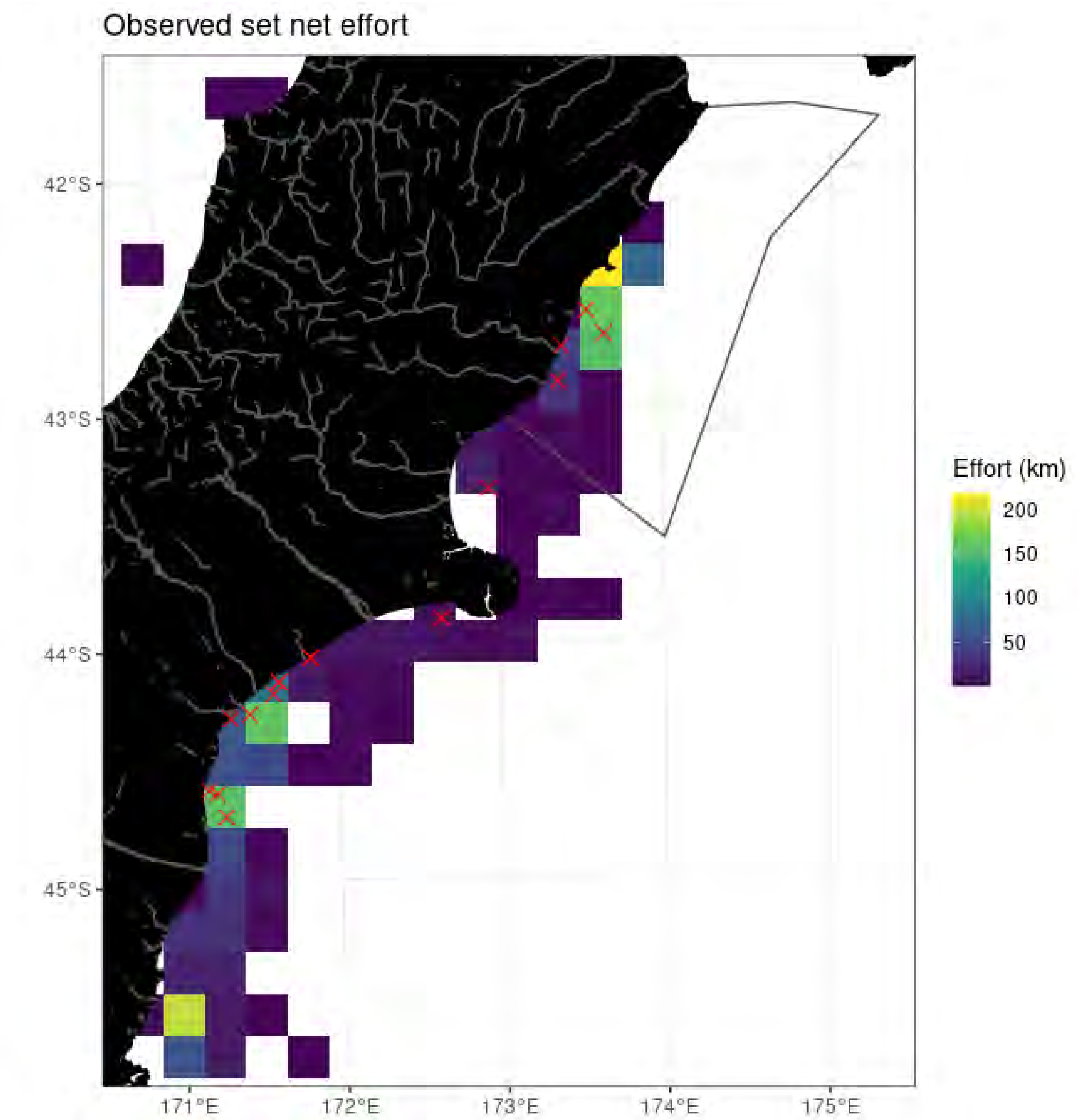

Figure F.4: Observed set net fishing effort (net length, km; gridded to 20-km resolution) and observed captures of Hector's dolphin in set nets (red crosses) from 1995–96 to 2019–20.

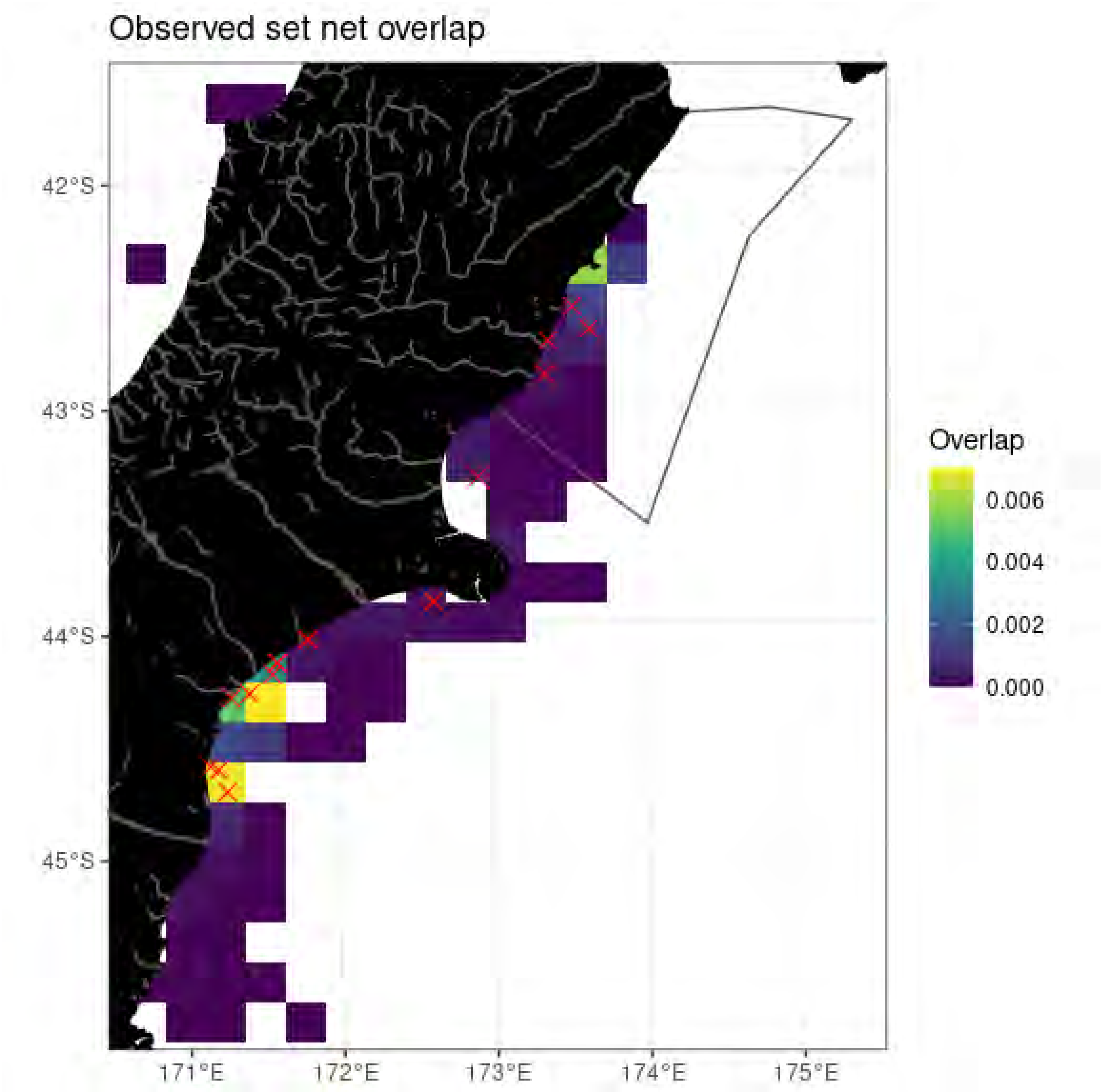

Figure F.5: **Observed set net fishing overlap (gridded to 20-km resolution) and observed captures of Hector's dolphin in set nets (red crosses) from 1995–96 to 2019–20.**

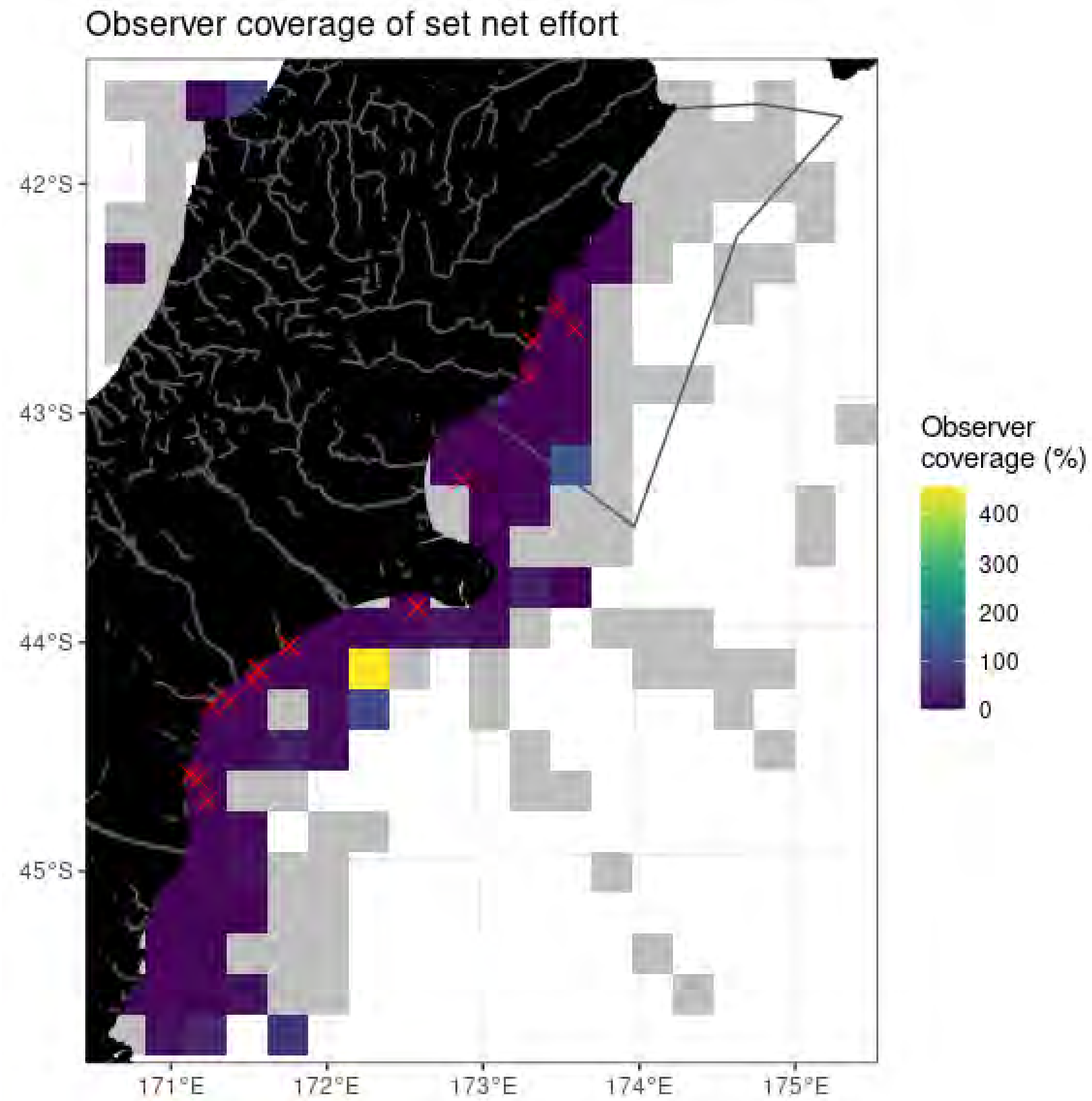

Figure F.6: **Observed set net fishing overlap (gridded to 20-km resolution) and observed captures of Hector's dolphin in set nets (red crosses) from 1995–96 to 2019–20. Note that the locations of some of the effort data were estimated by Fisheries New Zealand, leading to one of the grid cells shown here apparently having > 100% observer coverage, when this would be possible in reality.**

APPENDIX G. SEFRA MODEL POSTERIORS

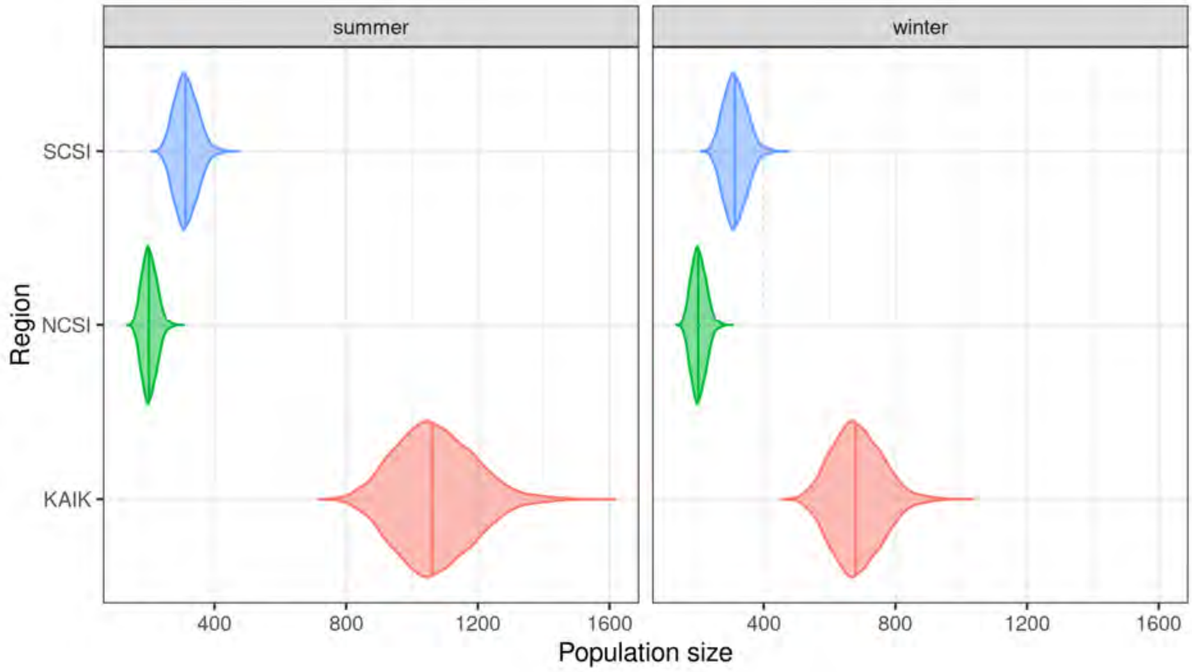

Figure G.1: Local-scale area population size of Hector's dolphins by summary area (Figure 1a) from model *update*. The median is indicated as vertical lines within each density.

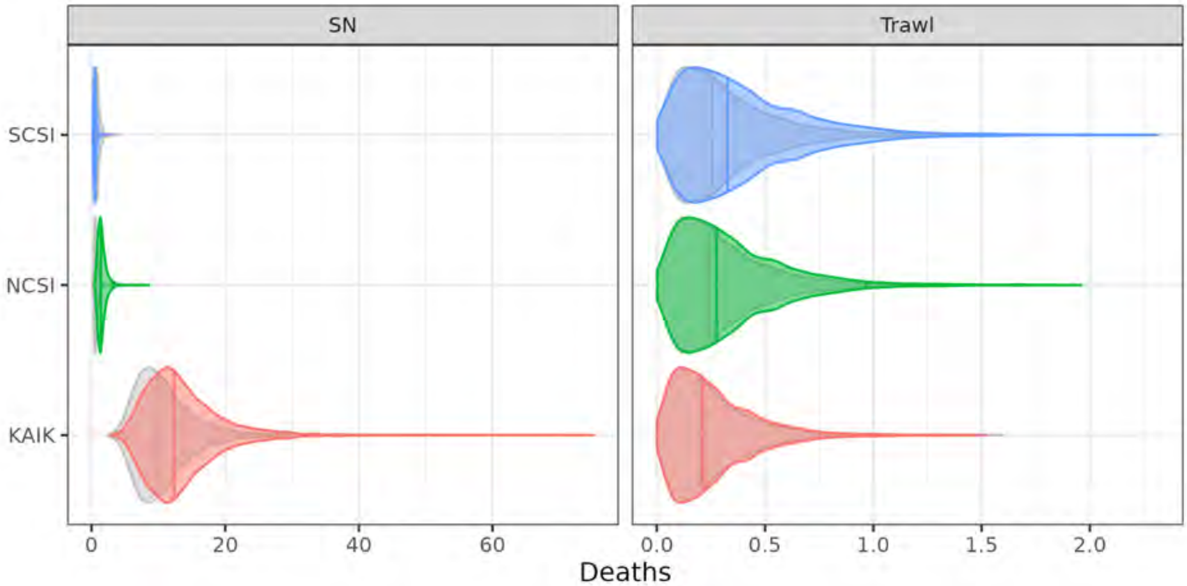

Figure G.2: Annual estimated annual commercial fishery (set net and inshore trawl) deaths for Hector's dolphins in fishing years 2014–15 to 2016–17 by summary area (Figure 1a) comparing model *update* (coloured violins) and *previous* (grey violins). The median and 97.5% quantiles are indicated as vertical lines within each density.

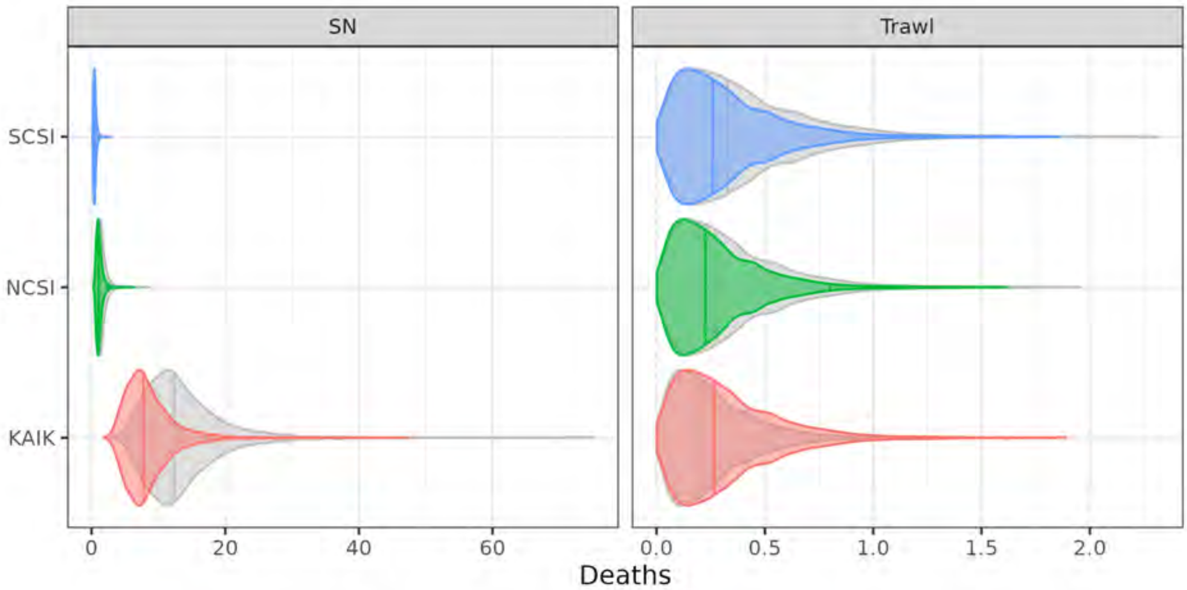

Figure G.3: Annual estimated annual commercial fishery (set net and inshore trawl) deaths for Hector's dolphins by summary area (Figure 1a) from model *update*, comparing fishing years 2017–18 to 2019–20 (coloured violins) and with 2014–15 to 2016–17 (grey violins). The median and 97.5% quantiles are indicated as vertical lines within each density.

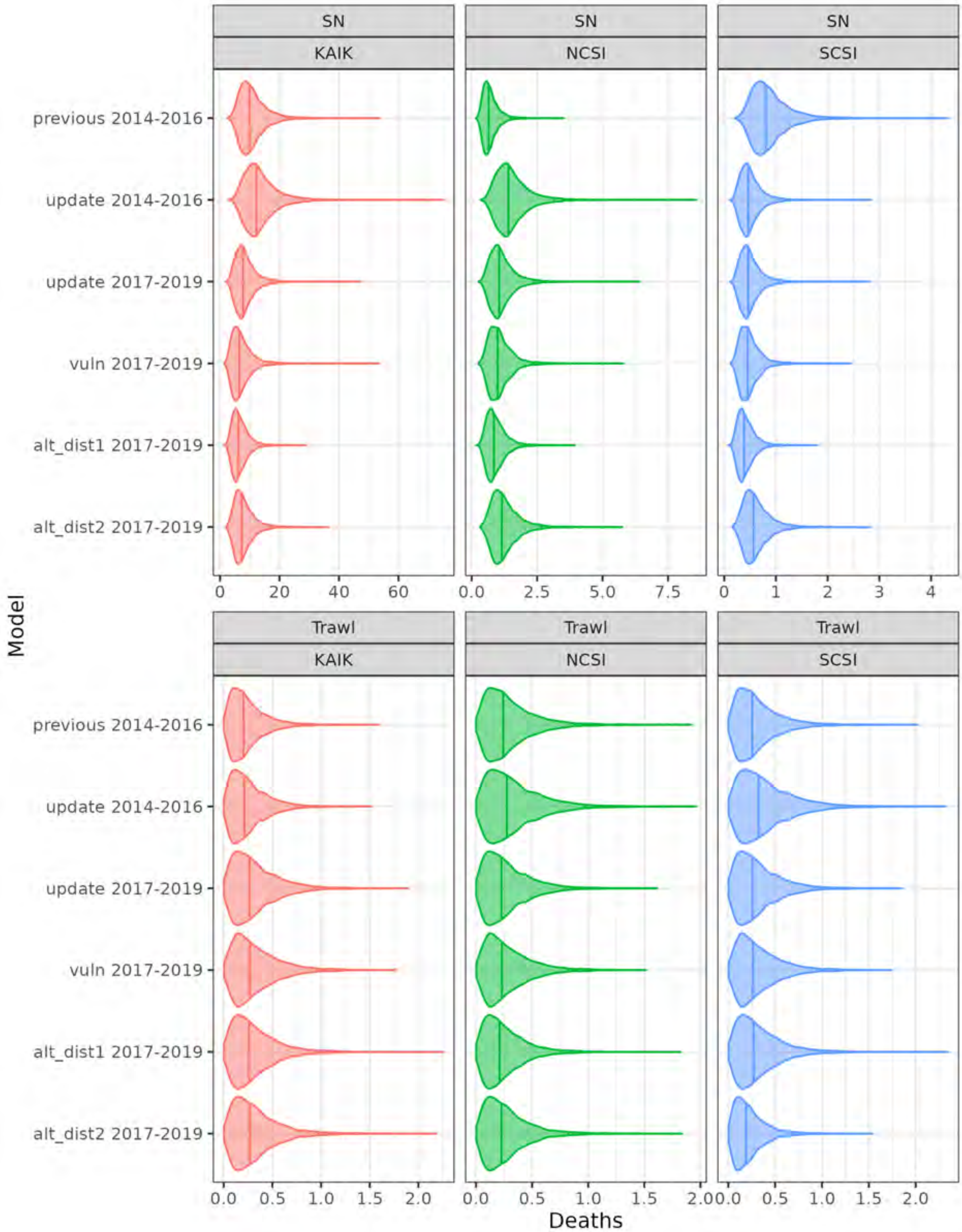

Figure G.4: **Annual estimated annual commercial fishery (set net and inshore trawl) deaths for Hector's dolphins by summary area (Figure 1a). Fishing years over which annual deaths were summarised are included in the model name (2014–2016 represents 2014–15 to 2016–17). The median and 97.5% quantiles are indicated as vertical lines within each density.**

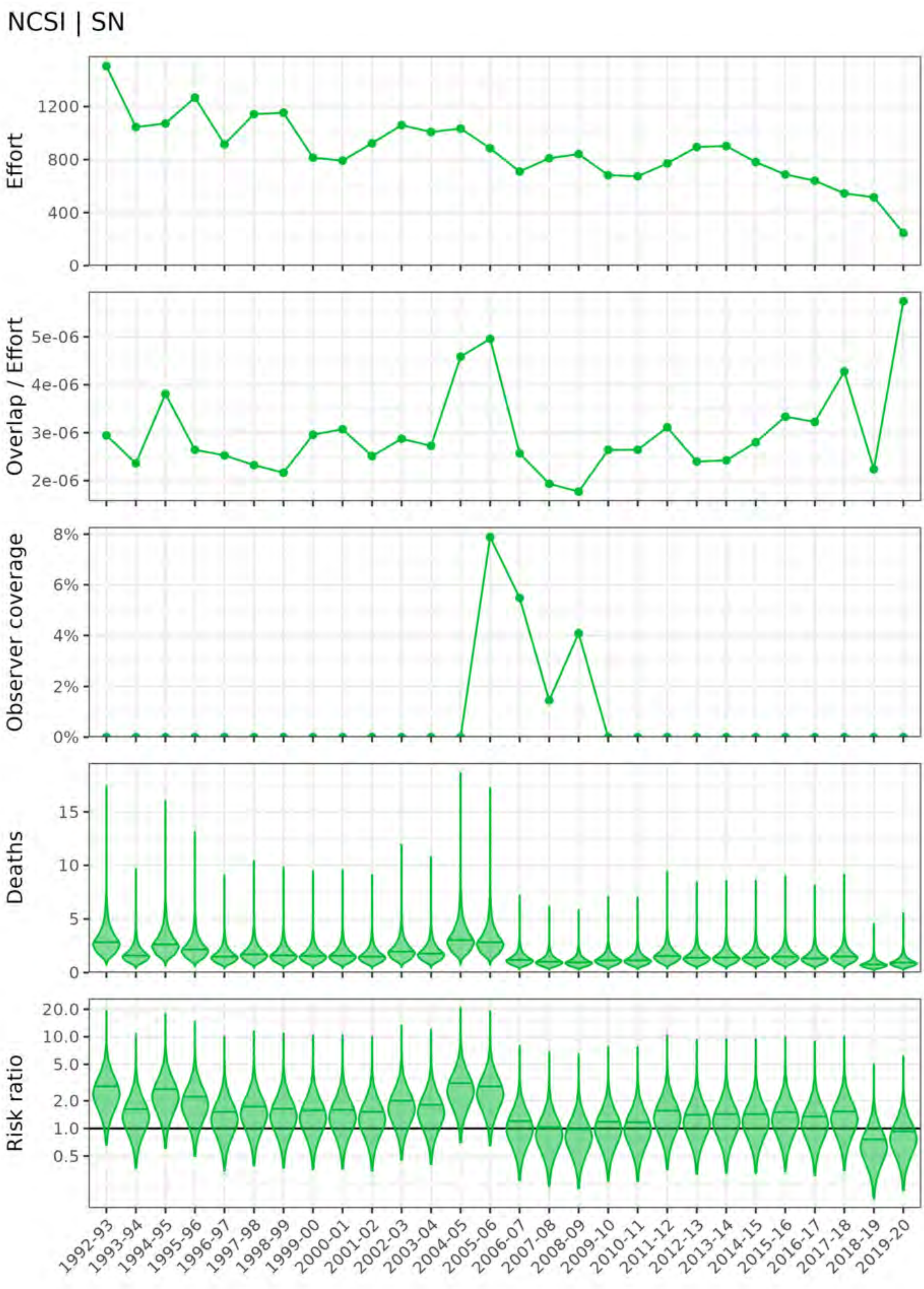

Figure G.5: Time series plots of outputs of model *update*, showing: commercial set net effort (km of net) [top], overlap per unit effort [second from top], percentage of the fishing effort that has been observed [middle], predicted number of deaths [second from bottom], and risk ratio [bottom] off the north coast of the South Island (NCSI) by fishing year for Hector's dolphins. This model run assumed a calibration coefficient (ϕ) of 0.2.

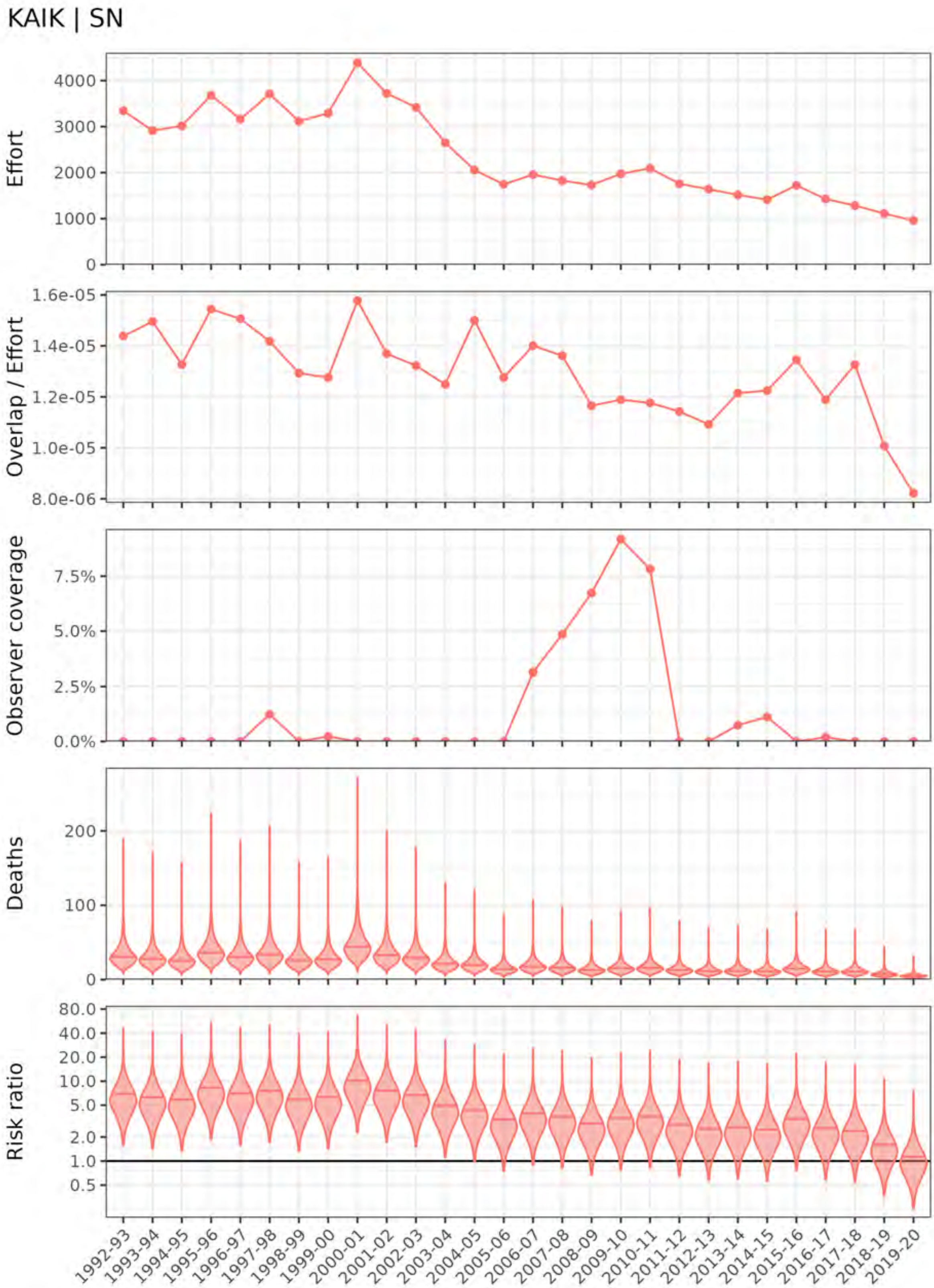

Figure G.6: Time series plots of outputs of model *update*, showing: commercial set net effort (km of net) [top], overlap per unit effort [second from top], percentage of the fishing effort that has been observed [middle], predicted number of deaths [second from bottom], and risk ratio [bottom] off Kaikōura (KAIK) by fishing year for Hector's dolphins. This model run assumed a calibration coefficient (ϕ) of 0.2.

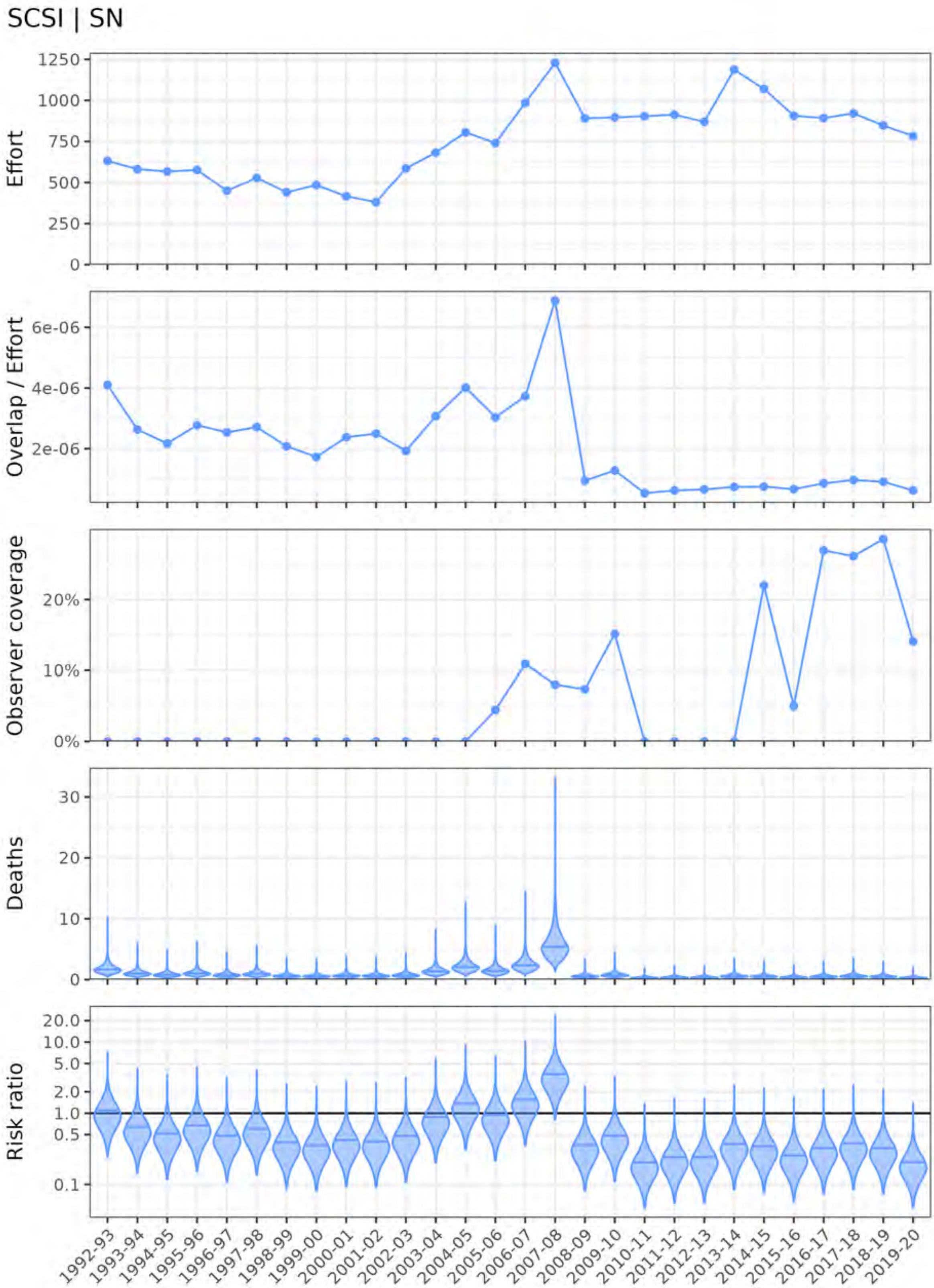

Figure G.7: Time series plots of outputs of model *update*, showing: commercial set net effort (km of net) [top], overlap per unit effort [second from top], percentage of the fishing effort that has been observed [middle], predicted number of deaths [second from bottom], and risk ratio [bottom] off the south coast of the South Island (SCSI) by fishing year for Hector's dolphins. This model run assumed a calibration coefficient (ϕ) of 0.2.

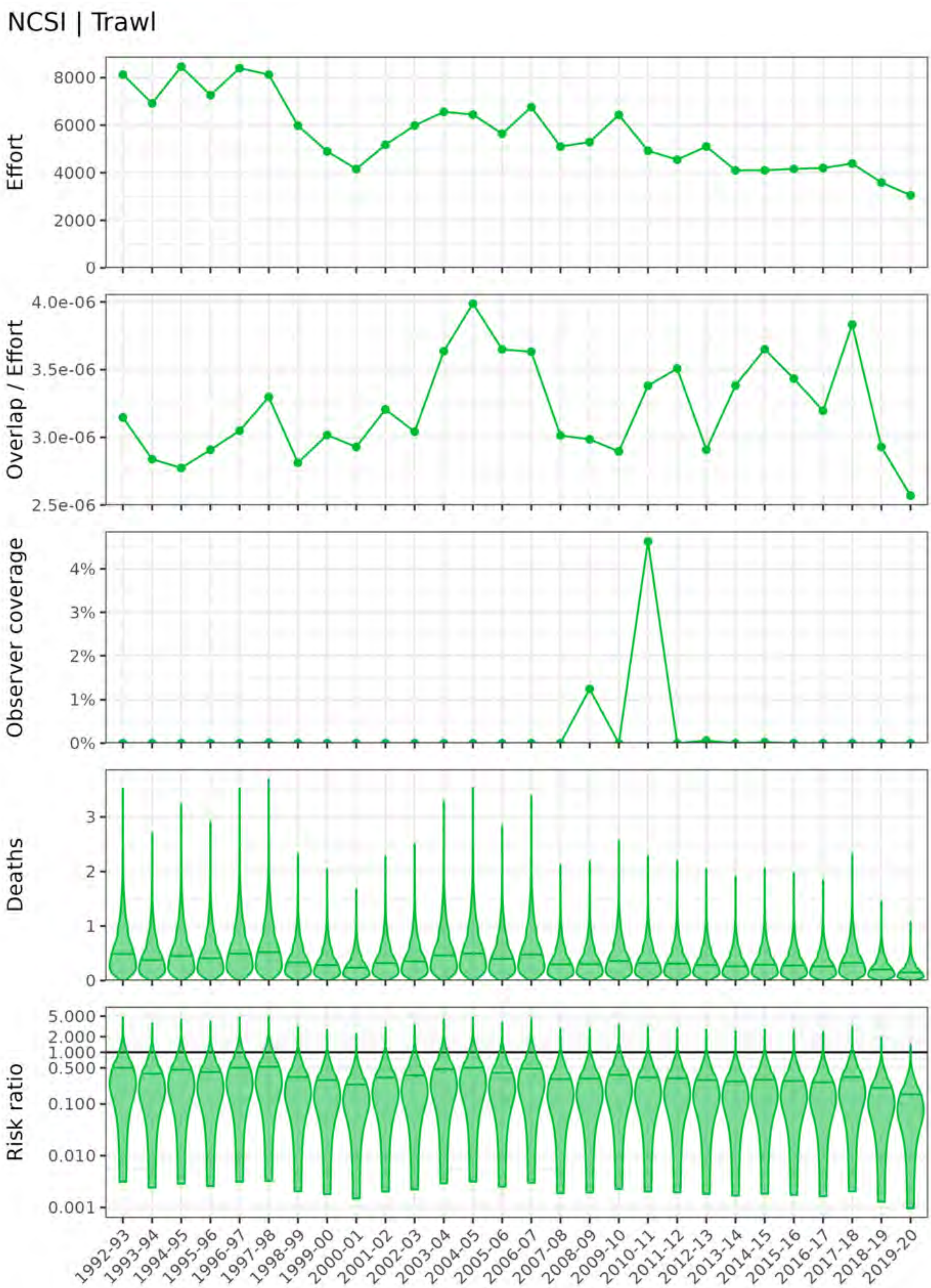

Figure G.8: **Time series plots of outputs of model *update*, showing: commercial trawl effort (number of tows) [top], overlap per unit effort [second from top], percentage of the fishing effort that has been observed [middle], predicted number of deaths [second from bottom], and risk ratio [bottom] off the north coast of the South Island (NCSI) by fishing year for Hector's dolphins. This model run assumed a calibration coefficient (ϕ) of 0.2.**

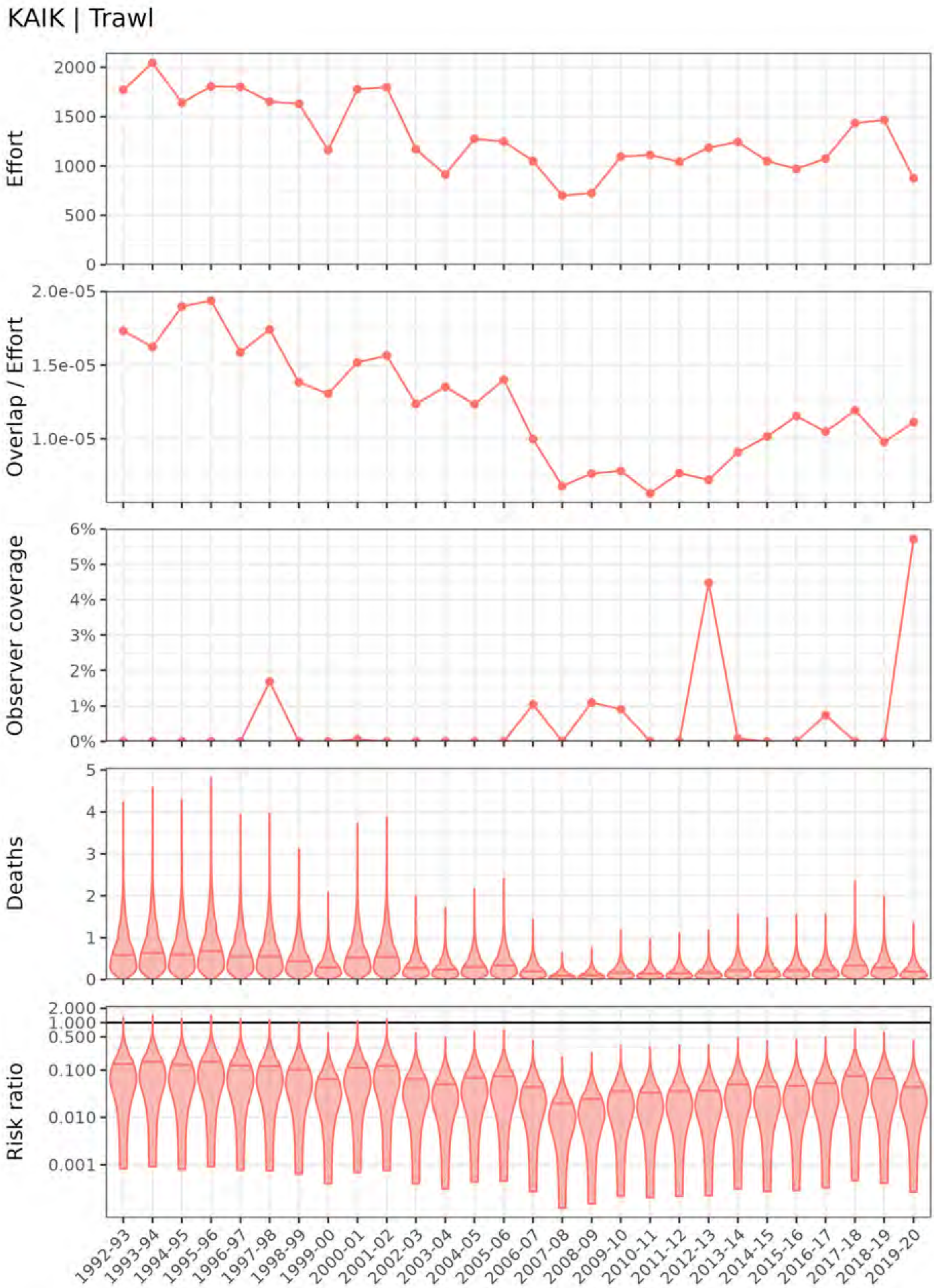

Figure G.9: **Time series plots of outputs of model *update*, showing: commercial trawl effort (number of tows) [top], overlap per unit effort [second from top], percentage of the fishing effort that has been observed [middle], predicted number of deaths [second from bottom], and risk ratio [bottom] off Kaikōura (KAIK) by fishing year for Hector's dolphins. This model run assumed a calibration coefficient (ϕ) of 0.2.**

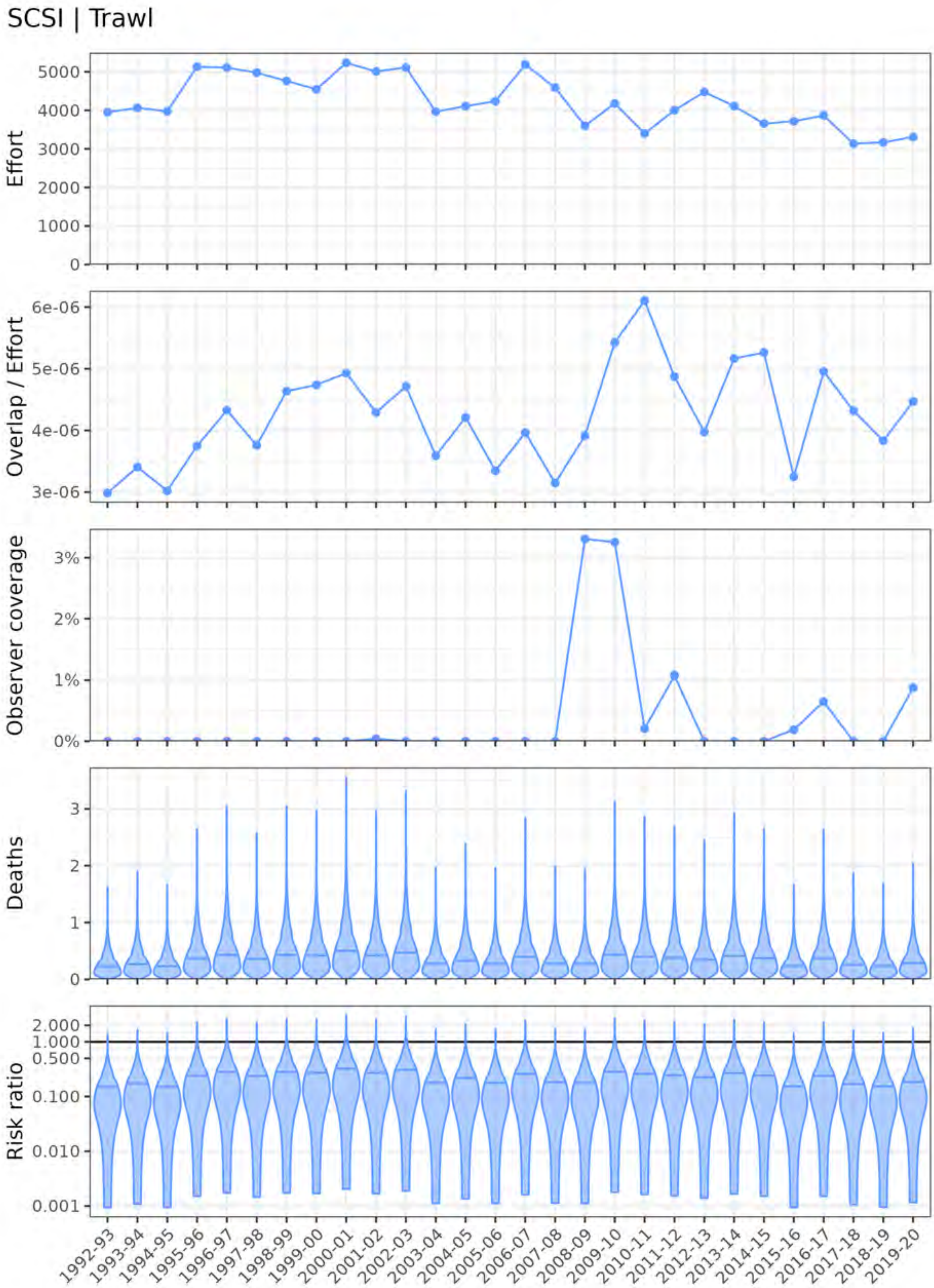

Figure G.10: Time series plots of outputs of model *update*, showing: commercial trawl effort (number of tows) [top], overlap per unit effort [second from top], percentage of the fishing effort that has been observed [middle], predicted number of deaths [second from bottom], and risk ratio [bottom] off the south coast of the South Island (SCSI) by fishing year for Hector's dolphins. This model run assumed a calibration coefficient (ϕ) of 0.2.

APPENDIX H. SPATIAL ESTIMATED OBSERVED CAPTURES

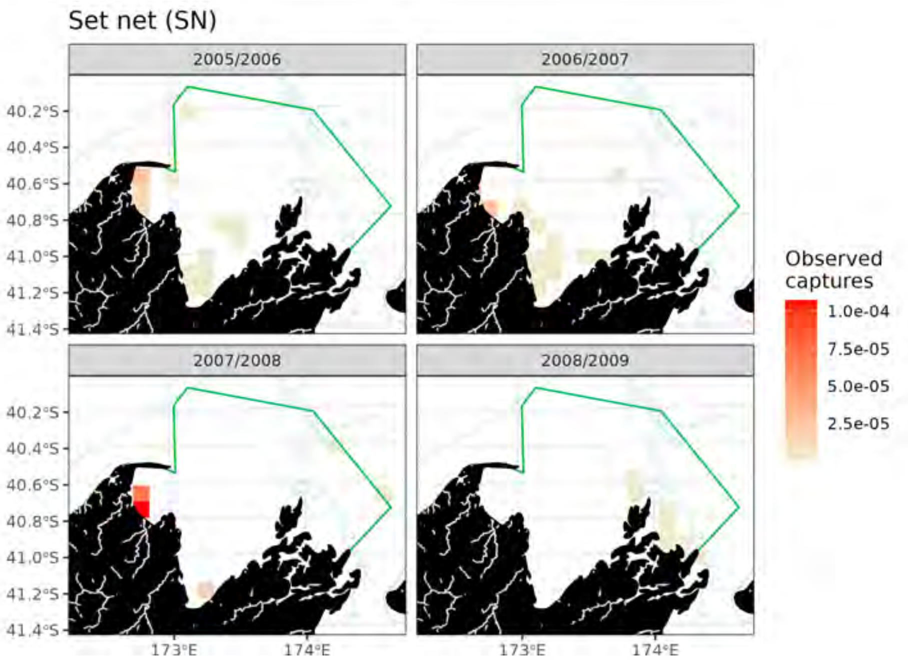

Figure H.1: Spatial plot of outputs of model *update*, showing the mean <u>predicted</u> number of Hector's dolphin observed captures by set nets (SN) in 10 km cells off the north coast of the South Island (NCSI) by fishing year. The NCSI region is shown in green and the 100 m depth contour in light blue. Note that only those years that had any observed fishing effort are shown.

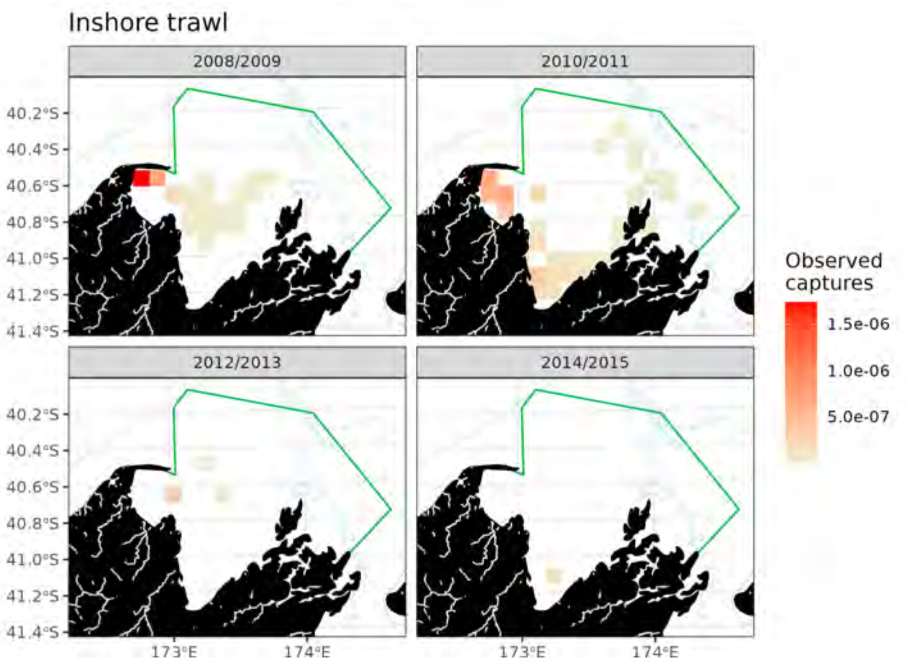

Figure H.2: Spatial plot of outputs of model *update*, showing the mean <u>predicted</u> number of Hector's dolphin observed captures by inshore trawls in 10-km cells off the north coast of the South Island (NCSI) by fishing year. The NCSI region is shown in green and the 100-m depth contour in light blue. Note that only those years that had any observed fishing effort are shown.

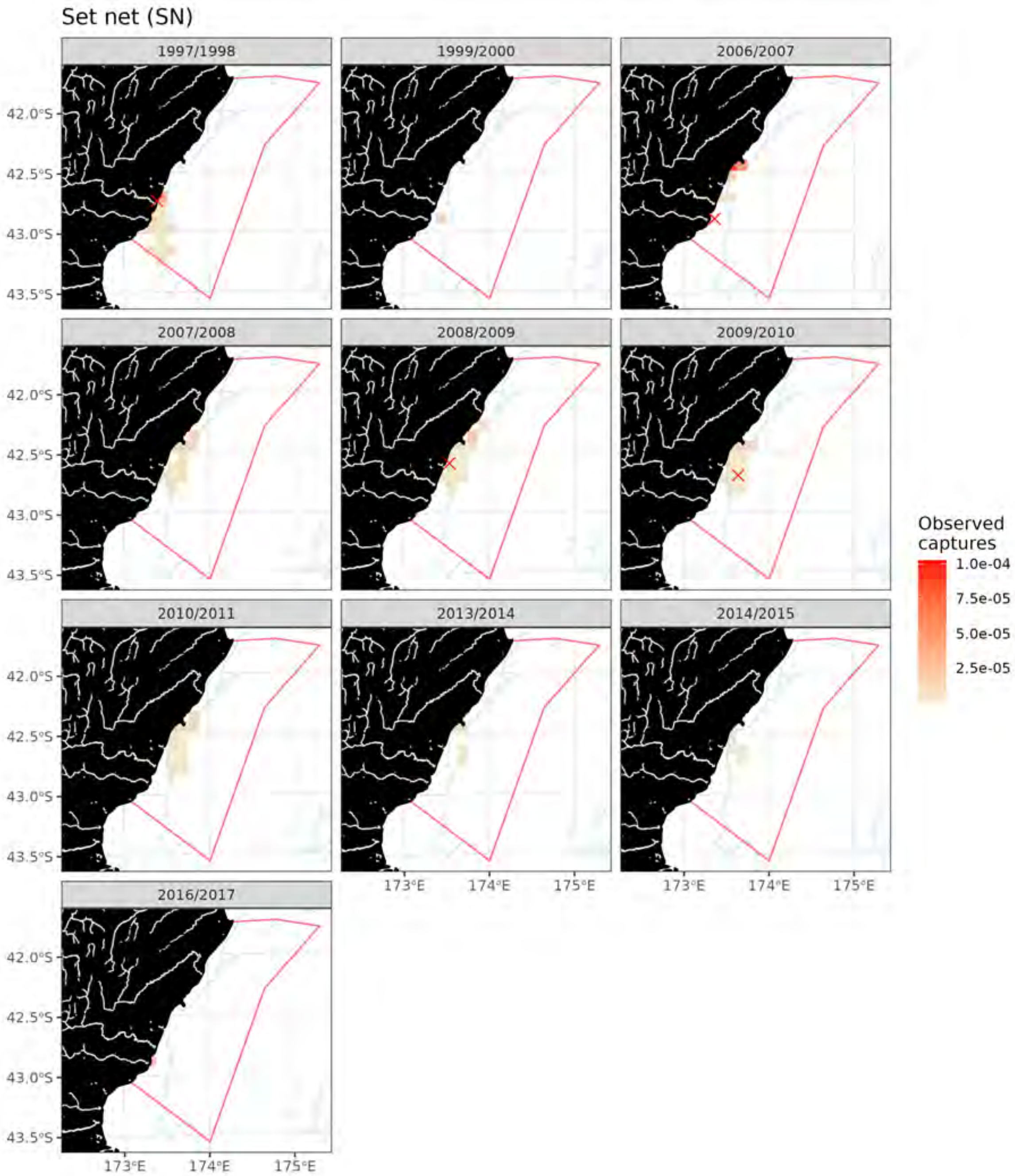

Figure H.3: Spatial plot of outputs of model *update*, showing the mean <u>predicted</u> number of Hector's dolphin observed captures by set nets (SN) in 10-km cells off Kaikōura (KAIK) by fishing year. The KAIK regions is shown in red and the 100-m depth contour in light blue. Note that only those years that had any observed fishing effort are shown.

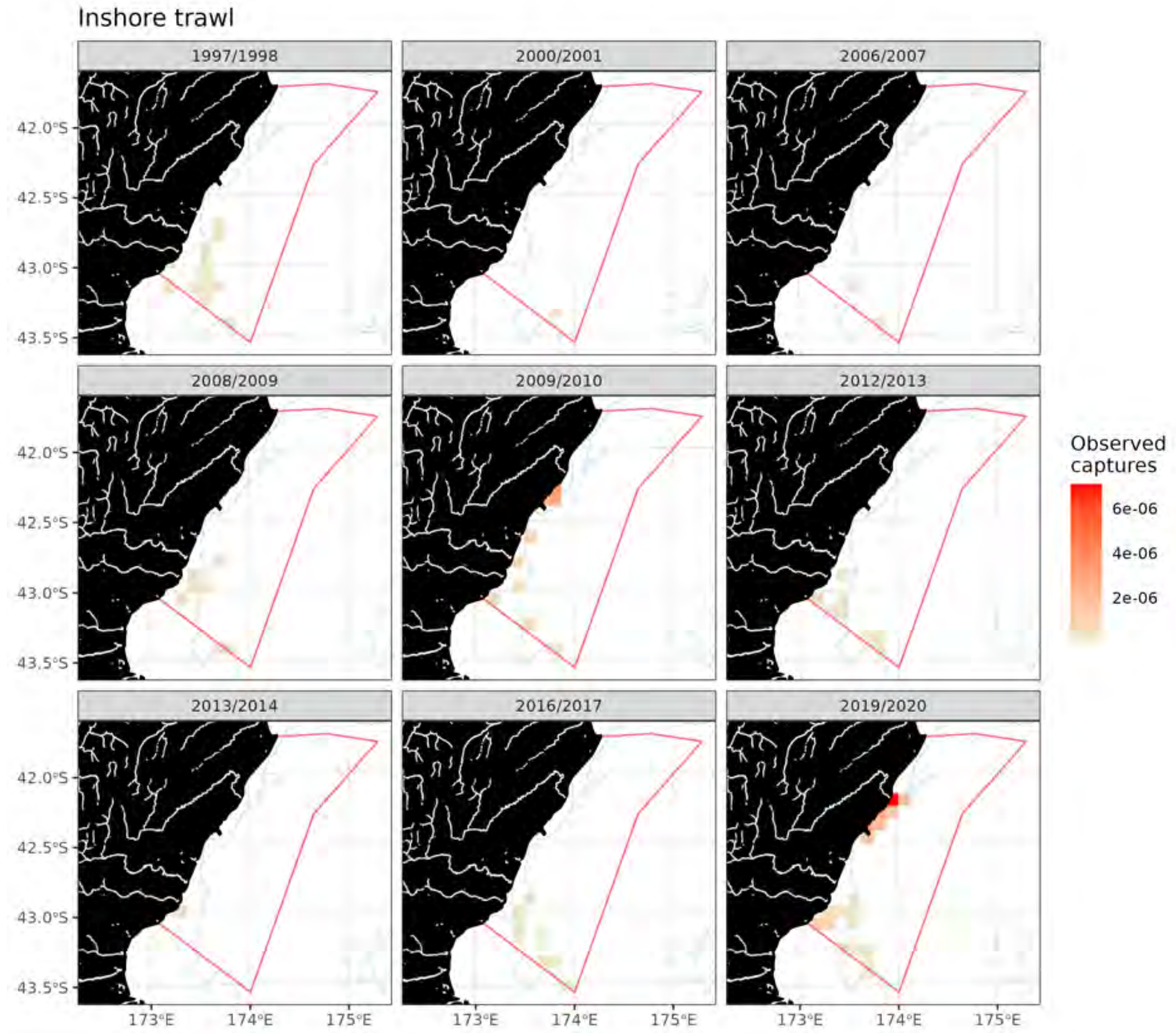

Figure H.4: **Spatial plot of outputs of model *update*, showing the mean <u>predicted</u> number of Hector's dolphin observed captures by inshore trawls in 10-km cells off Kaikōura (KAIK) by fishing year. The KAIK regions is shown in red and the 100-m depth contour in light blue. Note that only those years that had any observed fishing effort are shown.**

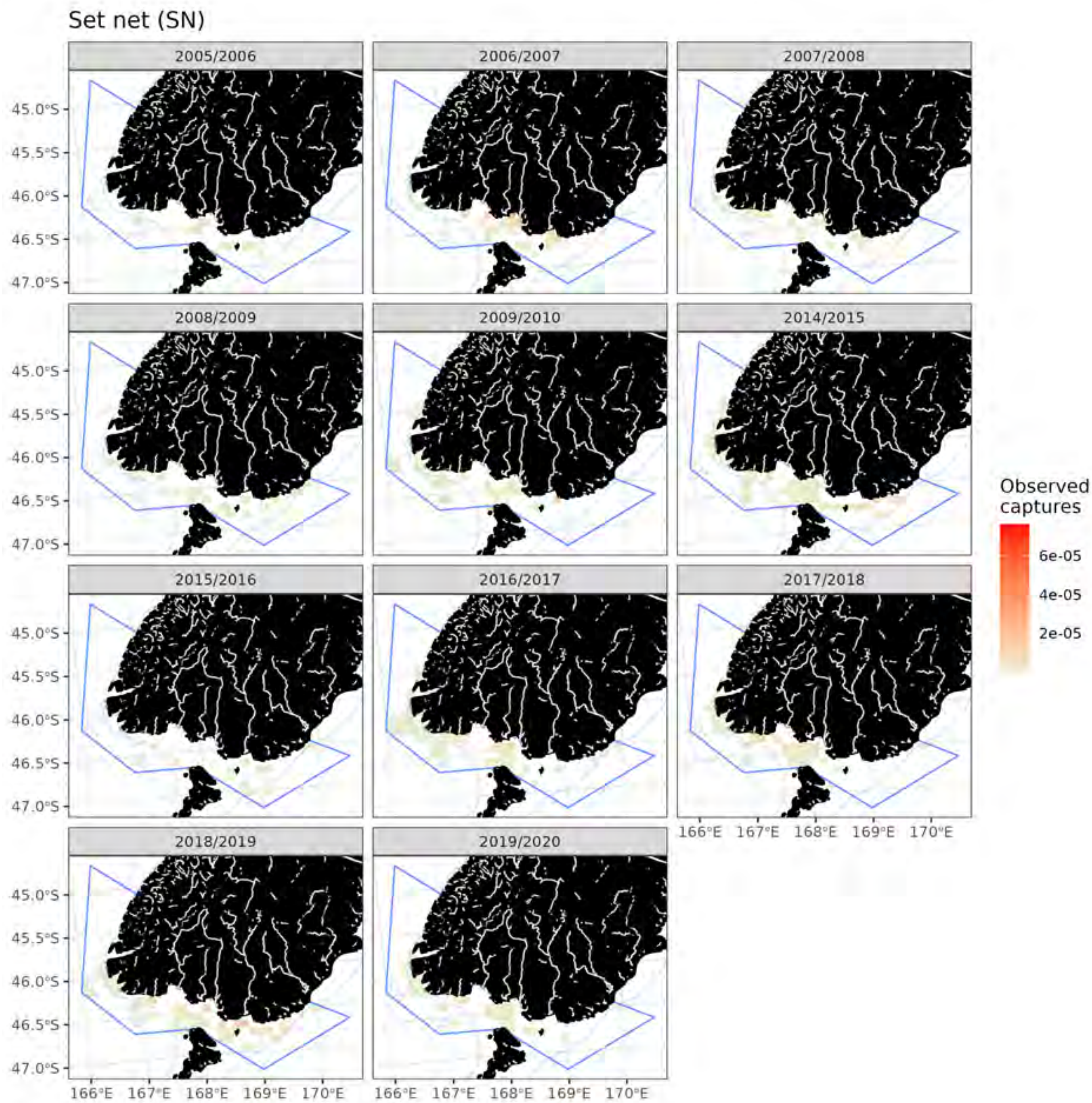

Figure H.5: Spatial plot of outputs of model *update*, showing the mean <u>predicted</u> number of Hector's dolphin observed captures by set nets (SN) in 10-km cells off the south coast of the South Island (SCSI) by fishing year. The SCSI regions is shown in blue and the 100-m depth contour in light blue. Note that only those years that had any observed fishing effort are shown.

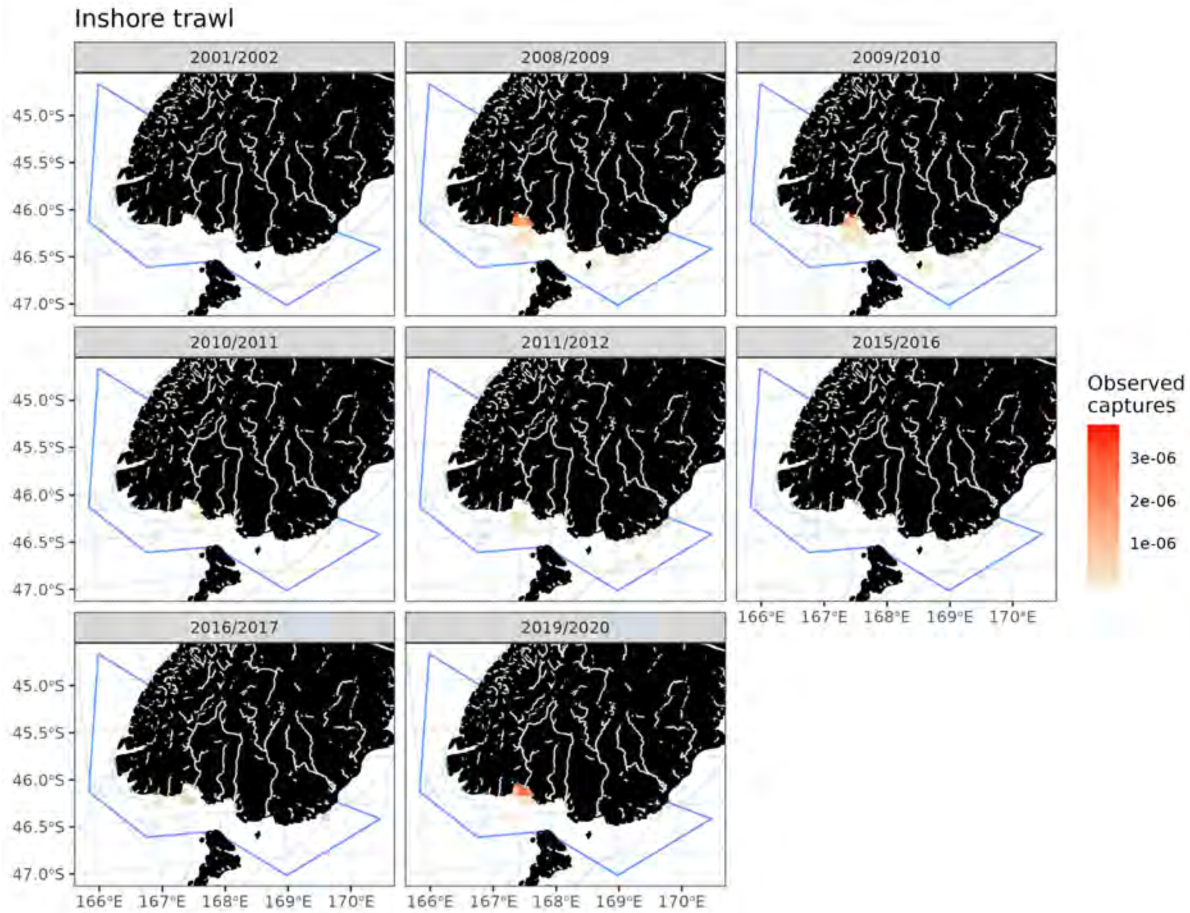

Figure H.6: Spatial plot of outputs of model *update*, showing the mean predicted number of Hector's dolphin observed captures by inshore trawls in 10 km cells off the south coast of the South Island (SCSI) by fishing year. The SCSI regions is shown in blue and the 100 m depth contour in light blue. Note that only those years that had any observed fishing effort are shown.